Development of Quantification Methods and Evaluation of Drugs Photostability in the Presence of Cyclodextrin Polymer and Human Serum Albumin Protein

Georgina Benson

A thesis submitted in partial fulfilment of the requirements for the degree of Doctor of Philosophy (PhD) to be awarded by De Montfort University

Leicester School of Pharmacy

De Montfort University

Leicester

March 2019

Abstract

This study aims to approach common issues encountered when detecting pharmaceuticals in surface waters and biofluids, using six compounds, Ethyl-3-aminobenzoate (3AB), Ethyl-2-aminobenzoate (2AB), Benzocaine (BZ), Mangiferin (MA), Tranilast (TR) and Axinitib (AXI).

The work can be seen as involving two main parts: an analytical and a physicochemical part.

In the analytical part two fluorimetric methods were developed to facilitate the detection of the compounds in different media. In the first section new quantification methods were developed to determine the drugs and molecules at the ppt level in both water and a real sample (canal water).

This method utilised β-CDP to increase the fluorimetric signal of the six compounds, up to ≈70 times. A recently proposed fluorimetric model was then used to characterise the drug-β-CDP inclusion complexes and stoichiometries, overcoming the limitations of the unknown molecular weight of β-CDP. This model was able to indicate that each compound formed either partial or multiple complexes with β-CDP, allowing for non-integer values to be considered, which could not be obtained using previous inclusion complex models.

To enable the compounds to be quantified in the presence of HSA, the decrease in the fluorimetric signal induced by an interaction between each of the six compounds and HSA was utilised. Through use of a novel application of Stern-Volmer equations, each compound was able to be successfully detected in the presence of HSA, providing a rapid, easy way to detect these compounds, without removal of the protein.

The proposed analytical methods using cyclodextrin nanosponge and human serum protein were proven to be robust and reliable, and each method was able to detect concentrations

of the compounds of ≈0.06ppb and ≈1ppb, respectively, representing a new way to improve detection and quantification of organic molecules, which could be extended to compounds other than those used in this study.

The physicochemical part dealt with the characterisation of the selected drugs and molecules in the absence and presence of nanosponges and human serum protein. After studying the evolution of the photodegradation of the compounds in a set of specific conditions, the -order kinetics tool made it possible to prove that the quantum yield of the forward and reverse photoreaction of TR in ethanol was wavelength dependent, increasing from 245nm-350nm, and that TR could be employed as an actinometer for the determination of unknown reaction parameters.

In addition the photostability of the studied molecules (TR and AXI) was significantly improved (more than 90% reduction of degradation) upon addition of increasing concentration of nanosponge or human serum albumin. This is particularly important for drug formulation and might explain the higher photostability of drugs in the blood stream.

In conclusion, each developed method was able to assist with the detection of the compounds in the outlined media, providing advantages that may be beneficial for future research of pharmaceuticals in biofluids and surface waters.

Contents

Acknowledgements

Firstly, I would like to thank my supervisor, Dr. Maafi. He has supported me and had faith in me throughout these years and has done more for me than I could ask of anyone. I am honoured to have had him as a supervisor.

I would also like to thank my second supervisor, Professor Grootveld, for encouraging me to pursue my dreams, and for his time and assistance.

Thirdly I would like to express how grateful I am to have such a loving family, I cherish them so much and am honoured to have them. I would especially like to thank my mother, she is truly one in a million. I can never repay her enough.

And lastly, to everyone who has stuck by for throughout these years. You are beautiful, genuine people, and I am honoured to know you all.

To have my work accepted would be a great honour. For those of you who have helped me I owe you everything.

List of Figures

Chapter 1

Chapter 2

Chapter 3

Chapter 4

Chapter 5

Chapter 6

Chapter 7

Chapter 8

List of Tables

Chapter 1

Chapter 2

Chapter 3

Chapter 4

Chapter 5

Chapter 6

Chapter 7

Chapter 8

List of Abbreviations

A= Native species of photounstable sample

$\boldsymbol{A_{tot}^{\lambda_{irr}}(0)}$= The total absorbance of the reaction irradiated photounstable parent compound before irradiation

$\boldsymbol{A_{tot}^{\lambda_{irr}}(\infty)}$= The total absorbance of the reaction solution at the photostationary phase of the reaction

$\boldsymbol{A_{tot}^{\frac{\lambda_{irr}}{\lambda_{obs}}}(t)}$= Absorbance reading at a specific time in the photoreaction, when irradiated at a particular wavelength and observed at another

$\boldsymbol{A_{tot}^{\frac{\lambda_{irr}}{\lambda_{obs}}}(\infty)}$= Absorbance reading at the photostationary state in the photoreaction, when irradiated at a particular wavelength and observed at another

$\boldsymbol{A_{tot}^{\frac{\lambda_{irr}}{\lambda_{obs}}}(0)}$ = Absorbance reading at the beginning of the photoreaction, when irradiated at a particular wavelength and observed at another

$\boldsymbol{A_{tot}^{\frac{\lambda_{irr}}{\lambda_{irr}}}(0)}$= Absorbance reading at the beginning of the photoreaction, when irradiated at a particular wavelength and observed at the same wavelength

$\boldsymbol{A_{tot}^{\frac{\lambda_{irr}}{\lambda_{irr}}}(\infty)}$= Absorbance reading at the photostationary state in the photoreaction, when irradiated at a particular wavelength and observed at the same wavelength

$\boldsymbol{A \rightleftarrows B}$= Reversible photoreaction between parent compound and photoproduct

AC= Association constant of the compound-cyclodextrin complex

AXI= Axitinib

B= Photoproduct

$\boldsymbol{B_1 \rightarrow B_2}$ = The phototransformation of photoproduct B_1 to a different photoproduct B_2

$\boldsymbol{B_2 \rightarrow B_3}$= The phototransformation of photoproduct B_2 to a different photoproduct B_3

BZ= Benzocaine

C$P_{\lambda irr}$= Calculated radiant power

C= Canal water

Cβ-CDP= β-cyclodextrin polymer and canal water

$C_B(\infty)$= The concentration of the photoproduct

C_A= The concentration of the unirradiated sample

CΦ= Quantum yield determined using the mathematical equations

$C\infty$ = The concentration of the sample at the phtostationary phase

[CD]= Concentration of β-cyclodextrin polymer

$[CD_p]_{0,x}$= Zero concentration of β-cyclodextrin polymer

$[CD_p]_{0,i,j}$= Concentration 'j' of β-cyclodextrin polymer

DMSO= Dimethyl sulfoxide

E$P_{\lambda irr}$= Experimentally determined radiant power

ELISA= Enzyme-Linked Immunosorbent Assay

EL-β-CDD= Ethylenediamine linked β-cyclodextrin dimer

ES-β-CD= Ethyl substituted β-cyclodextrin

EΦ = Experimentally determined quantum yield

FRED= Field-Ready Electrochemical Detector

F= Relative fluorescence intensity of the complexed guest compound

F_0= Relative fluorescence intensity of HSA in the absence of drug

F_{obs}= Relative fluorescence intensity of the guest compound with β-cyclodextrin polymer, at the appropriate maximum wavelength

$F_{\lambda_{irr}}(\infty)$= The time-independent photokinetic factor

$Fl_{tot,i,j}^{\lambda obs}$ = Total fluorescence intensity of the medium in the presence of 'j' concentration of β-cyclodextrin polymer and 'i' concentration of guest compound

Fl^{obs}= Observed fluorescence intensity

$Fl_{0,G,i}^{\lambda obs}$= The native fluorescence intensity of a specific 'i' concentration of the guest

$Fl_{0,(G_n:(CD_p)_m)}^{\lambda obs}$= The fluorescence intensity when every guest molecule is completely complexed

F_X= Relative fluorescence intensity of compound X

FPT, PCA and PGA= The main photoproducts of folic acid

[G]= Concentration of guest compound

$[G]_{0,i}^{n-1}$= A specific 'i' concentration of the guest compound

G_n: $(CD_p)_m$= The complex formed between one or more molecules of guest 'n' with one or more cyclodextrin polymer units 'm', which may be comprised of 'p' cyclodextrin monomer units

HP-β-CD= Hydroxypropyl-β-cyclodextrin

2-HP-β-CD= 2-Hydroxyl-propyl-β-cyclodextrin

HSA= Human Serum Albumin

ICH= International Conference on Harmonisation of Technical Requirements for Registration of Pharmaceuticals for Human Use

ICH Q1B= Harmonised Tripartite Guideline on Stability Testing of New Drug Substances and Products

k_q= The bimolecular quenching constant

$k_X^{\lambda_{irr}}$= The overall photoreaction rate of sample X

$k_{A\rightleftharpoons B}^{\lambda_{irr}}$= The exponential factor representing the overall rate-constant of an A⇌B photoreversible reaction

$K_{A\rightleftharpoons B}^{\lambda_{irr}}$= The equilibrium constant for thermodynamic reactions

K_{SV}= Stern-Volmer quenching constant

$K'_{G_n:(CD_p)_m}$= The drug-β-cyclodextrin polymer pseudo-association constant of the complex

$K_{G_n:(CD_p)_m}$= The drug-β-cyclodextrin polymer association constant of the complex

LOD= Limit of detection

LOQ= Limit of quantification

M-β-CD= Mono (6-ethylene-diamino-6-deoxy)-β-cyclodextrin

[M+H$^+$]= Molecular ion (used in LC/ MS)

n= Number of calibration points

Pp= Photoproduct

Ppb= Parts per billion

Ppt= Parts per trillion

Pss/ ∞= Photostationary state

$P_{\lambda irr}$= Irradiation radiant power

[Q]= Concentration of compound used as quencher

r= Correlation coefficient

RFI= Relative fluorescence intensity

RSD= Relative Standard Deviation

S= Stoichiometry of drug-β-cyclodextrin polymer complex

s.d.= Standard deviation

SIM= Positive single-ion monitoring (used in LC/ MS)

S-β-CD= Sulfobutylether-β-cyclodextrin

t= Specific reaction time in photoreaction when an equilibrium between the parent and photoproduct has been reached

TMS= Tetramethylsilane

TR= Tranilast

Try= Tryptophan

UV-A= Ultraviolet region from approximately 320nm-400nm

UV-B= Ultraviolet region from approximately 290nm-320nm

UV-C= Ultraviolet region from approximately 110nm-290nm

W= Water

3AB= Ethyl-3-aminobenzoate

2AB= Ethyl-2-aminobenzoate

$\boldsymbol{\lambda_{obs}}$= The wavelength at which the sample is observed

$\boldsymbol{\lambda_{irr}}$= The wavelength at which the sample is irradiated

$\boldsymbol{I_{\lambda_{obs}}}$= The optical path length of the light within the sample

$\boldsymbol{I_{\lambda_{irr}}}$= Optical pathlength of sample at the specific irradiation wavelength

$\boldsymbol{\lambda_{irr}/\lambda_{obs}}$= Photoreaction irradiated at a specific wavelength and monitored at a specific wavelength, which may or may not be the same wavelength

εB2= Extinction coefficient of photoproduct B_2

εB1= Extinction coefficient of photoproduct B_1

$\boldsymbol{\upsilon_0^{\lambda_{irr}/\lambda_{obs}}}$= The initial velocity of the photoreaction

$\boldsymbol{\upsilon_{0(cld.)}^{\lambda_{irr}/\lambda_{obs}}}$= The calculated initial velocity of the photoreaction

$\boldsymbol{\beta_{\lambda_{irr}}}$= A proportionality factor between the overall rate-constant and the radiant power

$\boldsymbol{\Phi_{A\rightarrow B}^{\lambda_{irr}}}$= The forward quantum yield of the photochemical reaction for the transformation from A→B, at a specific irradiation wavelength

$\boldsymbol{\Phi}_{B\rightarrow A}^{\lambda_{irr}}$= The reverse quantum yield of the photochemical reaction for the transformation from B→A, at a specific irradiation wavelength

***%$_{REC}$**= Average percentage recovery of compound recorded in the sample

≠C$_{Det}$/ ppb= Average concentration of compound detected in the sample

+C$_{Add}$/ ppb= Concentration of compound added to the sample

τ= The fluorescence lifetime of the unquenched molecule

α-CD= α-cyclodextrin

β-CD= β-cyclodextrin

γ-CD= γ-cyclodextrin

β-CDP= β-cyclodextrin polymer

Chapter 1:

Literature survey

Chapter 1: Literature survey

1.1.1 Detection of drugs

Concentrations of drugs, frequently below detection limits of most available instruments, can be present in surface waters (Owens, 2015), often existing for long periods of time (Rozman, Hrkal, Váňa, Vymazal, & Boukalová, 2017). The quantity of drug able to cause toxic effects is specific to each individual (Voicescu & Bandula, 2015). By accumulating or interacting with other compounds, potentially fatal consequences may result, such as antibiotic resistance (Owens, 2015). HPLC can be used to achieve low detection (Ulbrich & Lamprecht, 2011), however, less expensive methods, results often lack accuracy (Kumar et al., 2014). There is therefore the necessity for a technique that is able to accurately quantify low concentrations of compounds.

In addition, compounds are often sensitive to the polarity of the media. Such matrices are rarely free from interferences (Lakowicz, 2006), this can complicate analysis, requiring extensive sample preparation, use of an additional compound (Abdolmohammad-Zadeh & Talleb, 2015), or time-consuming and expensive equipment (Von Tungeln et al., 2011). As mentioned, HPLC can provide good detection, but at the expense of costly solvents, and sufficient separation of multiple compounds may be time-consuming (Ulbrich & Lamprecht, 2011). Cheaper techniques can provide sensitivity, specificity, and rapid analysis, able to detect concentrations as low as 0.04ppb, however, to accomplish this, sample preparation is required (Hurtado-Sánchez, Lozano, Rodríguez-Cáceres, Durán-Merás, & Escandar, 2015). To allow for routine testing to be conducted in biofluids, an easy-to-carry-out technique should

be developed which can detect relatively low concentrations of the pharmaceuticals, without need for sample preparation.

Pharmaceutical compounds do not necessarily interact with other pharmaceuticals in the sample. There are, however, a number found to interact with species present in the environment, and also with light. Such occurrences can have just as fatalistic consequences, as they can photodegrade to form toxic photoproducts which can cause such effects as photoxicity or photoallergy, affecting cellular function (Moore, 2004), or can inactivate the effects of the compound (Tønnesen, 2004). These photounstable compounds can alter in their photostability in different media, including blood (Nilsson, 2010). Such photoproducts may inhibit analysis, increasing or decreasing the compound concentration measured and resulting in incorrect quantification of the compound in the initial sample (Moore, 2004). The extent of the photodegradation of the sample should therefore be determined for accurate analysis of the sample.

1.1.2 Current detection methods and their limitations

There are currently a number of techniques available able to detect low concentrations of drug compounds in surface waters.

Techniques such as HPLC-UV and solid-phase microextraction coupled with gas chromatography isotope ratio mass spectrometry either lack the sensitivity required or are unsuitable for thermally unstable compounds. The most sensitive methods tend to be liquid chromatography tendem mass spectrometry, and gas chromatography coupled to mass spectroscopy, however solid-phase extraction is often required before an injection can be carried out (Mu, 2015). Even though techniques such as graphite furnace atomic absorption spectroscopy and inductively coupled plasma mass spectrometry are reliable, they are often

time-consuming and require expertise. Enzyme-Linked Immunosorbent Assay (ELISA) has the ability to provide rapid detection but is limited by its sensitivity (Kuang et al., 2013). In order to provide sensitive analysis in a short-period of time methods such as Field Ready Electrochemical Detector (FRED) (FREDSense, 2018) and lateral flow assay, using a heterogenously sized gold amplified probe to create a strip immunosensor, may be employed. These are easy, rapid, cost effective and able to provide lower sensitivity than ELISA, however, lateral flow assay does require some sample preparation (Kuang et al., 2013), and although FRED can be used on-site it takes ≈1 hour to generate results. Although able to provide detection of ≈190ppb and 1ppb (FREDSense, 2018; Kuang et al., 2013), and useful for routine analysis, both the latter methods lack the sensitivity able to be achieved using LC-MS/MS methods, which are able to detect concentrations as low as 0.05ppb (Mu, 2015).

In regards to compounds in biofluids, precision and accuracy of the compounds can be accomplished using LC-MS/ MS, however, not only did this require use of mobile-phase solvents, but centrifugation, evaporation and removal of the supernatant was also necessary (Sahoo, Sahu, Rao, & Ghosh, 2014). Furthermore, methods which overcome the requirement for sample pretreatment, such as Shodex ODP2 HP, a polymer-based reversed-phase HPLC column, can exclude the biological matrix, however, not only require more expensive equipment, but have relatively high limits of detection (Ito, K., Wakayama, R., Denko, K. K. S., Komiyama, Y., Showa Denko, S., Hara, 2013) (DIRECT ANALYSIS).

1.2.1 Cyclodextrins

Often used in pharmaceutical studies for drug delivery, cyclodextrins are cyclic oligosaccharides which possess a polar exterior and non-polar interior cavity, within which

they can encapsulate non-polar molecules by forming hydrogen bonds to create a complex. Hydroxyls on the cyclodextrin can rotate, reducing the cavity size more on the primary side, than the other, secondary side (Fig. 1). Such complexes have various pharmaceutical applications, including increasing drug stability and enhancing concentrations of drug compound present in the solution (Szejtli, 2005).

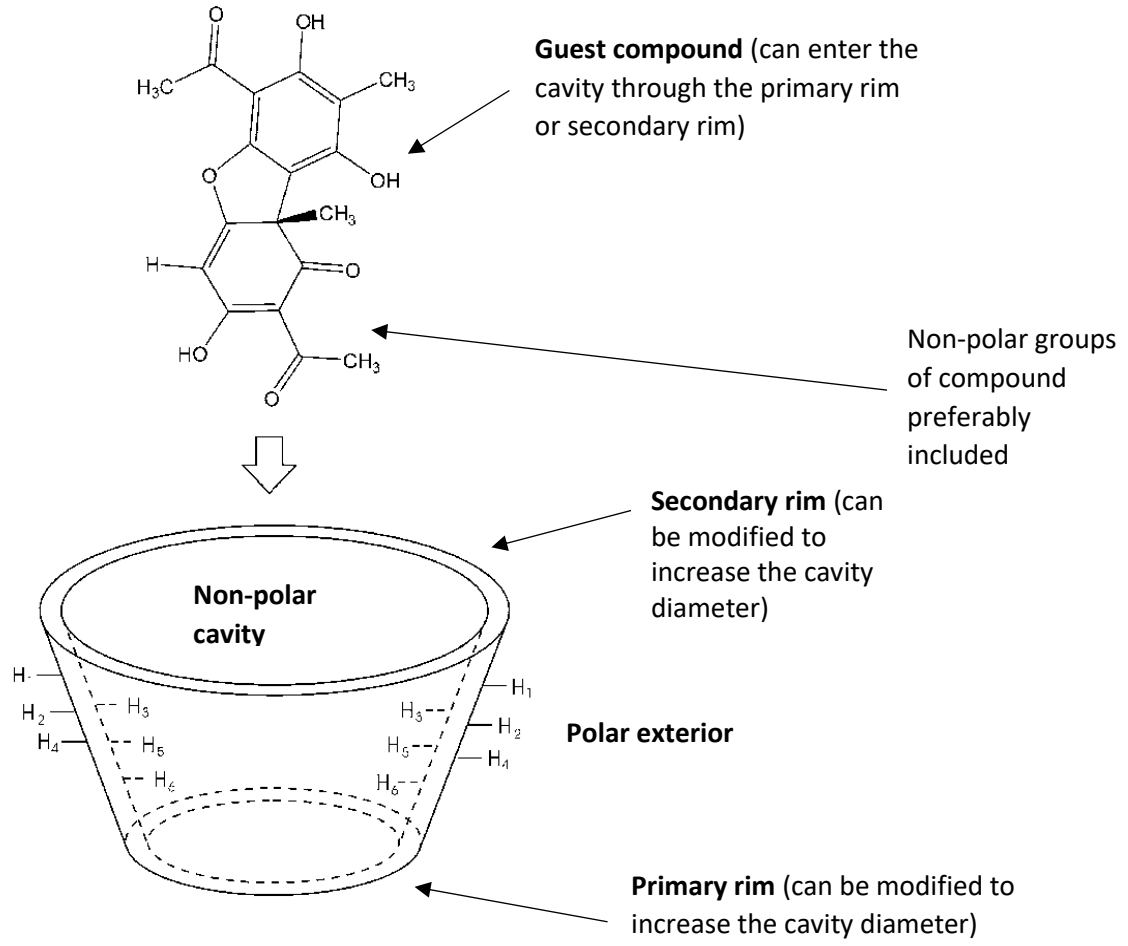

Figure 1: *Molecular structure of cyclodextrin, representing cavity, hydrophilic exterior and hydrophobic interior (Nikolić et al., 2013)*

Of the three main cyclodextrins, α-, β- and γ-cyclodextrin, β-cyclodextrin has proved the most useful. Inclusion complexes formed with guest molecules can be observed spectroscopically through various changes including increases, and shifts (Szejtli, 2005).

Such spectral observations can occur when the compound is protected from environmental effects, such as solvents and light (Tejashri, Amrita, & Darshana, 2013), often resulting in spectra intensity increases and shifts (Szejtli, 2005). This is not necessarily the case, however, as sometimes decreases (Ishiwata & Kamiya, 1997) or no observable effects (Varghese, Al-Busafi, Suliman, & Al-Kindy, 2015) are encountered.

1.2.2 Cyclodextrin derivatives

The functional groups on the primary or secondary face of the cyclodextrin can be modified with various substituents to form derivatives, sometimes increasing its solubility, and when complexed with a guest compound can provide advantageous effects to this compound (Huang, He, Lu, Ge, & Guo, 2011). As can be observed (Table 1), each compound can interact uniquely with the different forms of cyclodextrin, whether it be α-, β-, or γ-cyclodextrin, or a derivative form. If the latter has superior properties compared to those of the native cyclodextrins monomers, then a greater association constant and an enhancement in fluorescence intensity may occur for the compound (Table 1).

Table 1: *Details of the previously observed effects of cyclodextrin monomers on 3AB, 2AB, BZ, MA, TR and AXI, the fluorimetric increases and ratio of fluorescence increase (fold), their association constants (AC) and stoichiometries (S) formed. α-CD=α-cyclodextrin, β-CD=β-cyclodextrin, γ-CD=γ-cyclodextrin, S-β-CD=Sulfobutylether-β-cyclodextrin, HP-β-CD=Hydroxypropyl-β-cyclodextrin, ES-β-CD=Ethyl substituted β-cyclodextrin, M-β-CD=mono (6-ethylene-diamino-6-deoxy)-β-cyclodextrin, EL-β-CDD=Ethylenediamine linked β-cyclodextrin dimer, β-CDP=β-cyclodextrin polymer* (Ferreira et al., 2013; Hirayama, Utsuki, & Uekama, 1991; Iglesias, 2011; Maestrelli, González-Rodríguez, Rabasco, Ghelardini, & Mura, 2010; Merzlikine, Abramov, Kowsz, Thomas, & Mano, 2011; Pinto et al., 2005; Tang, Liang, Tong, & Li, 2006; Utsuki, Hirayama, & Uekama, 1993; Yan Lee, 2016; Yang et al., 2013).

Compound	Cyclodextrin	Medium	Increase/ fold	S/ AC
BZ	α-CD	Neutral	≈0.043-3.09/ 71.86	1:1
	β-CD	Neutral	≈0.048-0.529/11.02	1:1/ 780 dm^3 mol^{-1}
	γ-CD	Neutral	≈0.048-0.257/ 5.35	1:1
	S-β-CD	Neutral	-	1:1/ 759.24M^{-1}

	β-CD	Neutral	-	1:1/ 315M^{-1}
	HP-β-CD	Neutral	-	1:1/ 352M^{-1}
	β-CD	Neutral	-	1:1/ 549M^{-1}
2AB	α-CD	Neutral	≈0.604-4.2/ 6.95	1:1/ 49 dm^3 mol^{-1}
	β-CD	Neutral	≈0.723-6.6/ 9.13	1:1/ 184 dm^3 mol^{-1}
	γ-CD	Neutral	≈0.58-5.3/ 9.14	1:1/ 34 dm^3 mol^{-1}
3AB	α-CD	Neutral	≈0.024-1.96/ 81.67	1:1
	β-CD	Neutral	≈0.021-1.22/ 58.10	1:1/ 185 dm^3 mol^{-1}
	γ-CD	Neutral	≈0.036-0.77/ 21.39	1:1
MA	β-CD	pH=8	≈120-250/ 2	-
	ES-β-CD	pH=8	≈75-500/ 7	2:1/ 3.04 x $10^6$$L^2$/ mol^2
	HP-β-CD	pH=8	≈50-210/ 4	1:1/ 3480 ± 20 L/mol
	S-β-CD	pH=8	≈30-100/ 4	1:1/ 2103 ± 60 L/mol
	β-CD	pH=8	-	1:1/ 1113 ± 60 L/mol
	M-β-CD	pH=8	-	1:1/ 3763 ± 80 L/mol
	β-CD	pH=7	-	1:1/ 1.6 ± 0.7 x 10^5L mol^{-1}
	β-CD	pH=7	-	1:1
TR	γ-CD	pH=7	-	2:1 or 1:1 (dependant on concentration)
	α-CD	pH=7	-	1:1/ 60± 20 dm^3 mol^{-1}
	β-CD	pH=7	-	1:1/ 220± 15 dm^3 mol^{-1}
	γ-CD	pH=7	-	2:1/ 2210± 90 dm^3 mol^{-1}
	EL-β-CDD	pH=2	≈50-190/ 3.8	1:1/ 8.39 x $10^3$$mol^{-1}$
AXI	HP-β-CD	pH=7	2.51	1.09:0.82/ 2041 L/mol
	β-CDP	pH=7	93.1	0.98: 0.79/ 3.33 g/L

1.2.3 Cyclodextrin polymers

Although it has the lowest solubility of the three native cyclodextrins, the greater complexing ability of β-cyclodextrin, when compared to the other cyclodextrins, means that this cyclodextrin is most commonly used to create polymeric cyclodextrins (nanosponges)(Tejashri et al., 2013). Although similar in structure to the monomers, these polymers boast the advantages of both monomers and polymers (Gidwani & Vyas, 2014). This can enable them to include more guest molecules, both within their cavity, and adsorbed to their exterior (Morin-Crini & Crini, 2013), and their 'looser' structure may increase the size of their secondary cavities and increase their solubility (Szejtli, 2005), boosting their complexing and stabilising ability (Tejashri et al., 2013). Spectroscopic benefits of β-cyclodextrin polymer

(β-CDP) include movement restriction, and microenvironment alteration, effects to which spectroscopy is especially sensitive. There are fewer fluorimetric studies dedicated to these polymers when compared to those of the monomers, however, where they have been studied they can lead to greater increases in fluorescence intensity than those with the monomers (Hamai, 1999)(Table 1).

It has been observed that in the presence of β-CDP the fluorescence intensity of such compounds as Azulene and 2-anilino-6-naphthalenesulfonic acid have been increased, and their fluorescence spectrum red shifted and blue shifted respectively. The different effects on each compound indicated each was included within the β-CDP cavity, in an alternative way to the other (Hamai, 1999). Such increases in intensity and blue shifts occurring (Lakowicz, 2006) may be attributed to a change in molecular rotation of the compounds (Neckers, Volman, & Bünau, 1996), their relocation to a more polar environment, and a smaller amount of energy lost through excited state solvent collisions processes (Lakowicz, 2006). Such studies sometimes addressed the fluorimetric effects occurring but did not always quantify the drug compound (Hamai, 1999).

1.2.4 Inclusion complex

In order to evaluate how effective cyclodextrins are for the complexation of a specific guest molecule the stoichiometry and stability constant can be determined. The former provides information on the number of guest compounds binding to a single cyclodextrin unit, whilst the latter measures the strength of the guest: host binding (Jones, Marand, & McGrath, 2004), by comparing the ratio of host-guest complex formed to that of the free host and guest remaining (Angelova, Ringard-Lefebvre, & Baszkin, 1999)(Fig. 2). The higher the association constant is, the more stable the complex (Domańska, Pelczarska, & Pobudkowska, 2011).

It has been reported that β-CDP may be comprised of multiple units of β-cyclodextrin monomer, and thus that multiple drug molecules may be bound to its inclusion site. These effects are not accounted for when determining the inclusion complex and stability constant (Hamai, 1999), as an average molecular mass of β-CDP is provided (Fülöp, Kurkov, Nielsen, Larsen, & Loftsson, 2012).

Studies involving β-CDP have taken various other approaches to measure the stability constant, such as recording the heat of inclusion through titration microcalorimetry (Wenz & Weickenmeier, 1996), and through carrying out solubility experiments (Zhang et al., 2013). Furthermore, use of spectroscopic methods, such as absorbance spectroscopy, have been used to determine the stoichiometry, however, data conclusions were based solely on spectroscopic changes, such as the presence of isosbestic points, bathochromic shifts, and increases in spectra (Hamai, 1999).

Many analysis methods tend to require knowledge of the β-CDP molecular weight, which can range from 1-2,000kDa (Fülöp et al., 2012). Accurate determination of the molecular weight is challenging as it is not only influenced by the formation ratio of β-cyclodextrin, epichlorohydrin and glycidyltrimetylammonium chloride used, but is additionally influenced by the crosslinking step, the temperature at which the crosslinking was carried out and the reaction time (Junthip, Tabary, Leclercq, & Martel, 2015). Such issues have been addressed through techniques such as Job's continuous variation plot to determine the stoichiometry of one cyclodextrin monomer unit alone (Zhang et al., 2013). Alternatively, in studies, conduction of elemental analysis, with knowledge of the polymerisation degree, have been made on the β-CDP to determine the molecular weight of one unit of its monomer, and then

double reciprocal plots created, based on spectral changes, to determine the rate-constant (Hamai, 1999).

These inclusion complexes are based on a set of pre-determined stoichiometry values, and therefore such methods may not provide accurate information on the stability complex (Fülöp et al., 2012).

1.2.5 Modes of inclusion

It has been shown that the inclusion of compounds within the cyclodextrins cavity tend to occur predominantly through encapsulation of the aromatic ring of the compound, forming the greatest stability constant and thus the strongest complexation (Hergert & Escandar, 2003). It has been reported that although one molecule of cyclodextrin is often complexed with one molecule of the guest compound, forming a 1:1 complex (Huang et al., 2011), more than one molecule of either compound or cyclodextrin may interact with the other to form various other inclusions, including 2:2, 2:1 or 1:2 complexations (Deng et al., 2016)(Figure 2).

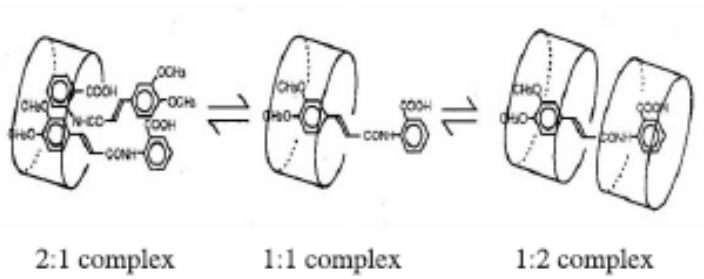

Figure 2: *Stoichiometries formed between guest compounds and cyclodextrins (Uekama, Hirayama, & Arima, 2006)*

Studies have shown that it may be energetically favourable for the compound to be included in more than one way (Aki, Niiya, Iwase, & Yamamoto, 2001) or not necessarily fully

encapsulated within the cyclodextrin cavity (Hamai, 1999). Such an effect has been observed with cyclodextrin monomers (Fernandes, Carvalho, Pereira da Costa, & Veiga, 2003).

In cases where multiple inclusion complexes have been reported, the results were supported through use of 2D NMR. Spectroscopic and evidence of interactions between both aromatic ends of the studied compound and the inner cavity of cyclodextrin were observed. Such effects have been reported in multiple studies and with various compounds, indicating that this phenomenon was possible and evidencing that cyclodextrins had the ability to accommodate more than one drug molecule (Fernandes et al., 2003).

As mentioned, β-CDP may have multiple binding sites (Hamai, 1999), and thus the use of pre-determined stoichiometries would not be useful for their evaluation. A technique has previously been proposed by our group which utilises fluorimetry and a set of mathematical equations. In this equation the molecular weight of β-CDP is represented in g/L, and multiple data sets are encompassed to determine the inclusion complex. Such a model has been proven to be able to determine the stoichiometry of both partial and multiple inclusions, increasing the reliability of the results (Yan Lee, 2016). The model has been utilised in the presence of both hydroxypropyl-β-cyclodextrin and β-CDP for the assessment of Axitinib and 8-Anilino-1-naphthalenesulfonic acid ammonium salt, however, it has not yet been applied to other compounds.

1.3 Human serum albumin (HSA)

The presence of proteins in biofluids (Abdolmohammad-Zadeh & Talleb, 2015), or organic compounds in surface waters has been found to influence drug concentrations (Sciences, 2014), resulting in challenging analysis of serum (Bonnier, Baker, & Byrne, 2016).

Although the sensitivity of fluorimetry may mean that it is the method of choice for pharmaceutical determination, proteins, such as HSA, have been found to possess a fluorophore, causing it to fluoresce and complicating analysis (Rub, Khan, Azum, & Asiri, 2017). Such a fluorophore (tryptophan residue) often fluoresces at a similar wavelength to that of pharmaceuticals, masking their signal (Tayyab, Zaroog, Feroz, Mohamad, & Malek, 2015). In addition the protein can bind to guest compounds, altering both its own properties and that of the quencher (Yue, Chen, Qin, & Yao, 2009).

As can be observed (Fig. 3) when the protein is in its native state, and thus folded, the structure of the protein protects the fluorescent tryptophan residue, allowing for the fluorophore to be spectroscopically detected. However, once the protein is unfolded the tryptophan residue is accessible to the polar solvent. This can be observed as wavelength shifts, depending on the medium, or when it is exposed to a guest compound (Yue et al., 2009).

If the tryptophan residue is inaccessible to the compound then no binding occurs, as would be observed by a small increase upon addition of the compound (Abdollahpour, Asoodeh, Saberi, & Chamani, 2011). If accessible and bound a decrease in fluorescence intensity may occur (fluorescence quenching), as will be explained with the following diagram (Figure 3):

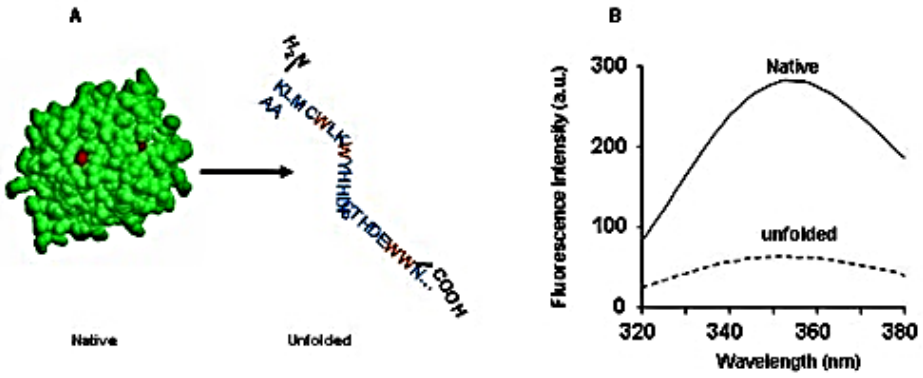

Figure 3: *Process of protein unfolding. When unfolded the tryptophan residue in the protein is exposed to the polar solvent and the fluorescence spectroscopic signal of the protein decreases (Fluorescence Spectroscopy: A tool for Protein folding/unfolding Study PC3267, 2007)*

The existence of HSA in proteins (Lakowicz, 2006) means that it is present in a number of biofluids, hindering spectroscopic analysis. Such biofluids are useful for representing drug concentrations in patients, and are relatively non-invasive. Although fluorescent detection limits in serum may sometimes be below 1ppb (Ferdig, Kaleta, Thanh Vo, & Buchberger, 2004), they are often thousands of ppb in size (Tang, Jia, & Shi, 2005). Therefore, low detection limits only appear to be achieved by using more expensive techniques alongside (Ferdig et al., 2004). There is therefore the lack of a method that involves little sample preparation, and can provide rapid quantification of drugs in serum, simply, cheaply and reliably (World Health Organization., 2010).

1.4.0 Photostability

1.4.1 Photostability

For the evaluation of a drug compound before it is released onto the market, The International Conference on Harmonisation of Technical Requirements for Registration of Pharmaceuticals for Human Use (ICH) Harmonised Tripartite Guideline on Stability Testing of New Drug Substances and Products (ICH Q1B) has proposed for it to be compulsory to provide

data on the photostability of a drug. Carried out through various stability measurements, including stress testing (H. Tønnesen, 2004) and forced degradation studies (*International Conference on Harmonisation of Technical Requirements for Registration of Pharmaceuticals for Human Use ICH Harmonised Tripartite Guideline Stability testing: Photostability Testing of New Drug Substances and Products Q1B*, 1996), these experiments should assess the overall photostability of the drug under various conditions (H. Tønnesen, 2004), including in its medium, which may be a real sample, such as blood (Cairns, 2012). If deemed photounstable it becomes necessary to identify the photodegradation pathways the compound takes and the photoproducts it forms (Cairns, 2012). It is crucial to conduct such stability studies before packaging and labelling the drug, to ensure its maximum preservation (H. Tønnesen, 2004), to identify whether its photoproducts are toxic and to determine the length of time the compound is stable for (Watson, 2012).

Issues arise when performing photostability experiments as there are currently no requirements on the specific photostability tests that should be carried out, and instead they are left for the experimenter to decide (H. Tønnesen, 2004).

1.4.2 Kinetics of photodegradation

Information on the rate of photodegradation is often acquired by measuring the absorbance spectrum of the compound, as the change in absorbance is proportional to the number of photons absorbed (Cairns, 2012), and the collected data is treated using reaction order kinetics.

Such results have been described by zero-, first- and second-order equations. When the data obeyed more than one reaction order, authors have been found to make conclusions based on small differences in the correlation coefficients of the equations of such plots (Roman,

Breier, & Steppe, 2011). Moreover, it has been acknowledged that different light environments can give different results (Guerra, Gosetti, Marengo, Llompart, & Garcia-Jares, 2019), and demonstrated that irradiation wavelength and power intensity influenced the degradation rate (W. Maafi & Maafi, 2013). Therefore, even though fitting to a single rate order may be the case (Tian & Acevedo, 2018), these models may be a poor representation of the data.

A new method has been proposed by our group (W. Maafi & Maafi, 2013) for the evaluation of photochemical reactions. This semi-empirical integrated rate-law has been found to relate two measureable quantities (absorbance and time), encompassing factors known to influence the rate of photodegradation. Such a model may therefore be useful for mathematical comparisons of data, and highlight the necessity for all other conditions to remain constant to allow for data comparisons (M. Maafi & Maafi, 2016), overcoming significant differences in results between stability testers (H. Tønnesen, 2004).

The model can not only determine whether a compound photodegrades in the UV-Vis region, but also the sub-band of UV light and specific wavelength range that is able to cause the most photodegradation to the compound (Table 2).

Table 2: *UV-Vis absorption region*

High energy wavelengths → Low energy wavelengths				
Region	UV-C	UV-B	UV-A	Visible
Wavelength	110-290	290-320	320-400	380-760

This method has been found useful for describing the photokinetics of a number of compounds (M. Maafi & Lee, 2015a, 2015b). In addition this model has been applied to

determine the quantum yield of a reaction to represent the efficiency of the reaction, and in actinometry to determine the light intensity from an unknown light source (M. Maafi & Al-Qarni, 2018). Such studies have only been applied to a small number of compounds, and thus there is the potential for further research in this area, using alternative compounds, to ascertain how they behave and whether they obey these rate equations, enhancing the reliability of the technique, and allowing for photoreaction information on the compounds to be determined.

1.4.3 Cyclodextrins and photostability

The application of cyclodextrins to allow for greater compound photostability has been demonstrated in a number of studies (Hirayama et al., 1991), and it is well documented that they can provide stability to compounds (Tejashri et al., 2013), although this is not always the case (Utsuki et al., 1993). The accommodation of the compound within the cavity protects it from the quencher, preventing it from forming hydrogen bonds with the solvent and reducing its molecular rotation by forming tight molecular bonds (Bortolus, Monti, Energia, & Area, 1996).

It has previously been evidenced that cyclodextrins can influence the rate of photodegradation, depending upon the specific ratio of compound to cyclodextrin used. When compounds undergo multiple photoprocesses, the macromolecules may not necessarily have the same influence on each stage of the photoreaction (Hirayama et al., 1991). Furthermore, whilst one cyclodextrin may reduce the rate of photodegradation, another may accelerate it (Utsuki et al., 1993).

1.4.4 HSA and photostability

It has been found that proteins may affect the photochemistry of a drug (Alarcón, Edwards, Aspée, Borsarelli, & Lissi, 2009), although there appears to be fewer photostability studies dedicated to this area than to the effects of cyclodextrins on photostability. Proteins such as β-lactoglobulin have been found to reduce the photodegradation of compounds by oxidising the protein residues, increasing its carbonyl content, and thus enhancing the stability of tryptophan residues (Wang et al., 2019).

The most abundant protein in human serum (Bonnier et al., 2016), HSA, has been found to maintain a greater fluorescence intensity of curcumin after 9 hours, when compared to that in its absence (Jain, 2017), and similar observations of its photoprotecting effects have been reported in other studies (Vayá, Lhiaubet-Vallet, Consuelo Jiménez, & Miranda, 2014). Of most interest to the current study was the reduction in photodegradation rate of folic acid in HSA. Further investigations in this study found that in tryptophan alone a decrease in photodegradation appeared to occur. However, this effect was less prominent than that with HSA, as was explained by the authors in Fig. 4 (Fig. 4):

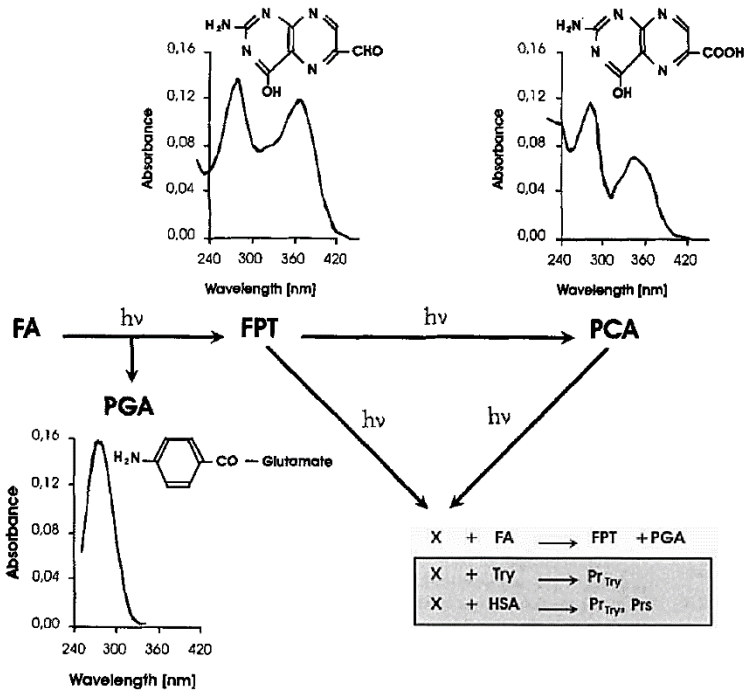

Figure 4: *A proposed scheme for folic acid photodegradation, including absorption spectra of the folic acid photoproducts. Photolysis of FPT and PCA form product X (which may be an excited form of protein or an active oxygen species) appearing to degrade folic acid. In tryptophan or the amino acids in HSA (including tryptophanyles) there is competition between the indole ring in tryptophan or the tryptophanyles. FPT, PCA and PGA are the main photoproducts of folic acid (Vorobey, Steindal, Off, Vorobey, & Moan, 2006)*

The study concluded that the photostabilisation was a result of the tryptophan in HSA. They supported their statement by stating that the enhanced photostability in HSA occurred because the tryptophan residue in the HSA (tryptophanyl) was more stable than the tryptophan in solution (Vorobey, Steindal, Off, Vorobey, & Moan, 2006). This highlighted the fact that proteins containing tryptophan residues may affect the photodegradation rate of compounds, and thus it would be necessary to conduct more research in this field.

1.4.5 New approaches for the assessment of photostabilisers on photounstable compounds

The recently proposed Φ-order kinetics method has previously been utilised to determine the photokinetics of pharmaceutical compounds in the presence of photoprotectants or

absorption competitors. Decreases in the rate-constant were observed using this model, and this effect was enhanced when the concentration of photoprotectant was increased (M. Maafi & Maafi, 2015). The model has additionally been applied to cyclodextrins to determine differences in rate-constants between their monomeric and polymeric forms (Yan Lee, 2016), providing increased photostability in each cyclodextrin and information on the rate of the photoreactions occurring (Yan Lee, 2016).

1.5.0 Conclusion

Poor detection of drug species in biofluids and surface waters can result in hazardous effects. Such issues can occur from imprecise quantification of the pharmaceuticals, or from techniques insensitive enough to be able to identify the low concentrations of the pharmaceuticals.

In addition, interactions with proteins in the biofluid, or the photodegradation of the drug, can make analysis more challenging.

Improved detection in such media is therefore required to ensure more accurate and precise analysis of drugs in these samples and to minimise unnecessary health costs and improve drug-containing surface water assessment.

Cyclodextrins have attracted attention for their ability to form strong complexations with pharmaceuticals and improve their solubility.

In addition they are able to protect the compound from such processes as photodegradation. Although photostability testing of drugs is now required there are no specified methods for treating such data, and thus, factors that can influence the photodegradation rate are not accounted for in analysis.

Polymeric derivatives of cyclodextrins have piqued interest in the pharmaceutical field as they have the ability to form stronger complexes, although there are fewer studies dedicated to these derivatives than other cyclodextrins.

Furthermore, pharmaceuticals in biofluids can prove difficult to detect as they can interact with other pharmaceuticals and possess proteins which can contain fluorescent amino acids.

There are various aspects able to influence the detection of pharmaceuticals. Therefore, each factor will be addressed in this study.

1.6.0 References

Abdollahpour, N., Asoodeh, A., Saberi, M. R., & Chamani, J. (2011). Separate and simultaneous binding effects of aspirin and amlodipine to human serum albumin based on fluorescence spectroscopic and molecular modeling characterizations: A mechanistic insight for determining usage drugs doses. *Journal of Luminescence*, *131*(9), 1885–1899.

Abdolmohammad-Zadeh, H., & Talleb, Z. (2015). Magnetic solid phase extraction of gemfibrozil from human serum and pharmaceutical wastewater samples utilizing a β-cyclodextrin grafted graphene oxide-magnetite nano-hybrid. *Talanta*, *134*, 387–393.

Aki, H., Niiya, T., Iwase, Y., & Yamamoto, M. (2001). Multimodal inclusion complexes between barbiturates and 2-hydroxypropyl-beta-cyclodextrin in aqueous solution: isothermal titration microcalorimetry, (13)C NMR spectrometry, and molecular dynamics simulation. *Journal of Pharmaceutical Sciences*, *90*(8), 1186–1197.

Alarcón, E., Edwards, A. M., Aspée, A., Borsarelli, C. D., & Lissi, E. A. (2009). Photophysics and photochemistry of rose bengal bound to human serum albumin. *Photochemical & Photobiological Sciences*, *8*(7), 933–943.

Angelova, A., Ringard-Lefebvre, C., & Baszkin, A. (1999). Drug–Cyclodextrin Association Constants Determined by Surface Tension and Surface Pressure Measurements. *Journal of Colloid and Interface Science*, *212*(2), 280–285.

Bonnier, F., Baker, M. J., & Byrne, H. J. (2016). Screening the Low Molecular Weight Fraction of Human Serum Using ATR-IR Spectroscopy. *Journal of Biophotonics*, *9*, 1085–1097.

Bortolus, P., Monti, S., Energia, A., & Area, C. N. R. (1996). *Photochemistry in Cyclodextrin Cavities* (Vol. 21).

Cairns, D. (2012). Kinetics of drug stability. In D. Cairns (Ed.), *Essentials of pharmaceutical chemistry* (pp. 239–248). London: Pharmaceutical Press.

Deng, Y., Pang, Y., Guo, Y., Ren, Y., Wang, F., Liao, X., & Yang, B. (2016). Host-guest inclusion

systems of daidzein with 2-hydroxypropyl-β-cyclodextrin (HP-β-CD) and sulfobutyl ether-β-cyclodextrin (SBE-β-CD): Preparation, binding behaviors and water solubility. *Journal of Molecular Structure*, *1118*, 307–315.

Domańska, U., Pelczarska, A., & Pobudkowska, A. (2011). Effect of 2-Hydroxypropyl-β-cyclodextrin on Solubility of Sparingly Soluble Drug Derivatives of Anthranilic Acid. *International Journal of Molecular Sciences*, *12*(4), 2383–2394.

Ferdig, M., Kaleta, A., Thanh Vo, T. D., & Buchberger, W. (2004). Improved capillary electrophoretic separation of nine (fluoro)quinolones with fluorescence detection for biological and environmental samples. *Journal of Chromatography A*, *1047*(2), 305–311.

Fernandes, C. M., Carvalho, R. A., Pereira da Costa, S., & Veiga, F. J. . (2003). Multimodal molecular encapsulation of nicardipine hydrochloride by β-cyclodextrin, hydroxypropyl-β-cyclodextrin and triacetyl-β-cyclodextrin in solution. Structural studies by 1H NMR and ROESY experiments. *European Journal of Pharmaceutical Sciences*, *18*(5), 285–296.

Ferreira, F. da R., Valentim, I. B., Ramones, E. L. C., Trevisan, M. T. S., Olea-Azar, C., Perez-Cruz, F., Goulart, M. O. F. (2013). Antioxidant activity of the mangiferin inclusion complex with β-cyclodextrin. *LWT - Food Science and Technology*, *51*(1), 129–134.

Fluorescence Spectroscopy: A tool for Protein folding/unfolding Study PC3267. (2007).

Fülöp, Z., Kurkov, S. V., Nielsen, T. T., Larsen, K. L., & Loftsson, T. (2012). Self-assembly of cyclodextrins: formation of cyclodextrin polymer based nanoparticles. *Journal of Drug Delivery Science and Technology*, *22*(3), 215–221.

Gidwani, B., & Vyas, A. (2014). Synthesis, characterization and application of Epichlorohydrin-β-cyclodextrin polymer. *Colloids and Surfaces B: Biointerfaces*, *114*, 130–137.

Guerra, E., Gosetti, F., Marengo, E., Llompart, M., & Garcia-Jares, C. (2019). Study of photostability of three synthetic dyes commonly used in mouthwashes. *Microchemical Journal*, *146*, 776–781.

Hamai, S. (1999). Inclusion complexes of poly-β-cyclodextrin with 2-anilino-6-naphthalenesulfonic acid, 1-chloronaphthalene, and azulene in aqueous solutions. *Journal of Photochemistry and Photobiology A: Chemistry*, *124*(3), 153–158.

Hergert, L. A., & Escandar, G. M. (2003). Spectrofluorimetric study of the β-cyclodextrin–ibuprofen complex and determination of ibuprofen in pharmaceutical preparations and serum. *Talanta*, *60*(2–3), 235–246.

Hirayama, F., Utsuki, T., & Uekama, K. (1991). Stoichiometry-dependent photodimerization of tranilast in a γ-cyclodextrin inclusion complex. *Journal of the Chemical Society, Chemical Communications*, *0*(13), 887–888.

Huang, L., He, J., Lu, R., Ge, X., & Guo, J. (2011). Investigation on a host–guest inclusion system by β-cyclodextrin derivative and its analytical application. *Bioorganic & Medicinal Chemistry Letters*, *21*(4), 1113–1117.

Hurtado-Sánchez, M. del C., Lozano, V. A., Rodríguez-Cáceres, M. I., Durán-Merás, I., & Escandar, G. M. (2015). Green analytical determination of emerging pollutants in environmental waters using excitation–emission photoinduced fluorescence data and

multivariate calibration. *Talanta*, *134*, 215–223.

Iglesias, E. (2011). Exploring the effect of supramolecular structures of micelles and cyclodextrins on fluorescence emission of local anesthetics. *Photochemical & Photobiological Sciences : Official Journal of the European Photochemistry Association and the European Society for Photobiology*, *10*(4), 531–542.

International Conference on Harmonisation of Technical Requirements for Registration of Pharmaceuticals for Human Use ICH Harmonised Tripartite Guideline Stability testing: Photostability Testing of New Drug Substances and Products Q1B. (1996). Retrieved from https://www.ich.org/fileadmin/Public_Web_Site/ICH_Products/Guidelines/Quality/Q1B/Step4/Q1B_Guideline.pdf

Ishiwata, S., & Kamiya, M. (1997). Cyclodextrin inclusion effects on fluorescence and fluorimetric properties of the pesticide warfarin. *Chemosphere*, *34*(4), 783–789.

Jain, B. (2017). A spectroscopic study on stability of curcumin as a function of pH in silica nanoformulations, liposome and serum protein. *Journal of Molecular Structure*, *1130*, 194–198.

Jones, J. W., Marand, H., & McGrath, J. E. (2004). *Quantification of Supramolecular Complexes Involving Charged Species in Non-Aqueous Solvents: Theory and Application* (Virginia Polytechnic Institute and State University). Retrieved from https://vtechworks.lib.vt.edu/bitstream/handle/10919/27775/JWJ_ETD.pdf?sequence=1&isAllowed=y

Junthip, J., Tabary, N., Leclercq, L., & Martel, B. (2015). Cationic β-cyclodextrin polymer applied to a dual cyclodextrin polyelectrolyte multilayer system. *Carbohydrate Polymers*, *126*, 156–167.

Kuang, H., Xing, C., Hao, C., Liu, L., Wang, L., & Xu, C. (2013). Rapid and Highly Sensitive Detection of Lead Ions in Drinking Water Based on a Strip Immunosensor. *Sensors*, *13*(4), 4214–4224.

Kumar, R., Gaurav, Heena, Malik, A. K., Kabir, A., & Furton, K. G. (2014). Efficient analysis of selected estrogens using fabric phase sorptive extraction and high performance liquid chromatography-fluorescence detection. *Journal of Chromatography A*, *1359*, 16–25.

Lakowicz, J. R. (2006). *Principles of fluorescence spectroscopy*. Springer.

Maafi, M., & Al-Qarni, M. A. (2018). Φ-order spectrophotokinetic characterisation and quantification of trans-cis oxyresveratrol reactivity, photodegradation and actinometry. *Spectrochimica Acta Part A: Molecular and Biomolecular Spectroscopy*, *188*, 64–71.

Maafi, M., & Lee, L.-Y. (2015a). Determination of Dacarbazine Φ-Order Photokinetics, Quantum Yields, and Potential for Actinometry. *Journal of Pharmaceutical Sciences*, *104*(10), 3501–3509.

Maafi, M., & Lee, L. Y. (2015b). Actinometric and Φ-order photodegradation properties of anti-cancer Sunitinib. *Journal of Pharmaceutical and Biomedical Analysis*, *110*, 34–41.

Maafi, M., & Maafi, W. (2015). Quantitative assessment of photostability and photostabilisation of Fluvoxamine and its design for actinometry. *Photochemical &*

Photobiological Sciences, *14*(5), 982–994.

Maafi, M., & Maafi, W. (2016). Modelling and elucidation of the kinetics of multiple 2 consecutive photoreactions AB 4 (4Φ) with Φ-order kinetics. Application to the photodegradation of riboflavin. *Journal of Pharmaceutical Sciences*, *105*(12), 3537–3548.

Maafi, W., & Maafi, M. (2013). Modelling nifedipine photodegradation, photostability and actinometric properties. *International Journal of Pharmaceutics*, *456*(1), 153–164.

Maestrelli, F., González-Rodríguez, M. L., Rabasco, A. M., Ghelardini, C., & Mura, P. (2010). New "drug-in cyclodextrin-in deformable liposomes" formulations to improve the therapeutic efficacy of local anaesthetics. *International Journal of Pharmaceutics*, *395*(1–2), 222–231.

Merzlikine, A., Abramov, Y. A., Kowsz, S. J., Thomas, V. H., & Mano, T. (2011). Development of machine learning models of β-cyclodextrin and sulfobutylether-β-cyclodextrin complexation free energies. *International Journal of Pharmaceutics*, *418*(2), 207–216.

Moore, D. E. (2004). Photophysical and Photochemical Aspects of Drug Stability. In 2nd ed. (Ed.), *Photostability of drugs and drug formulations* (pp. 2–6). Retrieved from https://www.crcpress.com/Photostability-of-Drugs-and-Drug-Formulations/Tonnesen/p/book/9780415303231

Morin-Crini, N., & Crini, G. (2013). Environmental applications of water-insoluble β-cyclodextrin–epichlorohydrin polymers. *Progress in Polymer Science*, *38*(2), 344–368.

Neckers, D. C., Volman, D. H., & Bünau, G. von. (1996). Advances in photochemistry. Volume 21. In D. C. Neckers, D. H. Volman, & G. von. Bünau (Eds.), *Advances in photochemistry. Volume 21*. Retrieved from https://books.google.co.uk/books?hl=en&lr=&id=ip_f68YoMTsC&oi=fnd&pg=PA1&dq=PHOTOCHEMISTRY+IN+CYCLODEXTRIN+CAVITIES+Pietro+Bortolus+and+Sandra+Monti&ots=vdq0Saq1Qg&sig=AIFQ6BFJUaV7bdLy1pv8T3RiCEE#v=onepage&q=PHOTOCHEMISTRY%2520IN%2520CYCLODEXTRIN%2520CAVITIES%252

Nikolić, V., Stanković, M., Nikolić, L., Nikolić, G., Ilić-Stojanović, S., Popsavin, M., … Kundaković, T. (2013). Inclusion complexes with cyclodextrin and usnic acid. *Journal of Inclusion Phenomena and Macrocyclic Chemistry*, *76*(1–2), 173–182.

Nilsson, G. (2010). *Stability of zopiclone in whole blood Studies from a forensic perspective* (Linköping University). Retrieved from https://www.diva-portal.org/smash/get/diva2:349342/FULLTEXT01.pdf

Owens, B. (2015). Pharmaceuticals in the environment: a growing problem. *The Pharmaceutical Journal*, *294*(7850). https://doi.org/10.1211/PJ.2015.20067898

Pinto, L. M. A., Fraceto, L. F., Santana, M. H. A., Pertinhez, T. A., Junior, S. O., & de Paula, E. (2005). Physico-chemical characterization of benzocaine-β-cyclodextrin inclusion complexes. *Journal of Pharmaceutical and Biomedical Analysis*, *39*(5), 956–963.

Roman, J., Breier, A. R., & Steppe, M. (2011). Stability Indicating LC Method to Determination of Sodium Montelukast in Pharmaceutical Dosage Form and its Photodegradation Kinetics. *Journal of Chromatographic Science*, *49*(7), 540–546.

Rozman, D., Hrkal, Z., Váňa, M., Vymazal, J., & Boukalová, Z. (2017). Occurrence of Pharmaceuticals in Wastewater and Their Interaction with Shallow Aquifers: A Case Study of Horní Beřkovice, Czech Republic. *Water*, *9*(218), 1-15.

Rub, M. A., Khan, J. M., Azum, N., & Asiri, A. M. (2017). Influence of antidepressant clomipramine hydrochloride drug on human serum albumin: Spectroscopic study. *Journal of Molecular Liquids*, *241*, 91–98.

Sciences, W. J. of P. (2014). Patent review on cyclodextrin based nanosponges prepared by different methods: physicochemical characterization, factors influencing formation and applications. *World Journal of Pharmaceutical Sciences*, *2*(4), 2321–3086.

Szejtli, J. (2005). Past, Present, and Future of Cyclodextrin Research. *Pure Appl. Chem.*, *76*(10), 1825–1845.

Tang, B., Jia, B., & Shi, X. (2005). Flow injection spectrofluorimetric study of the supramolecular interaction between β-cyclodextrin and dequalinium chloride and its analytical application. *Spectrochimica Acta Part A: Molecular and Biomolecular Spectroscopy*, *61*(9), 2203–2209.

Tang, B., Liang, H., Tong, L., & Li, P. (2006). Synthesis of ethylenediamine linked β-cyclodextrin dimer and its analytical application for tranilast determination by spectrofluorimetry. *Bioorganic & Medicinal Chemistry*, *14*(11), 3947–3952.

Tayyab, S., Zaroog, M. S., Feroz, S. R., Mohamad, S. B., & Malek, S. N. A. (2015). Exploring the interaction between the antiallergic drug, tranilast and human serum albumin: Insights from calorimetric, spectroscopic and modeling studies. *International Journal of Pharmaceutics*, *491*(1–2), 352–358.

Tejashri, G., Amrita, B., & Darshana, J. (2013). Cyclodextrin based nanosponges for pharmaceutical use: A review. *Acta Pharmaceutica*, *63*(3), 335–358.

Tian, Y., & Acevedo, N. C. (2018). Kinetic study on photostability of retinyl palmitate entrapped in policosanol oleogels. *Food Chemistry*, *255*, 252–259.

Tønnesen, H. (2004). Introduction: Photostability Testing of Drugs and Drug Formulations-Why and How? In H. H. (Hanne H. Tønnesen (Ed.), *Photostability of drugs and drug formulations* (2nd ed., pp. 1–9). Retrieved from https://books.google.co.uk/books?id=AFtAqwtrwucC&pg=PP12&lpg=PP12&dq=Chapter+1:+Introduction:+Photostability+Testing+of+Drugs+and+Drug+Formulations-+Why+and+How?&source=bl&ots=jSnQjZB6Mh&sig=ACfU3U3zzraeq4EKJDz4UoYrBB4cSuNWFA&hl=en&sa=X&ved=2ahUKEwjWn-iU5

Uekama, K., Hirayama, F., & Arima, H. (2006). Pharmaceutical Applications of Cyclodextrins and Their Derivatives. In H. Dodziuk (Ed.), *Cyclodextrins and Their Complexes* (pp. 381–422). https://doi.org/10.1002/3527608982.ch14

Ulbrich, W., & Lamprecht, A. (2011). Fluorimetric quantification of clodronate and alendronate in aqueous samples and in serum. *Talanta*, *84*(2), 437–442.

Utsuki, T., Hirayama, F., & Uekama, K. (1993). Different photodimerization behaviour of tranilast in α-, β- and γ-cyclodextrin complexes: cavity-size and stoichiometry dependence. *J. Chem. Soc., Perkin Trans. 2*, *0*(1), 109–114.

Varghese, B., Al-Busafi, S. N., Suliman, F. O., & Al-Kindy, S. M. Z. (2015). Study on the spectral and inclusion properties of a sensitive dye, 3-naphthyl-1-phenyl-5-(5-fluoro-2-nitrophenyl)-2-pyrazoline, in solvents and β-cyclodextrin. *Spectrochimica Acta Part A: Molecular and Biomolecular Spectroscopy*, *136*, 661–671.

Vayá, I., Lhiaubet-Vallet, V., Consuelo Jiménez, M., & Miranda, M. A. (2014). Photoactive Assemblies of Organic Compounds and Biomolecules: Drug/Protein Supramolecular Systems. *Chemical Society Reviews*, *43*(12), 4102–4122.

Voicescu, M., & Bandula, R. (2015). 3,6-diHydroxyflavone/bovine serum albumin interaction in cyclodextrin medium: Absorption and emission monitoring. *Spectrochimica Acta Part A: Molecular and Biomolecular Spectroscopy*, *138*, 628–636.

Von Tungeln, L. S., Zhou, T., Woodling, K. A., Doerge, D. R., Greenlees, K. J., & Beland, F. A. (2011). Benzocaine-induced methemoglobinemia in an acute-exposure rat model. *Food and Chemical Toxicology*, *49*(10), 2530–2535.

Vorobey, P., Steindal, A. E., Off, M. K., Vorobey, A., & Moan, J. (2006). Influence of Human Serum Albumin on Photodegradation of Folic Acid in Solution. *Photochemistry and Photobiology*, *82*(3), 817-822.

Wang, H., Shou, Y., Zhu, X., Xu, Y., Shi, L., Xiang, S., Han, J. (2019). Stability of vitamin B12 with the protection of whey proteins and their effects on the gut microbiome. *Food Chemistry*, *276*, 298–306.

Watson, D. G. (2012). Physical and chemical properties of drug molecules. In D. G. Watson (Ed.), *Pharmaceutical Analysis: A Textbook for Pharmacy Students and Pharmaceutical Chemists* (pp. 17–46). Retrieved from https://www.researchgate.net/profile/Tareq_Alasadi2/publication/303405281_David_G_Watson_Pharmaceutical_analysis_a_textbBookZZorg_1/links/5741c18708ae298602ee2449/David-G-Watson-Pharmaceutical-analysis-a-textbBookZZorg-1.pdf

Wenz, G., & Weickenmeier, M. (1996). Inclusion of Adamantan Derivatives. *Macromolecular Rapid Communications*, *17*, 731–736.

World Health Organization. (2010). *Screening donated blood for transfusion-transmissible infections : recommendations.* World Health Organization.

Yan Lee, L. (2016). *Study Of The Photodegradation And Photostability Of Anti-Cancer Drugs In Different Media Towards The Development Of Both New Actinometers And Liquid Formulations* (De Montfort University). Retrieved from https://www.dora.dmu.ac.uk/bitstream/handle/2086/12188/Lok Yan%27s Thesis.pdf?sequence=1&isAllowed=y

Yang, X., Zhao, Y., Chen, Y., Liao, X., Gao, C., Xiao, D., Yang, B. (2013). Host–guest inclusion system of mangiferin with β-cyclodextrin and its derivatives. *Materials Science and Engineering: C*, *33*(4), 2386–2391.

Yue, Y., Chen, X., Qin, J., & Yao, X. (2009). Characterization of the mangiferin–human serum albumin complex by spectroscopic and molecular modeling approaches. *Journal of Pharmaceutical and Biomedical Analysis*, *49*(3), 753–759.

Zhang, W., Gong, X., Cai, Y., Zhang, C., Yu, X., Fan, J., & Diao, G. (2013). Investigation of water-

soluble inclusion complex of hypericin with β-cyclodextrin polymer. *Carbohydrate Polymers*, *95*, 366–370.

Chapter 2:
Introduction

Chapter 2: Introduction

2.1.0 Aims

As has been previously reported pharmaceuticals can be excreted or disposed of into surface waters (Owens, 2015). When considering their removal, currently available techniques are limited by their poor selectivity and sensitivity (Saul, 2017), and lack precision. Furthermore, proteins, such as HSA, and environmental effects, such as light, may further hinder analysis of the pharmaceuticals.

The ingestion of pharmaceuticals, present in surface waters, by unsuitable subjects can result in toxicity (Tønnesen, 2004), or, in the case of antibiotics, a build-up can cause antibiotic resistance (Karthikeyan & Meyer, 2006). Such drug concentrations are often below the limits of detection (LODs) of even highly sensitive instruments, and techniques which overcome this limitation tend to lack the precision and accuracy required for routine screening. Current available methods are time consuming, lack the sensitivity required (Kuang et al., 2013), or are costly (Von Tungeln et al., 2011).

Fluorescence spectroscopy has the sensitivity to make it a potential technique for evaluating changes in the microenvironment of the guest compound (Hamai, 1999). Work published has also highlighted the benefits of cyclodextrins for enhancing concentrations of drug compounds present in solution (Szejtli, 2005), and the fact that cyclodextrins polymers display more advantageous properties than monomeric cyclodextrins (Tejashri, Amrita, & Darshana, 2013).

The first section of this thesis aims to reduce the concentration of drug able to be detected in canal water. It is intended for polymer cyclodextrins to be utilised to identify lower

concentrations of the compounds than have previously been determined using monomeric cyclodextrins.

To the best of our knowledge there is no published work able to accurately quantify low concentrations of the specific drugs in biofluids and surface waters, or on the photokinetics of these drugs in such matrix.

This study aims to address these issues using Ethyl-3-aminobenzoate, Ethyl-2-aminobenzoate, Benzocaine, Tranilast, Mangiferin and Axitinib as model drugs, and resolve them in the chapters.

The first section can be further split into two parts. The first part aims to reduce the concentration of drug able to be detected in canal water and serum, and the second section aims to provide photokinetic data on the photounstable drugs used in the study.

Such methods would require evaluating the interaction of the drug with both the matrix and the cyclodextrin. This will be achieved through current techniques, and a recently developed mathematical equation for the characterisation of cyclodextrin polymer complexes. The latter method overcomes the issues of unknown polymer molecular masses, and does not make assumptions on stoichiometries, allowing for the possibility of multiple stoichiometries and partial interactions to be considered.

In the second part of this section a novel method will be proposed with the goal of overcoming some of the current limits of drug detection in biofluids, using an easy to apply, rapid method.

Biofluids, such as human serum, are largely comprised of the protein, human serum albumin (Luque-Garcia & Neubert, 2007). Such protein levels can vary in individuals, potentially resulting in larger quantities of the free drug, and drug side effects (Deeb et al., 2014). In the

presence of an acidic pharmaceutical this protein can be denatured, and the polar regions on its primary structure may be exposed to the compound, altering its properties (Singh, Shandilya, Kundu, & Kayastha, 2015) and resulting in background noise (Luque-Garcia & Neubert, 2007).

The removal of this protein is therefore necessary, prior to analysis, and can be carried out using techniques such as affinity chromatography, antibody or size-exclusion filtration (Jain, Jawade, Pingle, Tumane, & Thakkar, 2015), centrifugal ultrafiltration or solid phase extraction. Such techniques are costly, time consuming, tend to require a large amount of sample preparation, are prone to errors and moreover, they can result in loss of components binding to the protein (Luque-Garcia & Neubert, 2007).

Once exposed to environmental effects, such as light, the drug may undergo photochemical changes. The current lack of photokinetic techniques able to provide specific information on the drug prevents accurate determination of the initial concentration of the drug at the time of sampling, hindering its analysis and resulting in the detection of under or overestimated concentrations.

This second half of the thesis aims to provide photokinetic data on the photounstable drugs used in the study. The intentions are to provide photostability to the drugs and to evaluate their photokinetics. It is intended for the recently developed Φ-order kinetics model to be used, as it has been shown to better describe the photostability of compounds, taking all known photodegradation factors into consideration. Such factors are the limitations of classic zero, first and second thermal reaction orders.

In this thesis the first three chapters provide information on previous attempts to overcome the complications addressed, the problems that will be covered and proposed methods to be used in the study. The final chapter will cover the work presented and the main results from the study, along with suggestions for future work in this area.

2.2.0 References

Deeb, S., Mckeown, D. A., Torrance, H. J., Wylie, F. M., Logan, B. K., & Scott, K. S. (2014). Simultaneous Analysis of 22 Antiepileptic Drugs in Postmortem Blood, Serum and Plasma Using LC-MS-MS with a Focus on Their Role in Forensic Cases. *Journal of Analytical Toxicology*, *38*(8), 485–494.

Hamai, S. (1999). Inclusion complexes of poly-β-cyclodextrin with 2-anilino-6-naphthalenesulfonic acid, 1-chloronaphthalene, and azulene in aqueous solutions. *Journal of Photochemistry and Photobiology A: Chemistry*, *124*(3), 153–158.

Jain, R. K., Jawade, A. A., Pingle, S. K., Tumane, R. G., & Thakkar, L. R. (2015). Separation of low molecular weight serum proteins using acetonitrile precipitation assessed by one dimensional gel electrophoresis. *Pelagia Research Library European Journal of Experimental Biology*, *5*(5), 18–23.

Karthikeyan, K. G., & Meyer, M. T. (2006). Occurrence of antibiotics in wastewater treatment facilities in Wisconsin, USA. *Science of The Total Environment*, *361*(1–3), 196–207.

Luque-Garcia, J. L., & Neubert, T. A. (2007). Sample preparation for serum/plasma profiling and biomarker identification by mass spectrometry. *Journal of Chromatography A*, *1153*(1–2), 259–276.

Owens, B. (2015). Pharmaceuticals in the environment: a growing problem. *The Pharmaceutical Journal*, *294*(7850). https://doi.org/10.1211/PJ.2015.20067898

Saul, L. (2017). *The Issues with Analysing Water | Technology Networks*. Retrieved from https://www.technologynetworks.com/applied-sciences/articles/solving-problems-within-analysis-of-contaminated-water-samples

Singh, K., Shandilya, M., Kundu, S., & Kayastha, A. M. (2015). Heat, Acid and Chemically Induced Unfolding Pathways, Conformational Stability and Structure-Function Relationship in Wheat α-Amylase. *PloS One*, *10*(6), 1–18.

Tejashri, G., Amrita, B., & Darshana, J. (2013). Cyclodextrin based nanosponges for pharmaceutical use: A review. *Acta Pharmaceutica*, *63*(3), 335–358.

Tønnesen, H. (2004). Introduction: Photostability Testing of Drugs and Drug Formulations-Why and How? In H. H. (Hanne H. Tønnesen (Ed.), *Photostability of drugs and drug formulations* (2nd ed., pp. 1–9). Retrieved from https://books.google.co.uk/books?id=AFtAqwtrwucC&pg=PP12&lpg=PP12&dq=Chapter+1:+Introduction:+Photostability+Testing+of+Drugs+and+Drug+Formulations-

+Why+and+How?&source=bl&ots=jSnQjZB6Mh&sig=ACfU3U3zzraeq4EKJDz4UoYrBB4cSuNWFA&hl=en&sa=X&ved=2ahUKEwjWn-iU5

Von Tungeln, L. S., Zhou, T., Woodling, K. A., Doerge, D. R., Greenlees, K. J., & Beland, F. A. (2011). Benzocaine-induced methemoglobinemia in an acute-exposure rat model. *Food and Chemical Toxicology*, *49*(10), 2530–2535.

Chapter 3:

Experimental

Chapter 3: Experimental

3.1.0 Chemicals, solvents and compounds

3.1.1 Chemicals and compounds

Ethyl-3-aminobenzoate (3AB), Ethyl-2-aminobenzoate (2AB), Benzocaine (BZ), Mangiferin (MA), Tranilast (TR), Axitinib (AXI), Human Serum Albumin (HSA), β-cyclodextrin polymer (β-CDP) and 2-hydroxyl-propyl-β-cyclodextrin (2-HP-β-CD) were purchased from Sigma-Aldrich, UK. These were used without any further modification.

3.1.2 Solvents

Ethanol (99.8%), 0.1M sodium hydroxide and 0.1M hydrochloric acid were purchased from Fisher Scientific, UK. 99% dimethyl sulfoxide (DMSO)(containing tetramethylsilane (TMS)), ≥99.9% HPLC grade acetonitrile, ≥99.9% HPLC grade methanol, ≥99.9% HPLC grade 0.1M acetic acid were purchased from Sigma-Aldrich, UK. Distilled water was also used as a solvent.

3.1.3 Chemicals

Buffer pH=7 and pH=4 tablets were purchased from Sigma-Aldrich, UK. All solvents and chemicals were of analytical grade or higher.

Table 1: *The molecular weight and structure for all compounds used in the study*

Compound	Structure	Compound	Structure
3AB	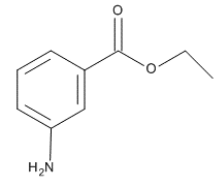 (165.19 g/mol)	**2AB**	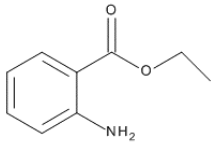 (165.19 g/mol)
BZ	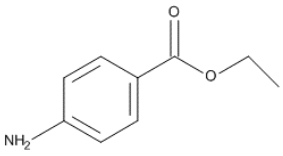 (165.19 g/mol)	**MA**	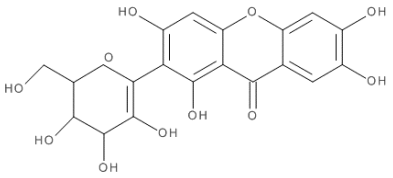 (422.34 g/mol)
TR	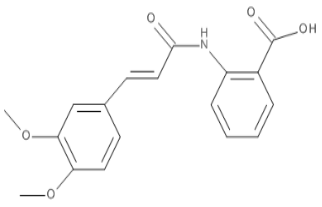 (327.33 g/mol)	**AXI**	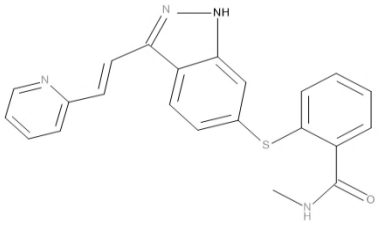 (386.47 g/mol)
HSA	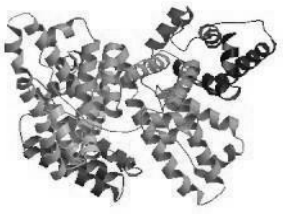 (66,478 g/mol)	**B-CDP**	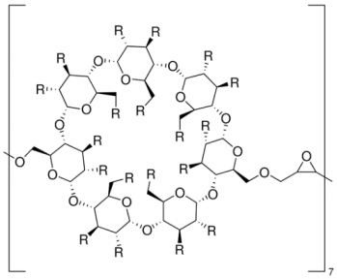 (2,000-300,000 g/mol)
2-HP-β-CD	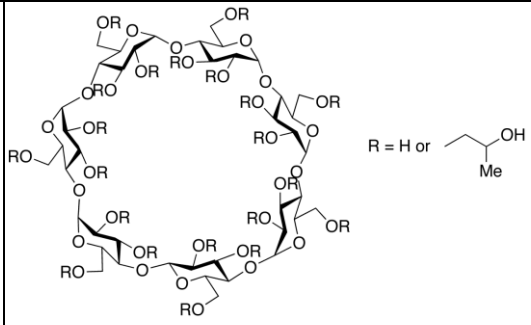 (1,460 g/mol)		

3.2.0 Instruments and apparatus

3.2.1 Fluorescence spectrometer

Fluorescence spectra were recorded using FL WinLab Version 4.00.03 software on a Perkin-Elmer Model LS 55 fluorescence spectrophotometer equipped with a 230V xenon lamp (UK). 10nm excitation and emission bandwidths were used with a monochromator scan rate of 500nm/min. Spectra were obtained in a 1cm 200-2500nm quartz macro cuvette (Hellma Analytics, UK), using the FL Win Lab Program provided by PerkinElmer (USA).

3.2.2 Syringes

Analyte was added to each sample using a 50µL microsyringe (Phenomenex, UK).

3.2.3 NMR analysis

Single pulse ^{1}H NMR spectra were acquired on an AV 500 Bruker Avance Spectrometer (George Porter building, University of Leicester, Leicester, UK) with an operating frequency of 499.94 MHz at 298 K. ^{1}H and ^{13}C NMR spectra were acquired with 6.5 µs pulses, 32,768 data points and a spectral width of 4,800 Hz, with 128 scans and 1024 scans, respectively. All data were processed in Topspin 2.1 (Bruker, UK).

3.2.4 Diode Array Spectrometer

For monochromatic irradiation studies, absorption spectra were recorded with an Agilent 8453 Diode Array Spectrophotometer, UK, using Agilent ChemStation kinetics software, UK from Agilent Technologies. Measurements were conducted in a thermostatically controlled Peltier 1cm cuvette holder.

3.2.5 Monochromatic irradiation set-up

For monochromatic irradiation an Ushio 1000 W xenon arc-lamp housed within a shell (model A6000) was used, and powered by a power supply (model LPS-1200), all from Photon Technology International Corporation. This lamp was connected to a monochromator (model 101), and a f/2.5 monochromator with a 1200 groove/300 nm blaze grating to enable selection of the irradiation wavelength.

3.2.6 Radiant Power Meter

A Radiant Power/ Energy Meter (Oriel Model 70260) was used to measure the radiant power.

Light intensity was given as milliwatts per centimetre squared (mW/cm^2).

3.2.7 HPLC analysis

Separation was achieved on a Waters (UK) Symmetry C_{18} 5µm (3.9x 150mm) column fitted to a PerkinElmer Series 200 LC pump (UK). The pump was equipped with a UV/Vis detector and vacuum degasser. Data was acquired using TotalChrom software (PerkinElmer, USA).

3.2.8 LC/MS analysis

The sample was irradiated using a UVP C-10 Mini Cabinet For Compact and Handheld Lamp P/N (6 Watt, 0.12 Amps, 254/265nm). An Agilent Technologies, UK, 6120 Quadrupole LC/MS was used for detection and Agilent OpenLAB CDS ChemStation Edition LCMS software used for data acquisition and analysis. Data was acquired using the same Waters Symmetry C_{18} 5µm (3.9x 150mm) column above (3.2.7). Operation was carried out at a flow-rate of 1mL/min, with a run-time of 7 mins.

3.3.0 Methods

3.3.1 Preparation of stock solutions

Stock solutions of each compound, 3AB, 2AB, BZ, MA, TR, AXI, β-CDP and HSA, were accurately prepared in the appropriate solvent. Solvents used were pH=7 for 3AB, 2AB, BZ, MA, β-CDP and HSA, ethanol for TR, and water: ethanol (98/2) for AXI. Prepared solutions were wrapped in foil and kept refrigerated at 3°C-5°C when not in use, thus reducing exposure to heat or light.

All samples for NMR analysis were prepared in 99% dimethyl sulfoxide (DMSO), containing tetramethylsilane (TMS) as an internal reference.

Ethanolic solutions were used for monochromatic and polychromatic studies. Dilutions for photostability studies (Chapter 8) were prepared in buffer pH=7. Studies for actinometry, HPLC and photokinetics (Chapter 7) were prepared in ethanol.

3.3.2 Preparation of diluted solutions

The concentration of the solutions was calculated using:

$$Concentration\ (M) = \frac{\frac{Mass\ (g)}{Molecular\ weight\ (\frac{g}{mol})}}{Volume\ (L)} \qquad \textbf{Eq. 1}$$

Working solutions were prepared using a Gilson® pipette and diluting a specific volume of the stock solution in the buffers outlined.

3.3.3 Real samples

Canal water was collected on 23rd May 2016 from the River Soar, Leicester, United Kingdom. This was purified by being filtered twice. The first filtration was carried out using Whatman

70mm filter paper, Grade 5, and the subsequent filtration used a 0.45µm Nylon Millipore syringe. The water was then diluted 1 in 50 times in buffer pH=7.

3.3.4.0 Fluorescence analysis

3.3.4.1 Calibration graphs

Blank solutions for fluorescence spectroscopy consisted of buffer pH=7 for 3AB, 2AB, BZ and MA, pH=4 for TR, and water: ethanol (98/2) for AXI. Various concentrations of sample were added to the relevant blank solution, and the sample thoroughly stirred. The excitation and emission spectra were recorded and the relative fluorescence intensity (RFI) at the appropriate maximum wavelength (F_{obs}) measured and plotted against increasing concentrations of the solution. The same procedure was used for all calibration graphs.

For analysis with macromolecules the cuvette was washed, replaced with 2mL of a specific concentration of β-CDP or HSA, and the fluorescence spectra obtained. The analyte was then added, and the sample analysed again.

3.3.4.2 Isotherm construction

The relative fluorescence intensities obtained for each analyte concentration were plotted against the concentrations of β-CDP, until a plateau in the relative fluorescence intensity was obtained. This was repeated with various concentrations of the compound to construct several isotherms, each of which was analysed in triplicate.

3.3.5 Proton NMR analysis

Samples were thoroughly mixed before being transferred to standard 5mm NMR tubes (Norell, UK). The proton and carbon spectra were acquired and assigned based on their

chemical shift and coupling patterns. Various concentrations of isomeric compound were observed in the presence of increasing β-CDP, and changes in the spectra characterised. This was then repeated using a constant concentration of β-CDP and increasing the concentration of the compound. Job's method of continuous variation was carried out by mixing equal molar concentrations of BZ and 2-HP-β-CD, in increasing ratios of 0.1-1, and plotting the change in chemical shift between each molar ratio.

3.3.6.0 Validation of the method

Analysis was carried out using the same procedure as described above (3.3.4).

3.3.6.1 Accuracy of the method

For recovery of the compounds in water and canal water known analyte concentrations from the upper, lower and middle ends of the linearity range of each compound were added to the samples. Percentage differences between the concentrations added and those calculated from the equation of the calibration graphs were determined. The same procedure was used for all recovery studies.

3.3.6.2 Robustness of the method

The excitation and emission wavelengths of each sample were analysed at ±2-5nm and recovery studies conducted. In addition, recovery studies were also carried out using a different fluorescence instrument, of the same model.

3.3.6.3 Effect of the pH

Solutions of buffer pH=7 were altered using various amounts of 0.1M hydrochloric acid or 0.1M sodium hydroxide to obtain solutions of pH≈1-11, measured using a Jenway 350 pH

meter (UK). The relative fluorescence intensity of the drug was plotted against the pH of the solution.

3.3.6.4 Limit of detection and quantification

The limits of detection (LOD) and quantification (LOQ) were defined as the lowest concentration of analyte able to be differentiated from the blank sample, with a limit of confidence; and the lowest concentration of the analyte able to be measured, with a limit of confidence, respectively. These were estimated as three or ten times the standard deviation of the blank experiment, accordingly.

Limits of detection and quantification were calculated through use of the following equations (Eq.2-3) (Shrivastava & Gupta, 2011):

$$LOD = \frac{s.d.\ RFI\ or\ s.d.\frac{F_{HSA}}{F_{obs}}}{slope\ of\ calibration\ graph} * 3.3 \qquad \textbf{Eq. 2}$$

$$LOQ = \frac{s.d.\ RFI\ or\ s.d.\frac{F_{HSA}}{F_{obs}}}{slope\ of\ calibration\ graph} * 10 \qquad \textbf{Eq. 3}$$

In which:

s.d.= Standard deviation of the samples

RFI= Relative fluorescence intensity

3.3.7.0 Photolysis procedures

The instrument setup was described in 3.2.4-3.2.5.

3.3.7.1 Continuous irradiation

The monochromator was set to a specific wavelength for irradiation (λ_{irr}) and the excitation beam guided through an optical fibre to the top of the sample cuvette so that the direction of the irradiation and analysis light were perpendicular.

2 mL of solvent was placed in the 1 cm quartz cuvette and a blank (zero concentration of the analyte) recorded on the spectrophotometer. Buffered double distilled water pH=7 was used for all studies. For studies in HSA or β-CDP the blank contained either the protein or polymer, respectively, to enable observation of only the spectra corresponding to the drug.

The optical fibre was placed perpendicularly onto the radiometer probe to measure the intensity of light. Readings taken before and after each photolysis confirmed the intensity remained the same throughout analysis.

Specific concentrations of the compound were added to the blank sample.

UV-Visible spectra were recorded at set intervals throughout photolysis, using the Agilent 8453 ChemStation kinetics computer program, UK. This was continued until the end of the photoreaction, indicated by little or no change in absorbance.

For all analyses the sample was continuously stirred with a magnetic flea, to ensure homogenisation of the solution and maximum exposure to light. A temperature of 22°C was maintained, and the sample was shielded from ambient light.

3.3.7.2 Polychromatic photolysis procedure

The same method as in 3.3.7.1 was used, however, at set intervals the sample was removed from the light source, and its absorption spectra measured.

For the calibration graph in UV-Vis the blank experiment consisted of 2mL of the solvent. Increasing concentrations of the drug were added to the cuvette and the absorbance spectrum measured and recorded. The absorbance against increasing concentrations of drug was plotted and the line of best fit outlining the linearity range was determined ($y = 31877x - 0.0099$).

3.3.7.3 Chromatographic analysis

Separation of the sample and its photoproducts was achieved using a mobile phase consisting of acetonitrile/ methanol/ 0.1M acetic acid (126/280/38). 20µL injections were made and the UV detector set to 330nm.

3.3.7.4 Kinetic data treatment

Based on the proposed photodegradation mechanism, differential equations were used to describe the concentration behaviour of the species in the reaction.

The values were converted into absorbance and fitted with the experimental data in Microsoft Excel. The data was inputted for the unknown reaction until there was a fit between the theoretical traces and experimental traces.

3.3.8 LC-MS analysis

LC-MS was carried out using the same mobile phase given above (3.3.7.3). 2 scan modes were used in the positive ion monitoring mode, mass range 150-750m/z. Positive single-ion monitoring (SIM) was also monitored at 328.3m/z, representing molecular ion [$M+H^+$] and sodium ion at 350 [$M+Na^+$]. Parameters used were: Drying gas flow 3.0L/min, nebulizer pressure 20psig, drying gas temperature 300°C and capillary voltage 3,000V at room

temperature. An initial chromatogram of the sample was obtained. The sample was then irradiated using the UV-light source and a second chromatogram recorded.

3.4.0 References

Shrivastava, A., & Gupta, V. (2011). Methods for the determination of limit of detection and limit of quantitation of the analytical methods. *Chronicles of Young Scientists*, *2*(1), 21–25.

Chapter 4:

The fluorescence properties of molecules in various media

Chapter 4: The fluorescence properties of molecules in various media

4.1.0 Introduction

4.1.1 Introduction

Precise and accurate detection of trace pharmaceuticals in biofluids and surface waters is limited as many techniques lack sensitivity and specificity (Saul, 2017). There is therefore the necessity for techniques that possess these properties and are rapid and low cost (Hurtado-Sánchez, Lozano, Rodríguez-Cáceres, Durán-Merás, & Escandar, 2015).

Such a technique is required as many drugs are successful through interacting with biological membranes. As a consequence, there is less of the free drug remaining in biofluids, because it can bind to proteins, making detection more challenging (Rub, Khan, Azum, & Asiri, 2017). Fluorimetry has the sensitivity to allow for these low concentrations to be detected, however, drug compounds can additionally bind to these proteins, altering the fluorescent properties of both themselves and HSA. To allow for reliable detection of the compounds in HSA the extent of the alteration in the compound needs to be controlled and considered (Lakowicz, 2006).

Furthermore, in both biofluids and surface waters, concentrations of drug compound below instrument detection limits may be present. Other approaches are therefore required.

Cyclodextrins have proved to have a number of beneficial effects, such as altering the environment of non-polar, poorly soluble compounds. This property has resulted in an improvement in drug solubility (Deng et al., 2016) and the compound is protected from bulk solution quenchers (Huang, He, Lu, Ge, & Guo, 2011), enhancing the fluorescence intensity (Lakowicz, 2006).

A groups of select compounds were chosen for their properties and their fluorimetric characteristics determined in water, and various environments, in the presence or absence of one of these macromolecules (HSA, β-CDP). This would be expected to provide fluorimetric information on their properties.

4.1.2 Fluorescence spectroscopy

Fluorescence spectroscopy is a quantitative and qualitative technique (Mura, 2014) that is able to provide information about the structure of trace concentrations of rigid, conjugated compounds, and their interaction with solvents and other compounds (Sheehan, 2009). As thus, it is able to provide information on the microenvironment of the compound, and the binding occurring.

Variations in polarity of the medium and the amount of vibrational energy each compound possesses can alter their fluorescence properties, making fluorimetry particularly useful for differentiating between compounds. The high sensitivity of the instrumentation enables it to be used to detect small changes in the environment of a species. Fluorimetry can therefore be used to differentiate between compounds, variations in the medium and interactions with other species (Lakowicz, 2006). The technique utilises high-energy UV-light to excite fluorophores from their ground state to excited singlet state. Through absorbing a specific number of high-energy photons, within a particular excitation wavelength range, the fluorescent compound can be promoted to its excited state. The maximum number of photons, 'extinction coefficient', a compound can embody falls into this wavelength range, and this specific wavelength can differ depending on environmental effects. The compound can then be promoted from its spin-paired ground state to its distinctive singlet excited state, where it is able to remain for an amount of time, 'excited state lifetime', before relaxing back

to its ground state and emitting photons at a longer wavelength. Over its excited state lifetime it loses energy through various internal conversion processes, including the transfer of heat to the solvent, intersystem crossing to the triplet state to produce phosphorescence, and interactions with other molecules. Such processes bring the compound to a lower excited state before emission. Similar to the excitation spectrum, the most intense fluorescence in this spectra range, 'emission maximum wavelength', is also affected by the environment (Lakowicz, 2006).

4.1.3 Factors influencing fluorescence properties

The fluorescence spectra produced by a compound can be affected by a number of factors. This includes: the structure of the compound; the solvent; and any interactions with other molecules (Sheehan, 2009)(Table 1).

Table 1: *Factors that can affect fluorescence spectra*

Fluorescence Factor			
Solvent polarity altered	Structure of compound	Different volume of sample solution	Change in sample concentration
↓	↓	↓	↓
SHOWN IN FLUORESCENCE SPECTRA			
↑	↑	↑	↑
Alteration in vibrations and rotations of compound	Number of functional groups on compound	Number of single and double bonds on compound	Interactions with other compounds

If the polarity of the solvent is varied then the fluorescence intensity and maximum emission wavelengths may be influenced. In the presence of more polar solvents, the amount of energy the compound possesses, following internal conversion, is reduced, increasing the amount of

energy lost via vibrations to the solvent and therefore shifting the emission spectra to higher wavelengths. The greater the polarity the greater the shift. This effect can also occur when the compound is able to form hydrogen bonds with the solvent (Lakowicz, 2006).

The proportion of photons emitted to those initially absorbed is the 'quantum yield'. The quantum yield of a specific compound, and thus the fluorescence intensity, can additionally be affected by factors in the Beer-Lambert law: the concentration of the sample; the absorption coefficient (and thus the wavelength of the compound); and the pathlength of the cell (Lakowicz, 2006).

In order to be fluorescent, the compound should possess a rigid structure, however the more non-bonding pairs of electrons it has, the more freely they can move, increasing its excited state lifetime, and red shifting the spectra, and may increase the fluorescence intensity. If these non-bonding pairs of electrons are electron donating, such as amine or alcohol groups, the fluorescence intensity can be enhanced (Brandt, 1999). If the structure of the compound contains more single σ-bonds than double π-bonds, then more energy is required to break them, demanding more excitation energy and red shifting their emission spectrum (Sauer, Hofkens, & Enderlein, 2011).

Some compounds are able to interact with other molecules. When such interactions occur the planarity of the compound can be altered, as can the extinction coefficient, influencing the energy required for excitation (Sauer et al., 2011). Interaction of a compound with a protein may quench the protein as it undergoes changes in its structure. This may involve energy transfer from the protein, which acts as a hydrogen donor, to the compound, and thus less photon energy is emitted. In addition, the wavelength of the compound can be red shifted if the compound binds to the polar region of the protein (Lakowicz, 2006).

Alternatively, if presented with a macromolecule, such as cyclodextrin, the compound may be 'shielded', protecting it from the solvent, and quenching from oxygen. This reduces non-radiative processes in internal conversion, and the compound can accept protons from the -OH (hydroxyl) groups within the cyclodextrin cavity, increasing the quantum yield and thus the fluorescence intensity (Lakowicz, 2006). Encapsulation within the cyclodextrin, restricts movement of the compound, thereby reducing its vibrations and rotations and thus increasing its fluorescence intensity (Mitra et al., 2014).

4.2.0 Selection of the molecules for analysis by fluorescence spectroscopy in water

Aromatic compounds selected as models for fluorimetric analysis were chosen for a variety of reasons. Each was a poorly water-soluble compound, and thus they represented assorted medicines. Although BZ and its isomer 3AB are popular for their local anaesthetic properties (da Silva, Grobério, Zacca, Maldaner, & Braga, 2018), the former licenced for use to manage acute or chronic pain for a short period of time (Shipton, 2012), 2AB tends to be used as a wine flavouring (Moio, 1995). The medicinal properties of the other compounds varied. MA is used in Indian medicine for the treatment of immune-deficiency diseases, such as arthritis (de Souza et al., 2009), TR has been used to treat asthma, keloids, hypertrophic scarring and allergic conjunctivitis in South Korea and Japan (U.S. Food & Drug Administration, 2018), and AXI has been identified as an anti-cancer drug (Yan Lee, 2016), able to increase levels of various enzymes and proteins in the body (Shi et al., 2011). The latter two compounds, AXI and TR, were able to reduce tumour growth and insulin levels in the body by inhibiting vascular endothelial growth factor receptors (Gross-Goupil, Françlois, Quivy, & Ravaud, 2013), and inhibiting the secretion of insulin, respectively. The latter through binding to calcium permeable channels (Darakhshan & Pour, 2015).

Various groups on the compounds would not only be responsible for their pharmaceutical effect, but would be able to influence their interactions with various media and host molecules (Table 2). Each of the compounds possessed non-bonding pairs of electrons, thus enabling them to form hydrogen bonds to interact with both electron withdrawing groups, such as halogens, and electron donating groups, such as: electron donating groups on solvents; amines on proteins; alcohols within cyclodextrins; and hydroxyls on the exterior of cyclodextrins. Research shows that amides, with a low electronegativity, are the group most electrostatically attracted to hydrogen atoms to form hydrogen bonds. The position of the amide functional group on BZ and its isomers 2AB and 3AB can alter the fluorescence spectra. The highly acidic carboxylic acid group on TR could act as a proton donor, whilst dipole-dipole interactions could form between other functional groups, such as ketone groups on MA and BZ, and ions or negatively charged parts of other compounds.

Table 2: *The structures of compounds used in the study*

3AB, 2AB, BZ 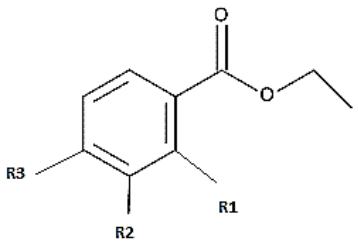 **R= NH_2** **R1**= 2AB **R2**= 3AB **R3**= BZ	**TR** 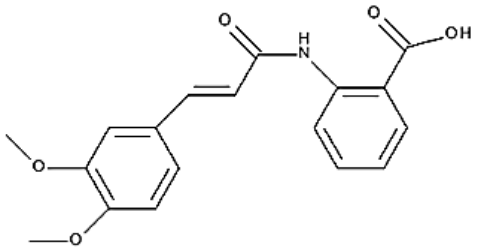
MA 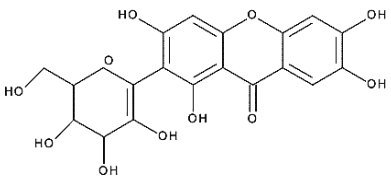	**AXI** 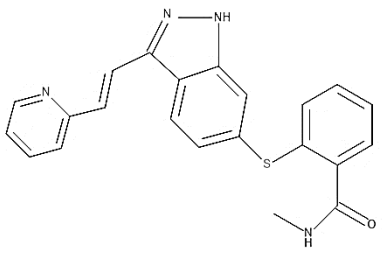

The size of such groups can affect the overall size and shape of the compound, influencing their binding with other molecules. Such effects can occur from functional groups in the solvent medium and interactions with macromolecules and proteins. Each different interaction would therefore have a unique effect on the fluorescence spectra.

With the exception of AXI, the compounds were all derived from natural sources, enabling their administration in the form of herbal teas or foods (Medina Ramírez et al., 2016). It was possible to obtain TR and MA, from nandina plants (Ogawa et al., 2010), and mangos (Medina Ramírez et al., 2016), respectively, and BZ from the esterification of mushroom and whole grain-derived (Medline Plus, 2019) para-aminobenzoic acid (Aronson, 2016), enabling their acquisition and worldwide use.

It would be interesting to observe BZ and its isomers for several reasons. BZ is used as a bulking agent in street cocaine (da Silva et al., 2018), users of this illicit drug may therefore have traces of BZ in their biofluids. Ingestion of such drugs, through consumption of contaminated tap water can have toxic effects, which are not necessarily specific to this category of drug (Karthikeyan & Meyer, 2006). Each of the compounds had previously been observed by fluorimetry, implying they possessed the necessary properties to be able to absorb light and emit fluorescence (Huang et al., 2011; Iglesias, 2011; Tang, Liang, Tong, & Li, 2006; Tayyab et al., 2016). Their analysis through this technique could therefore be monitored.

To allow for comparisons of the compounds in different environments, three environments were elected: canal water was selected as a surface water, likely to have a different environment to water; HSA was selected as a protein in a biofluid, which could form

interactions with various compounds; and β-CDP was chosen as a supramolecular molecule able to encapsulate compounds within its structure (Iglesias, 2011).

4.3.0 Results

4.3.1 Fluorimetric properties of the compounds in water

Initially, the fluorimetric properties of the compounds, including their various wavelength positions and shapes, were observed in water to see how they responded to this neutral medium, and to compare the spectra between the various compounds, and how this was reflected in their fluorescence properties (Fig. 1). Such a medium was deemed typical of both surface water and biofluid conditions (Huang et al., 2011; Iglesias, 2011; Tayyab et al., 2016; Yan Lee, 2016).

Previous fluorimetric observation of these compounds had been acquired in water. Despite the large number of σ-bonds the chemical structure of MA was comprised of, and the indistinguishable chemical formulas of BZ and its isomers, each compound was able to produce a distinct, detectable fluorescence spectrum (Fig. 1, Annexe Fig. 4-5).

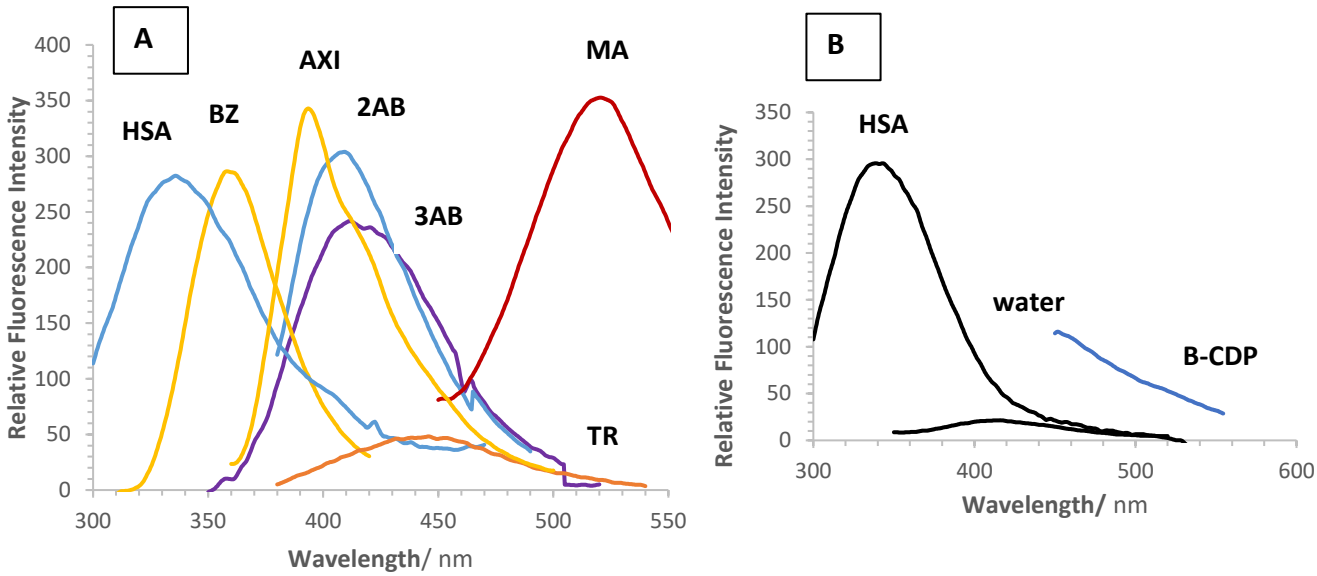

Figure 1: *Emission spectra of (A)(left to right) 9.73 x 10^{-7}M HSA, 4.93 x 10^{-6}M BZ, 1.16 x 10^{-6}M AXI, 6.10 x 10^{-8}M 2AB, 2.44 x 10^{-7}M 3AB, 4.89 x 10^{-6}M TR and 8.54 x 10^{-7}M MA in water, (B) Emission spectra of hosts and media (left to right) 9.21 x 10^{-8}M HSA, buffer pH=7, 12.17mg/mL β-CDP (the host was subtracted from the spectra in the presence of the compound)*

The different species fluoresced at different wavelengths, and, as previously suggested (4.2.0), their spectra varied in intensity and shape.

It can be observed (Fig. 1, Annexe Fig. 4-5) that the emission spectra of BZ and MA differ by almost 200nm. The much longer wavelength of emission observed for MA would be indicative of its electron donating groups and high ratio of single bonds, requiring more energy for excitation (Sauer et al., 2011), and thus absorbing light at a longer wavelength.

In order to obtain emission spectra of a similar intensity, various concentrations of each compound were used. It can be observed that 2AB has an intensity ≈6 times greater than TR, but using a concentration ≈80 times lower. TR may exhibit a smaller intensity, as it possesses a greater number of electron accepting groups than 2AB. These excess vibrations are lost through internal conversion processes and so less energy is emitted as photons (Sauer et al., 2011).

In comparison to TR the shape of the spectrum of AXI appears narrower. A possible explanation for this could be that TR was able to undergo more molecular vibrations than AXI, resulting in poorly-resolved, broad vibrational transitions, and thus broad emission spectrum (Sheehan, 2009).

Of additional interest is the emission spectra of BZ and its isomers. Not only does the similar shape in spectrum of 2AB and BZ, and much broader one of 3AB, suggest more vibrational collisions occurred in the latter compound, but the intensity and wavelengths differed.

The increase in emission wavelengths of the isomers, in the order 3AB>2AB>BZ, differed slightly to those previously observed in another study, which were attributed to the different electron densities. In addition, these compounds have been found to be sensitive to solvent effects. These effects could therefore not only contribute towards the different emission wavelengths observed for each compound, when compared to the previous study (Iglesias, 2011), but also the spectral shifts.

Whilst 2AB and 3AB have similar wavelengths, that of BZ is much shorter. A much shorter wavelength would indicate less energy was required for non-radiative internal conversion processes with this compound than the other two compounds. A similar effect has previously been observed for isomers and assigned to the longer lifetimes in the meta and ortho position. This would account for the greater red shift of 3AB and 2AB, when compared to that of BZ (Promkatkaew et al., 2014). The emission spectra of proteins tend to be characterised by their amino acid spectra. In HSA this is tryptophan, which can be excited at 280nm, emitting fluorescence from ≈320nm-355nm. The specific emission wavelength is dependent on the polarity of the environment. In the relatively polar medium of water, the indole on the protein can be denaturised, reducing energy and red shifting as a result of energy lost through the

unfolding of the protein (Lakowicz, 2006). This would explain the presence of an emission peak at 343nm (Fig. 1, Annexe Fig. 3).

4.3.2 Effect of AXI degradation on its fluorimetric properties

AXI had previously been deemed to be photounstable (Yan Lee, 2016), therefore prior to analysing its behaviour in various media, its behaviour in experimental light conditions was observed. Studying the fluorescence intensity of an AXI sample over a period of 3 hours showed a decrease of ≈4 times before a plateau was observed. In the presence of β-CDP an increase of ≈30% was observed in the spectrum before a plateau was reached, suggesting it was being stabilised against photodegradation (Glass et al., 2001). This effect was found to be reproducible in both water and canal water medium.

Comparison of the fluorescence spectrum of the compound, and the compound-β-CDP solution, prior to light exposure, showed little or no differences in fluorescence intensity increase (Fig. 2, Annexe Fig. 6).

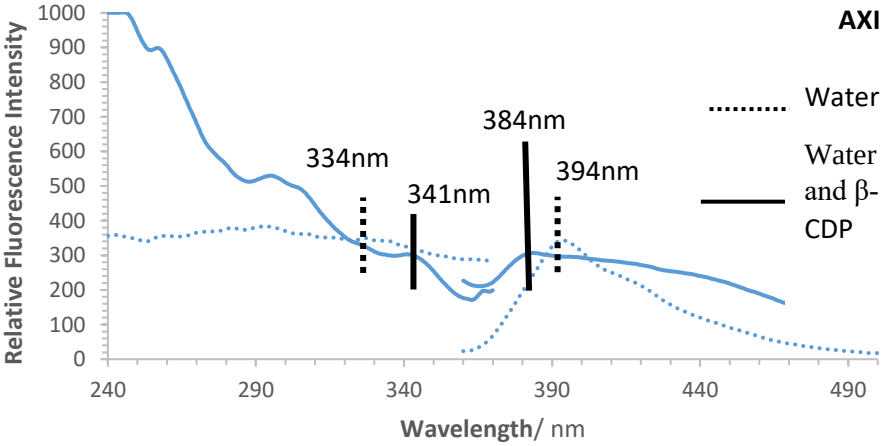

Figure 2: *Excitation and emission spectra of 3.01ppb AXI in water and ethanol (98/2)(dashed lines), and 3.01ppb AXI in 15.08mg/mL β-CDP, respectively (plain lines), at room temperature, the maximum spectra of which are labelled*

Following irradiation, ≈7 times greater intensity was observed at the plateau region of the compound isotherms, in the presence of β-CDP, when compared to that in its absence

(Annexe Fig. 7). Such an effect may be attributed to stabilisation of the compound by cyclodextrin, decreasing the production of photoproducts (Ioele, De Luca, Tavano, & Ragno, 2014).

Further fluorimetric analysis of the compound was therefore conducted after light exposure of the sample cuvette for a period of 3 hours.

4.3.3 Fluorimetric properties of 3AB, 2AB, BZ, MA, TR and AXI in the various environments

To ascertain the effect of altering the environment on the fluorescence properties of the compound, the excitation and emission spectra of the compounds were recorded in canal water, in both the presence and absence of β-CDP, and in HSA (Fig. 3, Annexe Fig. 1-3).

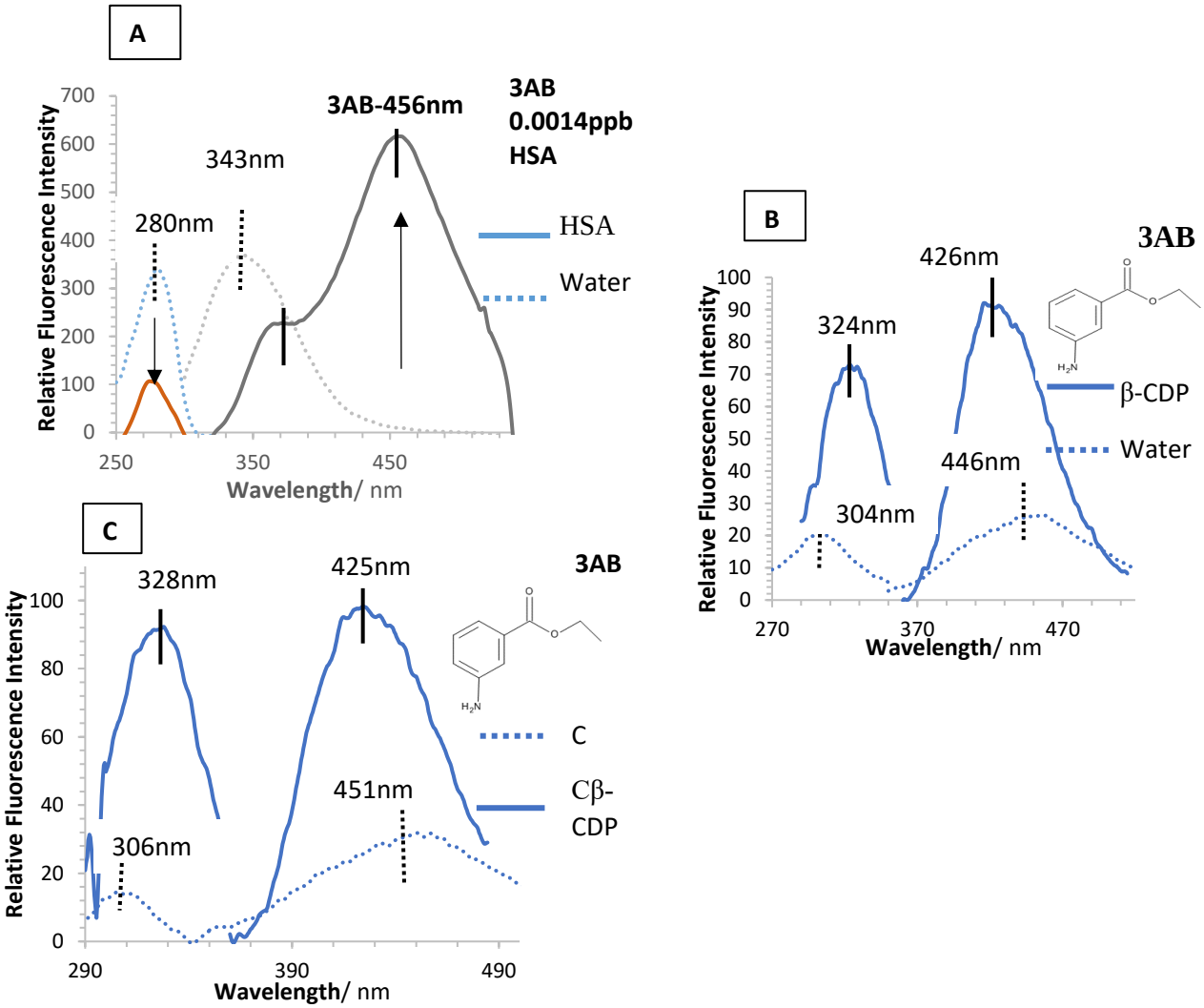

Figure 3: Excitation and emission spectra of (A) 0.0014ppb HSA in the absence (dashed lines) and presence (solid lines) of 1.94ppb 3AB, and 24.33ppb 3AB (dashed lines), respectively, (B) 0.65ppb 3AB and 25.20mg/mL β-CDP (plain lines), and 29.24ppb 3AB in canal water (C) (dashed lines) and (C) 0.65ppb 3AB in 25.13mg/mL β-CDP and canal water (Cβ-CDP)(plain lines), at room temperature, the maximum spectra of which are labelled

In canal water (Fig. 3, Annexe Fig. 2) red shifts in the emission spectra were observed, when compared to water (Fig. 3, Annexe Fig. 1), as can occur when the compound is transferred to a more polar environment (Lakowicz, 2006). Such effects have been attributed to the energy required for hydrogen bond formation between the solvent and compound, reducing the energy of the fluorophore following internal conversion, and causing it to emit photons at a longer wavelength (Sheehan, 2009).

In the presence of HSA, the emission spectra of the compound additionally red shifted. This was indicative of compound-drug binding, as would occur if the compound was binding to the polar amino acid residues on the HSA (Sheehan, 2009). When a compound binds to a protein the hydrogen bonds are destroyed and structure of the protein broken down. This can alter its secondary structure, causing the protein to unfold, reducing its α-helix content, β-sheet and turn structures (Moradi, Ashrafi-Kooshk, Chamani, Shackebaei, & Norouzi, 2018). It has been hypothesised that this involves π-π stacking forces, van der Waals forces and hydrogen bonding between polar groups on the compound, such as hydroxyl groups, and the main polypeptide chain of the amino acid (Liu et al., 2018).

It can additionally be observed that the fluorescence intensity of HSA was reduced in the presence of five of the compounds (Fig. 3, Annexe Fig. 3). This may be attributed to the unfolding of the protein, and exposure of its fluorophores to the polar quencher (Lakowicz, 2006). Furthermore, the fluorescence emission spectrum of BZ overlaps the absorption spectrum of HSA (Annexe Fig. 3). Such an effect can result in the transfer of energy from HSA to the compound, decreasing the energy of this donor and increasing the intensity of BZ. Such an interaction involves dipole-dipole interactions and the passing of excited state energy from the fluorescing HSA to BZ. This can arise when the donor and acceptor compound share a common vibration level, and transfer energy between the two until one emits (C. A. Parker, 1967). This can be supported by the greater emission intensity of BZ in the presence of HSA, when compared to that in its absence. The fluorescence spectrum of BZ obstructed the spectrum of the protein as a result and therefore the effect of BZ on HSA was observed at ≈320nm. Although the fluorescence intensity of two of the concentrations of HSA were quenched in the presence of AXI, the protein displayed a different effect in 0.0011ppm HSA.

Such an effect may indicate AXI may be bound to a hydrophobic region on the protein, forming more hydrogen bonds and stabilising the complex (Naik, Pawar, Tandel, & J, 2018).

In the presence of β-CDP blue shifts, previously observed between a compound and β-CDP (Hamai, 1999), were observed in the wavelengths of the compounds in both canal water and water. This would indicate that the compounds were being located to a less polar environment, such as that in the β-CDP cavity, and the presence of isosbestic points in all compound-β-CDP spectra would indicate the compound in its bound and complexed state (Hamai, 1999). Larger shifts observed when canal water was used over water would evidence that canal water had a more polar environment than the cavity, requiring a larger amount of energy for realignment (Connors, 1997).

A greater intensity of the compounds in both media was additionally observed. This could also be attributed to shielding from internal conversion processes (Lakowicz, 2006), which could potentially occur from vibrational restriction of the compound, which would reduce excess vibrational energy loss (Mitra et al., 2014).

Comparison of the spectral shifts of the compound in the various environments may be able to provide information on the amount of time the compound resides in its excited state for. This can be affected by various factors including interactions with other molecules and the solvent (Sheehan, 2009). Such information can be obtained from the Stoke's shift, by measuring the energy difference between the fluorescence emission and excitation wavelengths.

The smaller Stoke's shifts observed in water and canal water, in the presence of β-CDP (Table 3), could be attributed to the lower polarity groups on the compound when within the cavity of the β-CDP (Hamai, 1999). Differences in the Stoke's shift of each compound, in water and

canal water, were compared in the presence and absence of β-CDP (Table 3). The greater shifts of 3AB, 2AB and TR in canal water may implicate that this environment was more polar for the compounds, when compared to water, requiring more energy for realignment of the solvent (Lakowicz, 2006). Greater shifts observed in water in the presence of the other compounds, MA and AXI, was suggestive of more non-fluorescent pathways. This may be attributed to more similar polarities of the two compounds, to that of the buffered solution, and thus less vibrational energy lost through solvent vibrations (Sheehan, 2009). The energy difference between the compounds in the different media could be indicative of the proton donating and accepting abilities of the compound. Such evidence as the lower pKa values of 2AB and 3AB, in comparison to BZ, may indicate their greater ability to accept electrons and therefore form hydrogen bonds with the hydroxyl groups on the β-CDP (Hamai, 1999).

Table 3: *Fluorescence features of 3AB, 2AB, BZ, MA, TR and AXI in water and canal water (W, C, respectively), in water and β-CDP (β-CDP), in canal water and β-CDP (Cβ-CDP), and the emission spectra of the compounds in HSA (HSA)*

Compound	Medium	Fluorescence excitation/ nm[a]	Fluorescence emission/ nm	Stoke's shift/ nm[b]
3AB	W	(283) 304	446	142
	β-CDP	(300) 324	426	102
	C	306	451	145
	Cβ-CDP	328 (314)	425	97
	HSA	-	456	-
2AB	W	329	424	95
	β-CDP	342	409	67
	C	329	424	95
	Cβ-CDP	341	407	66
	HSA	-	413	-
BZ	W	286	360	74
	β-CDP	296	(328) 344	48
	C	284	(344) 359	75
	Cβ-CDP	(279) 295	(329) 344	49
	HSA	-	357	-
MA	W	377	528	151
	β-CDP	378	520	142
	C	379	529	150
	Cβ-CDP	(279) 378	521	143
	HSA	-	522	-
TR	W (pH=4)	323	441	118
	β-CDP	326	436	110
	C	326	437	111
	Cβ-CDP	342	434	92
	W (pH=7)	326	427	101
	HSA	-	414	-
AXI	W	334	394	60
	β-CDP	341	384	43
	C	328	394	66
	Cβ-CDP	333	394	61
	HSA	-	404	-

[a] The maximum excitation and emission spectra of the compounds, alone (See Table 3), are underlined, whilst shoulders are displayed in brackets

[b] The Stoke's shift is calculated from the difference in the energy of the maximum emission spectra and the maximum excitation spectra of the compound

The change in polarity between the environment of the canal water and that of water was further evidenced by the slightly lower intensity of the species in canal water, in the absence of β-CDP. This may indicate that the compound was more ionised in water than in canal water (Sahoo, Sahu, Rao, & Ghosh, 2014).

In the presence of β-CDP the intensity of each of the compounds was increased. This could indicate that β-CDP shielded the compounds from non-radiative processes by reducing their rotations and donating protons (Lakowicz, 2006).

Comparisons between the three isomers found that 3AB exhibited larger Stoke's shifts in each of the medium used. This may be attributed to the difference in the electron density of 3AB in comparison to its isomers (Lakowicz, 2006).

4.4.0 Conclusion

The properties of selected pharmaceuticals: 3AB, 2AB, BZ, MA, TR and AXI, which may be present in surface waters and biofluids, were observed by fluorimetry in water and their spectra compared to those in a macromolecule or in canal water. In the presence of β-CDP the fluorescence intensity was increased for all compounds, indicating their stabilisation against non-radiative processes. In the presence of the compounds the spectrum of HSA was quenched, implying an alteration in the structure of the protein. Shifts in the spectra of all compounds in the presence of one of these macromolecules, or in canal water, were indicative of their transfer to a less polar environment.

4.5.0 References

Aronson, J. K. (2016). Benzocaine. In J. K. Aronson & L. Meyler (Eds.), *Meyler's side effects of drugs : the international encyclopedia of adverse drug reactions and interactions* (16th ed., pp. 858–862). Amsterdam: Elsevier Science.

Brandt, M. (1999). *Fluorescence Spectroscopy*. Retrieved from https://www.rose-

hulman.edu/~brandt/Fluorescence/Fluorescence_Introduction.pdf

C. A. Parker. (1967). Fluorescence and Phosphorescence Analysis. *Fluorescence and Phosphorescence Analysis*, *4*(5), 139–140.

Connors, K. A. (1997). The Stability of Cyclodextrin Complexes in Solution. *Chemical Reviews*, *97*(5), 1325–1358.

da Silva, A. F., Grobério, T. S., Zacca, J. J., Maldaner, A. O., & Braga, J. W. B. (2018). Cocaine and adulterants analysis in seized drug samples by infrared spectroscopy and MCR-ALS. *Forensic Science International*, *290*, 169–177.

Darakhshan, S., & Pour, A. B. (2015). Tranilast: A review of its therapeutic applications. *Pharmacological Research*, *91*, 15–28.

de Souza, J. R. R., de Carvalho, J. I. X., Trevisan, M. T. S., de Paula, R. C. M., Ricardo, N. M. P. S., & Feitosa, J. P. A. (2009). Chitosan-coated pectin beads: Characterization and in vitro release of mangiferin. *Food Hydrocolloids*, *23*(8), 2278–2286.

Deng, Y., Pang, Y., Guo, Y., Ren, Y., Wang, F., Liao, X., & Yang, B. (2016). Host-guest inclusion systems of daidzein with 2-hydroxypropyl-β-cyclodextrin (HP-β-CD) and sulfobutyl ether-β-cyclodextrin (SBE-β-CD): Preparation, binding behaviors and water solubility. *Journal of Molecular Structure*, *1118*, 307–315.

Glass, B. D., Brown, M. E., Daya, S., Worthington, M. S., Drummond, P., Antunes, E., Maharaj, D. (2001). Influence of cyclodextrins on the photostability of selected drug molecules in solution and the solid-state. *International Journal of Photoenergy*, *3*(4), 205–211.

Gross-Goupil, M., Françlois, L., Quivy, A., & Ravaud, A. (2013). Axitinib: A Review of its Safety and Efficacy in the Treatment of Adults with Advanced Renal Cell Carcinoma. *Clinical Medicine Insights: Oncology*, *7*(2013), 269–277.

Hamai, S. (1999). Inclusion complexes of poly-β-cyclodextrin with 2-anilino-6-naphthalenesulfonic acid, 1-chloronaphthalene, and azulene in aqueous solutions. *Journal of Photochemistry and Photobiology A: Chemistry*, *124*(3), 153–158.

Huang, L., He, J., Lu, R., Ge, X., & Guo, J. (2011). Investigation on a host–guest inclusion system by β-cyclodextrin derivative and its analytical application. *Bioorganic & Medicinal Chemistry Letters*, *21*(4), 1113–1117.

Hurtado-Sánchez, M. del C., Lozano, V. A., Rodríguez-Cáceres, M. I., Durán-Merás, I., & Escandar, G. M. (2015). Green analytical determination of emerging pollutants in environmental waters using excitation–emission photoinduced fluorescence data and multivariate calibration. *Talanta*, *134*, 215–223.

Iglesias, E. (2011). Exploring the effect of supramolecular structures of micelles and cyclodextrins on fluorescence emission of local anesthetics. *Photochemical & Photobiological Sciences : Official Journal of the European Photochemistry Association and the European Society for Photobiology*, *10*(4), 531–542.

Ioele, G., De Luca, M., Tavano, L., & Ragno, G. (2014). The difficulties for a photolabile drug in topical formulations: The case of diclofenac. *International Journal of Pharmaceutics*, *465*(1–2), 284–290.

Karthikeyan, K. G., & Meyer, M. T. (2006). Occurrence of antibiotics in wastewater treatment facilities in Wisconsin, USA. *Science of The Total Environment*, *361*(1–3), 196–207.

Lakowicz, J. R. (2006). *Principles of fluorescence spectroscopy*. Springer.

Liu, Y., Cai, Y., Ying, D., Fu, Y., Xiong, Y., & Le, X. (2018). Ovalbumin as a carrier to significantly enhance the aqueous solubility and photostability of curcumin: Interaction and binding mechanism study. *International Journal of Biological Macromolecules*, *116*, 893–900.

Medina Ramírez, N., Monteiro Farias, L., Apolonio Santana, F., Viana Leite, J., De Souza Dantas, M., Lopes Toledo, R., Machado Rocha Ribeiro, S. (2016). Extraction of Mangiferin and Chemical Characterization and Sensorial Analysis of Teas from Mangifera indica L. Leaves of the Ubá Variety. *Beverages*, *2*(33), 1–13.

Medline Plus. (2019). Para-aminobenzoic acid: MedlinePlus Medical Encyclopedia. Retrieved February 22, 2019, from https://medlineplus.gov/ency/article/002518.htm

Mitra, A. K., Ghosh, S., Sarangi, M. K., Chakraborty, S., Saha, C., & Basu, S. (2014). Photophysics of a solvent sensitive keto-tetrahydrocarbazole based fluorophore and its interaction with triethylamine: A spectroscopic inquest under surfactant and β-CD confinement. *Journal of Molecular Structure*, *1074*, 617–628.

Moio, L., & Etievant, P. X. (1995). Ethyl Anthranilate, Ethyl Cinnamate, 2,3-Dihydrocinnamate, and Methyl Anthranilate: Four Important Odorants Identified in Pinot noir Wines of Burgundy. American Journal of Enology and Viticulture, 46(1995), 392-398.

Moradi, N., Ashrafi-Kooshk, M. R., Chamani, J., Shackebaei, D., & Norouzi, F. (2018). Separate and simultaneous binding of tamoxifen and estradiol to human serum albumin: Spectroscopic and molecular modeling investigations. *Journal of Molecular Liquids*, *249*, 1083–1096.

Mura, P. (2014). Analytical techniques for characterization of cyclodextrin complexes in aqueous solution: A review. *Journal of Pharmaceutical and Biomedical Analysis*, *101*, 238–250.

Naik, R. S., Pawar, S. K., Tandel, R. D., & J, S. (2018). Insights in to the mechanism of interaction of a thrombin inhibitor, dabigatran etexilate with human serum albumin and influence of β-cyclodextrin on binding: Spectroscopic and computational approach. *Journal of Molecular Liquids*, *251*, 119–127.

Ogawa, Y., Dogru, M., Uchino, M., Tatematsu, Y., Kamoi, M., Yamamoto, Y., Tsubota, K. (2010). Topical tranilast for treatment of the early stage of mild dry eye associated with chronic GVHD. *Bone Marrow Transplantation*, *45*(3), 565–569.

Promkatkaew, M., Suramitr, S., Karpkird, T., Wanichwecharungruang, S., Ehara, M., & Hannongbua, S. (2014). Photophysical properties and photochemistry of substituted cinnamates and cinnamic acids for UVB blocking: effect of hydroxy, nitro, and fluoro substitutions at ortho, meta, and para positions. *Photochemical & Photobiological Sciences*, *13*(3), 583-594.

Rub, M. A., Khan, J. M., Azum, N., & Asiri, A. M. (2017). Influence of antidepressant clomipramine hydrochloride drug on human serum albumin: Spectroscopic study. *Journal of Molecular Liquids*, *241*, 91–98.

Sahoo, N., Sahu, M., Rao, P., & Ghosh, G. (2014). Development and Validation of Liquid Chromatography- Mass Spectroscopy/Mass Spectroscopy Method for Quantitative Analysis of Naproxen in Human Plasma after Liquid-Liquid Extraction. *Tropical Journal of Pharmaceutical Research*, *13*(9), 1503-1510.

Sauer, M., Hofkens, J., & Enderlein, J. (Jörg). (2011). Basic Principles of Fluorescence Spectroscopy. In *Handbook of fluorescence spectroscopy and imaging : from single molecules to ensembles* (pp. 1–30). Retrieved from https://www.wiley.com/en-us/Handbook+of+Fluorescence+Spectroscopy+and+Imaging%3A+From+Ensemble+to+Single+Molecules-p-9783527316694

Saul, L. (2017). *The Issues with Analysing Water | Technology Networks*. Retrieved from https://www.technologynetworks.com/applied-sciences/articles/solving-problems-within-analysis-of-contaminated-water-samples

Sheehan, D. (2009). *Physical biochemistry : principles and applications* (2nd ed.). Retrieved from https://www.wiley.com/en-us/Physical+Biochemistry%3A+Principles+and+Applications%2C+2nd+Edition-p-9780470856031

Shi, H., Wang, Y., Fang, B., Talmon, Y., Ge, W., Raghavan, S. R., & Zakin, J. L. (2011). Light-Responsive Threadlike Micelles as Drag Reducing Fluids with Enhanced Heat-Transfer Capabilities. *Langmuir*, *27*(10), 5806–5813.

Shipton, E. A. (2012). New formulations of local anaesthetics-part I. *Anesthesiology Research and Practice*, *2012*, 1–11.

Tang, B., Liang, H., Tong, L., & Li, P. (2006). Synthesis of ethylenediamine linked β-cyclodextrin dimer and its analytical application for tranilast determination by spectrofluorimetry. *Bioorganic & Medicinal Chemistry*, *14*(11), 3947–3952.

Tayyab, S., Izzudin, M. M., Kabir, M. Z., Feroz, S. R., Tee, W.-V., Mohamad, S. B., & Alias, Z. (2016). Binding of an anticancer drug, axitinib to human serum albumin: Fluorescence quenching and molecular docking study. *Journal of Photochemistry and Photobiology B: Biology*, *162*, 386–394.

U.S. Food & Drug Administration. *Compounding - Section 503A of the Federal Food, Drug, and Cosmetic Act*., (2018).

Yan Lee, L. (2016). *Study Of The Photodegradation And Photostability Of Anti-Cancer Drugs In Different Media Towards The Development Of Both New Actinometers And Liquid Formulations* (De Montfort University). Retrieved from https://www.dora.dmu.ac.uk/bitstream/handle/2086/12188/Lok Yan%27s Thesis.pdf?sequence=1&isAllowed=y

Chapter 5:

Complexation of guest molecules with cyclodextrin to form a G_n: $(CD_p)_m$ complex

Chapter 5: Complexation of guest molecules with cyclodextrin to form a G_n: $(CD_p)_m$ complex

5.1.0 Introduction

5.1.1 Introduction

Knowledge of the stoichiometry and inclusion complex formed between a host and guest is necessary as it assesses the ability of the host to: solubilise guest compounds, improve drug release and efficiently encapsulate insoluble drugs (Gidwani & Vyas, 2014).

Cyclodextrins have been found to form water-soluble inclusion complexes with various compounds (Limousin et al., 2007), allowing them to be used in the pharmaceutical industry as drug delivery agents. Cyclodextrins have been the subject of a number of studies, with over 170,000 studies published by the end of 2003 (Szejtli, 2005).

Increasing attention has been paid to cyclodextrin polymers, as polymerising monomers enables them to maintain the advantages of β-cyclodextrin (β-CD), with the addition of polymer benefits, including a high molecular weight and solubility (Gidwani & Vyas, 2014). These polymeric derivatives have a high adsorption capability, enabling them to rapidly adsorb (Moulahcene et al., 2015) a greater number of poorly soluble compounds (Erdoğar & Bilensoy, 2018) with large structures (Li, Xiao, Li, & Zhong, 2004) (Li et al., 2004). Furthermore, they can increase the fluorescence intensity of guest compounds (Cavalli et al., 2009), and protect these guests against chemical degradation processes (di Cagno, Terndrup Nielsen, Lambertsen Larsen, Kuntsche, & Bauer-Brandl, 2014).

The complexation between a molecule of guest compound and unit of cyclodextrin monomer is often evaluated using Job's continuous variation plot (Upadhyay & Kumar, 2009), however,

this method utilises concentrations of drug and cyclodextrin, and involves plotting the changes in fluorimetric signal against varying molar ratios to provide an indication of the stoichiometry (Upadhyay & Kumar, 2009). As the molecular weight of β-CDP is affected by the polymerisation reaction conditions (Junthip, Tabary, Leclercq, & Martel, 2015), and number of monomers it contains (Murdan, 2013), its molecular weight can not be accurately determined. When utilising a cyclodextrin polymer, fluorimetric determination of a complexation has only been possible through methods, such as assigning a 'molecular weight' to a unit of polymer (Hamai, 1999).

The application of isothermal models (Limousin et al., 2007) to guest-β-CDP complexes does not appear to have yet been reported in the literature.

Although studies for the evidence of β-CDP complexes have been conducted using fluorimetry (Hamai, 1999), these are more often evidenced by thermal analysis techniques, such as Differential Scanning Calorimetry (Tejashri, Amrita, & Darshana, 2013). The current study aims to monitor the guest-β-CDP interaction and quantify and analyse the findings to determine the stoichiometry of the complex.

A new method has been proposed by our group and demonstrated (Yan Lee, 2016). Outlined in the next section (5.1.2) this method was applied to the six compounds: 3AB, 2AB, BZ, MA, TR and AXI, in the presence of β-CDP.

5.1.2 Mathematical model for a G_n: $(CD_p)_m$ complex

The association between one or more molecules of guest with one or more cyclodextrin polymer units, which may be comprised of 'p' cyclodextrin monomer units, form a G_n: $(CD_p)_m$ complex. Thus, when a monomer cyclodextrin is complexed, 'p'=1 (Pinto et al.,

2005). It is expected that the complex occurs rapidly (Moulahcene et al., 2015) and each of the binding sites on the cyclodextrin has a different stability complex (Fülöp, Kurkov, Nielsen, Larsen, & Loftsson, 2012).

The association reaction can be represented by:

$$nG + mCD_p \rightleftharpoons G_n{:}\,(CD_p)_m \qquad \textbf{Eq. 1}$$

The variation in the fluorescence intensity signal occurring ($Fl^{\lambda obs}_{tot,i,j}$), with concentration 'j' of β-cyclodextrin polymer ($[CDp]_{0,i,j}$), for a $G_n{:}\,(CD_p)_m$ complex can be described by Eq. 2:

$$\frac{(Fl^{\lambda obs}_{0,(G_n:(CDp)_m)} - Fl^{\lambda obs}_{tot,i,j})^n}{Fl^{\lambda obs}_{tot,i,j} - Fl^{\lambda obs}_{0,G,i}} = \frac{(Fl^{\lambda obs}_{0,(G_n:(CDp)_m)} - Fl^{\lambda obs}_{0,G,i})^{n-1}}{n \times K_{G_n:(CD_p)_m} \times [G]^{n-1}_{0,i}} \times \frac{1}{[CD_p]^m_{0,i,j}} \qquad \textbf{Eq. 2}$$

In which ($Fl^{\lambda obs}_{0,(G_n:(CD_p)_m)}$) is the fluorescence intensity when every guest molecule is completely complexed, $Fl^{\lambda obs}_{0,G,i}$ is the native fluorescence intensity of a specific 'i' concentration of the guest $[G]^{n-1}_{0,i}$, and $K_{G_n:(CD_p)_m}$ represents the drug-β-cyclodextrin polymer association constant of the complex.

Linearising Eq. 2 allows for the following formula to be derived (Eq. 3). This can enable the stoichiometry of the complex to be determined in three stages.

$$In\left[\frac{Fl^{\lambda obs}_{tot,i,j} - Fl^{\lambda obs}_{0,G,i}}{Fl^{\lambda obs}_{0,(G_n:(CDp)_m)} - Fl^{\lambda obs}_{0,G,i}} \times [G]_{0,i}\right] = n \times ln\left[\frac{Fl^{\lambda obs}_{0,(G_n:(CDp)_m)} - Fl^{\lambda obs}_{tot,i,j}}{Fl^{\lambda obs}_{0,(G_n:(CDp)_m)} - Fl^{\lambda obs}_{0,G,i}{}_0} \times [G]_{0,i}\right] + ln\left[n \times K_{G_n:(CD_p)_m} \times [CD_p]^m_{0,i,j}\right] \qquad \textbf{Eq. 3}$$

The gradient of the linear relationship, Eq. 3, is 'n'. This can be determined from Eq. 3 if the total fluorescence intensity of the medium ($Fl^{\lambda obs}_{tot,i,j}$) is recorded for 'i' experiments at a specific β-CDP concentration $[CD_p]_{0,x}$. This can be achieved by vertically drawing a line on the

isotherms and obtaining the fluorescence intensity readings where the line intersects each isotherm. The intercept $ln\left[n \times K_{G_n:(CD_p)_m} \times [CD_p]_{0,x}^{m}\right]$ for the particular $[CD_p]_{0,\mathrm{x}}$ concentration will therefore be a constant.

Once 'n' has been determined the data obtained from one of the 'i' isotherms (where $[G]_{0,\mathrm{i\ x}}$ is a constant and $[CD_p]_{0,\mathrm{i,j}}$ is a variable) can be treated using the following equation derived from Eq.2 (Eq. 4):

$$ln\left[\frac{\left(Fl_{0,(G_n:(CD_p)_m)}^{\lambda obs}-Fl_{tot,i,j}^{\lambda obs}\right)^{n}}{Fl_{tot,i,j}^{\lambda obs}-Fl_{0,G,i}^{\lambda obs}}\right]=-m\times Ln\left[CD_p\right]_{0,i,j}+Ln\left[\frac{(Fl_{0,(G_n:(CD_p)_m)}^{\lambda obs}-Fl_{0,G,i}^{\lambda obs})^{n-1}}{n\times K_{G_n:(CD_p)_m}\times [G]_{0,i}^{n-1}}\right] \quad \textbf{Eq. 4}$$

Using the gradient from Eq. 4 will allow the determination of parameter 'm'.

Once 'm' and 'n' have been determined the value of the association constant (Eq. 5) can be established from the intercept formula and the value of Eq. 4:

$$K_{G_n:(CD_p)_m}=\frac{\left(Fl_{0,(G_n:(CD_p)_m)}^{\lambda obs}-Fl_{0,G,i}^{\lambda obs}\right)^{n-1}}{n\times e^{intercept}\times [G]_{0,i}^{n-1}} \quad \textbf{Eq. 5}$$

For the majority of cyclodextrin polymers the relative molecular mass cannot be accurately determined, therefore, the cyclodextrin concentrations can be expressed in g/L, rather than molarity. An 'alternative pseudo-association' constant $K'_{G_n:(CD_p)_m}$(Eq. 6) can be used, given in $(g/L)^{1-m-n}$, or similar.

$$K'_{G_n:(CD_p)_m}=K_{G_n:(CD_p)_m}\times [RMM(G)]_{0,i}^{1-n}\times [RMM(CD_p)]_{0,i}^{-m} \quad \textbf{Eq. 6}$$

The shape of the isotherms may be able to reflect the stoichiometry of the inclusion complex. It has previously been suggested that if the isotherm is 'S-shaped' then the host molecule may

have large pores, enabling it to adsorb more than one guest molecule (Limousin et al., 2007). Simulations performed indicated this could suggest that m>1. Alternatively, if the isotherms are exponential-like in shape then it is expected that m=1, and one unit of cyclodextrin polymer is involved in the complexation of the guest (Yan Lee, 2016). The shape of the isotherm can therefore provide information on the number of β-CDP units involved in the complexation.

The model treats the data collected for a series of isotherms of 'i' concentrations of guest molecule, in the presence of increasing 'j' host concentrations. To overcome problems with a single isotherm it uses various concentrations of guest in the presence of a constant host concentration. The method is similar to Job's continuous variation, in that the variation in host concentration is also accounted for.

For a Job's continuous variation plot to be constructed, the total concentration of guest and host should remain constant, whilst the molar fraction of guest [G] to cyclodextrin [CD] is varied. Such methods, however, are not often applied in fluorimetry, as significantly lower concentrations of the guest are required for analysis (Tang, Liang, Tong, & Li, 2006), as large concentrations of compounds can result in self-adsorption and self-quenching (Sheehan, 2009).

In addition, Job's method requires knowledge of the molecular weight of the compounds. As this cannot be accurately determined for the majority of cyclodextrin polymers, the proposed method uses g/L unit for concentrations instead of molarity units.

Unlike Job's plot, the proposed model doesn't base the treatment of the isotherm data on the current complex stoichiometries in the literature (H Aki, Niiya, Iwase, & Yamamoto, 2001).

The approach therefore allows for all stoichimetries to be taken into consideration and, what's more, provides information on the association constant of the complex.

5.2.0. Results

5.2.1.1 Fluorimetric effects of altering the guest concentration in β-CDP

The excitation and emission spectra of the compounds: 3AB, 2AB, BZ, MA, TR and AXI have been recorded in both water and canal water, and in the presence of β-CDP (Chapter 4).

It was observed that when using either water or canal water as media, the fluorescence properties of the compounds were altered, and their emission spectra blue shifted in the presence of β-CDP. Furthermore, the excitation spectra of each compound was red shifted (≈1-22nm) when presented with β-CDP (Chapter 4- Fig 3., Annexe Fig. 1-2), and the Stoke's shift subsequently increased (Chapter 4-Table 3).

When compared to those recorded in the absence of β-CDP, the relative fluorescence intensities in both canal water and water were ≈70 times (BZ in water), and ≈60 times (3AB in canal water) greater in the presence of β-CDP (Table 1).

Such increases in the fluorescence intensity of low polarity drugs in the presence of β-CDP have been attributed to a reduction in non-fluorescent pathways. The effect can occur when the compound is relocated to a less polar environment, in which its molecular vibrations are reduced and rigidity increased (Sheehan, 2009).

Table 1: *Fluorescence features of 3AB, 2AB, BZ, MA, TR and AXI in the presence and absence of β-CDP*

$\frac{Fl^{\lambda obs}_{0,(G_n:(CD_p)m)}}{Fl^{\lambda obs}}$[a]						
Compound / **Medium**	**3AB**	**2AB**	**BZ**	**MA**	**TR**	**AXI**
Water	1	1	1	1	1	1
β-CDP	12.68	7.38	69.5	14.93	14.64	5.53
Canal water	1	1	1	1	1	1
Canal water and β-CDP	58.38	6.73	45.5	8.18	8.40	17.44

[a] The fluorescence intensity of the numerator corresponds to either the maximum fluorescence intensity of 3AB, 2AB, BZ, MA, TR or AXI, when in water, or canal water, or the maximum intensity observed when in excess β-CDP, whilst the denominator corresponds to the fluorescence intensity of 3AB, 2AB, BZ, MA, TR or AXI in water or canal water ($Fl^{obs}$is equal to $Fl^{\lambda obs}_{0,G,i}$)

The data (Table 1) was indicative of the formation of a guest-β-CDP inclusion complex, indicating all six compounds were capable of forming a complex with β-CDP.

This enhancement in the fluorescence intensity of the compounds agreed with previous results obtained for these species (Ferreira et al., 2013; Hirayama, Utsuki, & Uekama, 1991; Huang, He, Lu, Ge, & Guo, 2011; Iglesias, 2011; Pinto et al., 2005; Tang et al., 2006; Utsuki, Hirayama, & Uekama, 1993; Yan Lee, 2016; Yang et al., 2013) , in which greater, or similar increases were observed in the presence of cyclodextrin monomers (Ferreira et al., 2013; Hirayama et al., 1991; Huang et al., 2011; Iglesias, 2011; Pinto et al., 2005; Tang et al., 2006; Utsuki et al., 1993; Yang et al., 2013), or β-CDP (Yan Lee, 2016). The enhancement was suggested to alter between the compounds as they each possessed differing polarities, and were of various sizes, affecting how they interacted with the host (Iglesias, 2011). AXI was the only compound in which the increase in fluorescence intensity had previously been observed in the presence of β-CDP (Yan Lee, 2016). Although the increases in fluorescence intensity observed with AXI in the current study were greater than those observed in the presence of

hydroxyl-propyl-β-cyclodextrin (HP-β-CD), they were not as high as those previously observed with β-CDP (Yan Lee, 2016). This difference could occur from slightly differences in the preparation of the samples, which could potentially influence the solution polarity, as has previously been found to occur in the presence of low concentrations of ethanol (as used to prepare the AXI solutions)(Bortolus, Monti, Energia, & Area, 1996).

5.2.1.2 Effect of guest concentration in the presence of β-CDP

In the presence of increasing concentrations of β-CDP the fluorescence intensity was seen to increase (Fig. 1, Annexe Fig. 10-11).

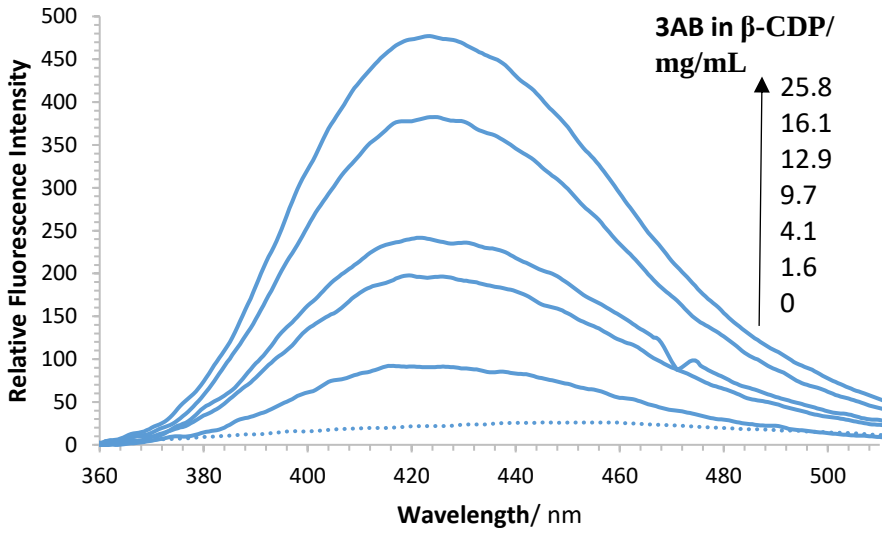

Figure 1: *Evolution of the fluorescence emission spectra of 2.60ppb 3AB in water, with increasing concentrations of β-CDP, at room temperature*

Various drug concentrations were selected so that their spectra did not exceed the limit of the fluorimeter upon addition of excess β-CDP, and so that isotherms spanned the range of the fluorimeter. Based on how the fluorescence intensity of the compounds evolved in the presence of β-CDP, increasing concentrations of β-CDP were added. Isotherms were constructed for the compounds, at the fluorescence emission maxima. Increasing

concentrations of β-CDP were found to result in a subsequent fluorescence intensity increase of the compounds, before reaching a plateau was reached (Fig. 2, Annexe Figure 12-13). Various concentrations of each guest appeared to reach plateaus at approximately the same concentrations of β-CDP, producing isotherms of a similar shape. This indicated that altering guest concentration had no influence on the stoichiometry of the complex.

All constructed isotherms appeared to be ‘‘L’-shaped’, in which increasing the β-CDP above a specific concentration did not result in any further enhancement in the relative fluorescence intensity of the drug. This indicated that cyclodextrin had a limited sorption capacity for the drug molecules (Hernandez-Montelongo et al., 2014). The absence of an ‘S’ shaped isotherm (Hernandez-Montelongo et al., 2014) may indicate that a single polymer unit of cyclodextrin was involved in the complexation (Pinto et al., 2005), and thus that ‘m’ was close to unity for the complexes formed with each of the studied compounds.

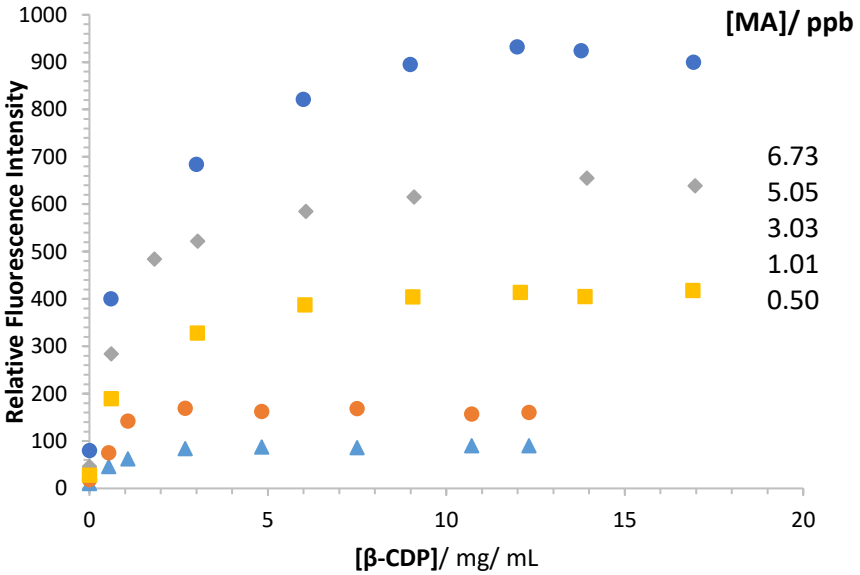

Figure 2: *Isotherms of 0.50ppb-6.73ppb MA, in water, with increasing concentrations of β-CDP, at room temperature*

5.2.1.3 Determination of the stoichiometry of the complex

The isotherm data for 'i' concentrations of compound in the presence of varying 'j' concentrations of β-CDP were treated using Eq. 4. For each isotherm the fluorescence spectra were recorded in the absence of the β-CDP, $Fl_{0,G,i}^{\lambda obs}$, at a specified concentration of β-CDP, $Fl_{tot,i,j}^{\lambda obs}$, (e.g. 12mg/mL for MA) and at the plateau region, $Fl_{0,(G_n:(CD_p)_m)}^{\lambda obs}$. Plots were then acquired for Y_n against X_n (Eq. 7) to produce straight lines.

$$X_n = Ln\left[\frac{\left(Fl_{0,(G_n:(CD_p)_m)}^{\lambda obs} - Fl_{tot,i,j}^{\lambda obs}\right)\times[G]_{0,i}}{Fl_{0,(G_n:(CD_p)_m)}^{\lambda obs} - Fl_{0,G,i}^{\lambda obs}}\right] \quad \textbf{Eq. 7a}$$

$$Y_n = Ln\left[\frac{Fl_{tot,i,j}^{\lambda obs} - Fl_{0,G,i}^{\lambda obs}\times[G]_{0,i}}{Fl_{0,(G_n:(CD_p)_m)}^{\lambda obs} - Fl_{0,G,i}^{\lambda obs}}\right] \quad \textbf{Eq. 7b}$$

The gradient of this linear plot (Y_n=f(X_n)) represents the number of guest molecules in the complex 'n' (Eq. 4). Using Eq. 8 the intercept of (Y_m=f(X_m)) can allow for the number of host molecules 'm' to be determined, using data from one of the isotherms.

$$X_m = Ln[CD_p]_{0,i,j} \quad \textbf{Eq. 8a}$$

$$Y_m = Ln\left[\frac{\left(Fl_{0,(G_n:(CD_p)_m)}^{\lambda obs} - Fl_{tot,i,j}^{\lambda obs}\right)^n}{\left(Fl_{tot,i,j}^{\lambda obs} - Fl_{0,G,i}^{\lambda obs}\right)}\right] \quad \textbf{Eq. 8b}$$

The association constant of each guest can then be determined for monomers using Eq. 5 and the value of the intercept. Eq. 5 requires knowledge of the molecular weight of the cyclodextrin. This is not accurately known for β-CDP, and thus only the pseudo-association constant can be determined (Eq. 9).

$$K'_{G_n:(CD_p)_m} = K_{G_n:(CD_p)_m} \times RMM(CD_p) = \frac{e^{intercept}}{n \times [CD_p]_{0,i,j}^m} \quad \textbf{Eq. 9}$$

In which $[CD_p]^m_{0,i,j}$ is given in g/L, and $K'_{G_n:(CD_p)_m}$ is given in (g/L)$^{1\text{-m-n}}$, or similar.

As can be observed (Fig. 3, Table 2, Annexe Fig. 14-17) the various stoichiometries obtained ranged from 0.65:0.85 for MA and 0.74:1.51 for 3AB. A previous study had already determined the stoichiometry between AXI and β-CDP to be 0.98:0.79 (Yan Lee, 2016). Although not comparable to the pseudo-order association constants, similar stoichiometries of 1:1 had previously been observed between 3AB, 2AB, BZ, MA and TR and monomeric β-cyclodextrins (Iglesias, 2011; Pinto et al., 2005; Utsuki et al., 1993; Yang et al., 2013).

The current results using β-CDP indicate that in the solution any one molecule of compound may interact with a single β-CDP unit differently to another molecule of this compound. This model represents an average of the overall complexes formed (Fernandes, Carvalho, Pereira da Costa, & Veiga, 2003), is multimodal, and therefore accounts for the multiple interactions (Hatsumi Aki et al., 2004).

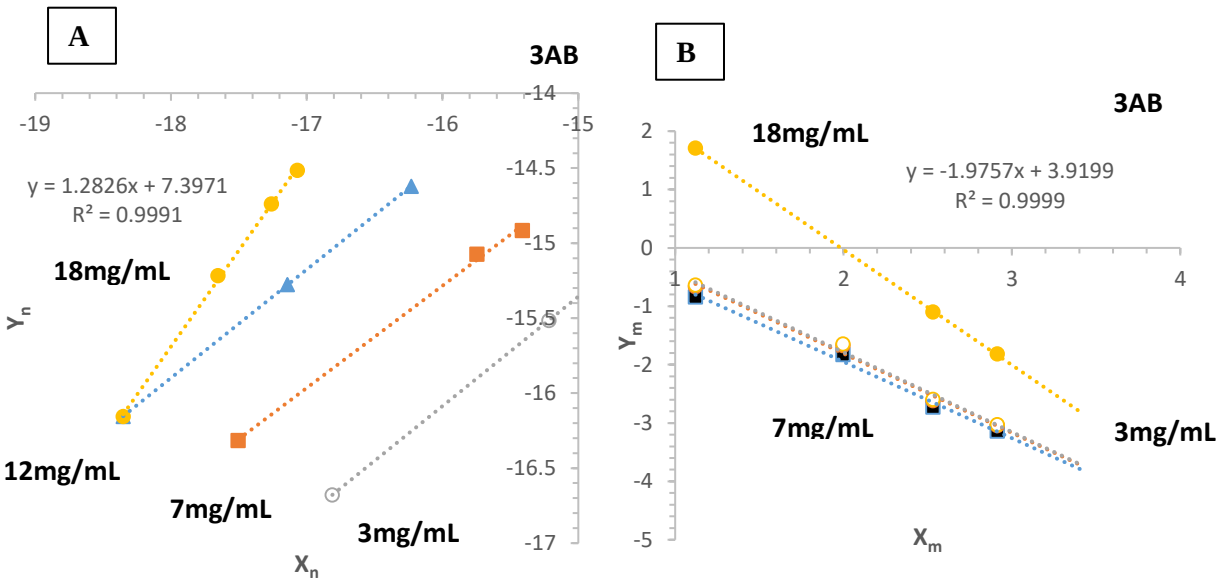

Figure 3: *Determination of coefficient (A) 'n' and (B) 'm' for 3AB-β-CDP complexes, using various concentrations of β-CDP (circles=18mg/mL β-CDP, open circles=3mg/mL β-CDP, squares=7mg/mL β-CDP, triangles=12mg/mL β-CDP)*

Table 2: *Correlation coefficients, stoichiometries and association constants for 3AB, 2AB, BZ, MA and TR complexes with β-CDP*

Complex	Conc. of β-CDP (mg/mL)	n[a]	Intercept[b]	r[c]	m[d]	int	r	K' (g/L)
3AB/ β-CDP	12	0.74	-2.51	1	1.51	1.25	0.99	16.13
2AB/ β-CDP	6	1.19	4.63	1	1.53	1.95	1	5.32
BZ/ β-CDP	3	0.90	0.61	1	1.74	-0.29	1	31.50
MA/ β-CDP	2.7	0.65	-3.90	1	0.85	-2.03	1	3.41
TR / β-CDP	7.5	0.86	-0.41	0.99	1.53	0.93	0.99	16.73

[a] 'n' is the number of guest molecules
[b] int is the intercept of the linear relationship
[c] r is the correlation coefficient of the linear relationship
[d] 'm' is the number of cyclodextrin molecules

The stoichiometries obtained for 3AB, BZ, MA and TR may indicate partial inclusion of the compounds, whilst that obtained for 2AB may indicate it possesses multiple binding sites (Fernandes et al., 2003). This could imply either full or partial inclusion of each compound within the cavity of a single cyclodextrin unit, to form the most energetically favourable inclusion complex (Connors, 1997); and is expected to vary between each molecule of a single compound.

The K' values determined for 3AB were ≈9 times greater than those determined for MA. This may indicate that the differing sizes of the compounds affected their ability to have a complementary fit within the cavity of the cyclodextrin. The larger value of K' would imply a better fit (Mennini, Bragagni, Maestrelli, & Mura, 2014), and would indicate fewer 2AB molecules remained uncomplexed in the final solution, when compared to MA. Each complexed compound formed greater K' than had previously been observed between AXI and β-CDP (3.33g/L)(Yan Lee, 2016).

Former studies have determined the dimensions of β-CDP monomer as ≈6.8Å wide and ≈7.8Å long (Iglesias, 2011)(Fig. 4). When comparing the sizes of this β-CD monomer to those previously reported for 3AB, 2AB and BZ (Yousef, Zughul, & Badwan, 2007), it is possible that (assuming one unit of β-CDP has the same dimensions as one unit of β-CD monomer) 2AB and 3AB could be encapsulated diameter-wise within the cavity. The greater length that had been determined for BZ may prevent it from being completely included within the cavity (Iglesias, 2011), although the results indicated partial inclusions with both BZ and 3AB (Table 2).

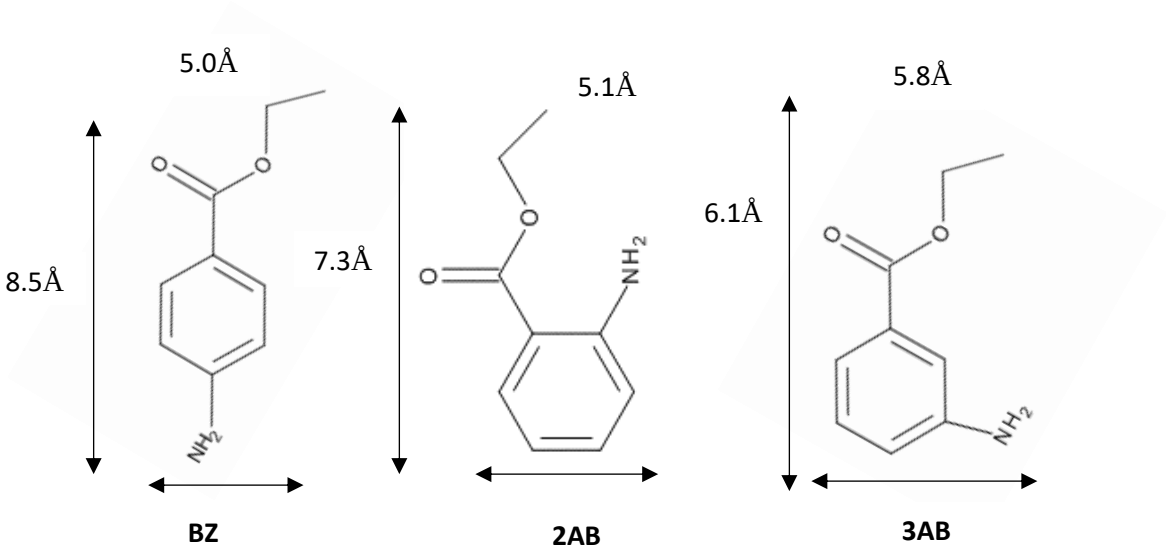

Figure 4: *Dimensions of the molecules of 3AB, 2AB and BZ, respectively*

Potential modes of complexation were considered. Past studies have suggested that the aromatic ring of BZ may be completely inserted within the cyclodextrin cavity (Pinto et al., 2005; Voicescu & Bandula, 2015), in which the amine group on each of the three isomers could form hydrogen bonds with the alkoxide group of the cyclodextrin cavity, or alternatively, hydrogen bonds may form between the ester group of the isomer and –OH group of cyclodextrin (Iglesias, 2011). The former compound-cyclodextrin complexation has

only been reported in alkaline medium (Iglesias, 2011), but may occur for all three of the isomers with β-CDP.

Although the sizes of TR and MA had not been measured, previous literature has proposed that the aromatic ring of either of these compounds could be encapsulated within the cavity, close to the primary hydroxyl groups on the cyclodextrin (Yang et al., 2013)(Fig. 5g, i), or its other aromatic ring included (Fig. 5h, j)(Utsuki et al., 1993). The latter inclusion had not previously been reported for MA. As the size of the β-CDP cavity can be altered through the addition of substituents (Baglole, Boland, & Wagner, 2005), or the polymer type (Letellier, Maupas, Gramond, Guyon, & Gareil, 1995). This would merely be theoretical for β-CDP, proving an indication of the mode of complexation.

The K' values obtained for β-CDP in our study were in the order of BZ>TR>3AB>2AB>MA. Such results could indicate that the position of the amine group, in respect to the ester group, could influence the strength of hydrogen bonds between the ester group on the guest and the OH on the H-3 proton of the cyclodextrin (Pescitelli, Bilia, Bergonzi, Vincieri, & Di Bari, 2010). Furthermore, the complexes observed are expected to be stronger than β-CD with β-CDP (di Cagno et al., 2014). When compared to the other compounds, the molecular weight is much greater for MA. The larger number of functional groups it posesses may therefore imply that more 'bulky' compounds form a lower K'.

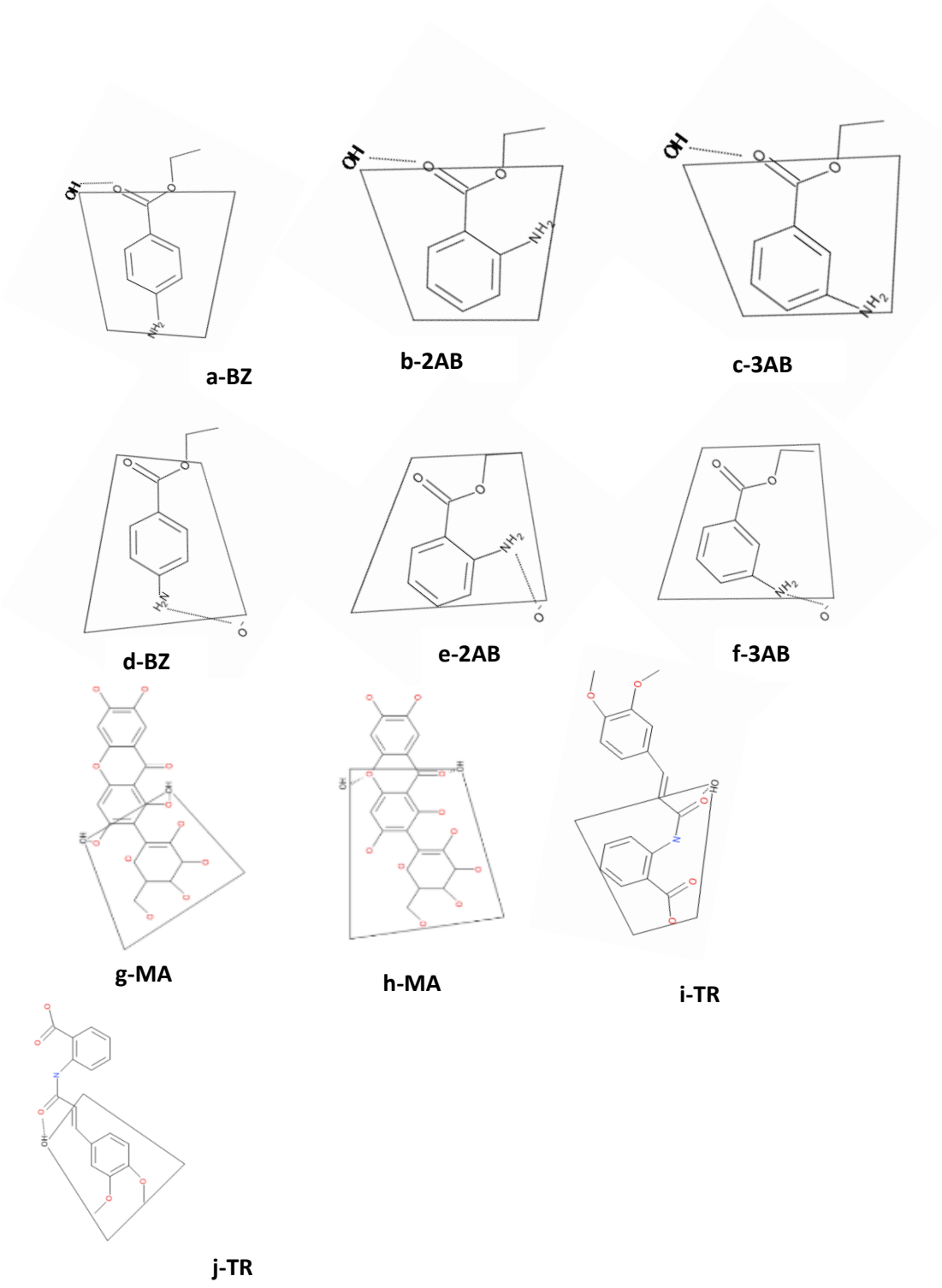

Figure 5: *Possible complex formations between a β-cyclodextrin unit and BZ (a, d), 2AB (b, e), 3AB (c, f), MA (g, h) and TR (i, j), respectively*

Larger association constants with β-cyclodextrin monomers have previously been determined, when compared to those with either α- or γ-cyclodextrin (Utsuki et al., 1993; Iglesias, 2011). The greatest association constant formed occurred between β-CD and BZ, supporting the induced-fit hypothesis (Utsuki et al., 1993). Moreover, use of cyclodextrin derivatives have influenced the strength of inclusion complexes. This has been observed in previous studies for MA, in which mono (6-ethylene-diamino-6-deoxy)-β-cyclodextrin was superior to hydroxylpropyl-β-cyclodextrin or sulfobutyl ether β-cyclodextrin (Yang et al., 2013), and TR, in which a stronger complex was formed with ethylenediamine linked β-cyclodextrin dimer (Tang et al., 2006), to that in native cyclodextrins (Utsuki et al., 1993). Although incomparable to these complex strengths, β-CDP is expected to form more stable complexes than either monomer. This is expected to involve both hydrogen bonds and van der Waals forces (Astray, Gonzalez-Barreiro, Mejuto, Rial-Otero, & Simal-Gándara, 2009), and, as mentioned in 5.1.2, may form multiple associations with each compound.

Implications of multimodal associations have previously been proposed for nicardipine hydrochloride and with either β-cyclodextrin or hydroxyl-propyl-β-cyclodextrin. In this study both aromatic ends of the guest were able to be energetically-favourably included within the cavity to form a rigid inclusion complex, and the inclusion mode considered to be dynamic (Fernandes et al., 2003).

5.2.1.4 NMR analysis of compounds in the presence of cyclodextrin

To provide further evidence of a complexation the proton and carbon NMR spectra were acquired and assigned for all compounds but MA and AXI. Job's plot of continuous variation was firstly applied to BZ in the presence of 2-hydroxyl-propyl-β-cyclodextrin (2-HP-β-CD). Using equal concentrations of drug and 2-HP-β-CD, the ratio was varied from 0.1-1, and the change in chemical shift between each molar ratio concentration plotted. Duplicate measurements showed a maximum change in the chemical shift at 0.5-0.7, indicative of a 1:1 stoichiometry (Baglole et al., 2005), alongside downfield drug chemical shifts (Fig. 6).

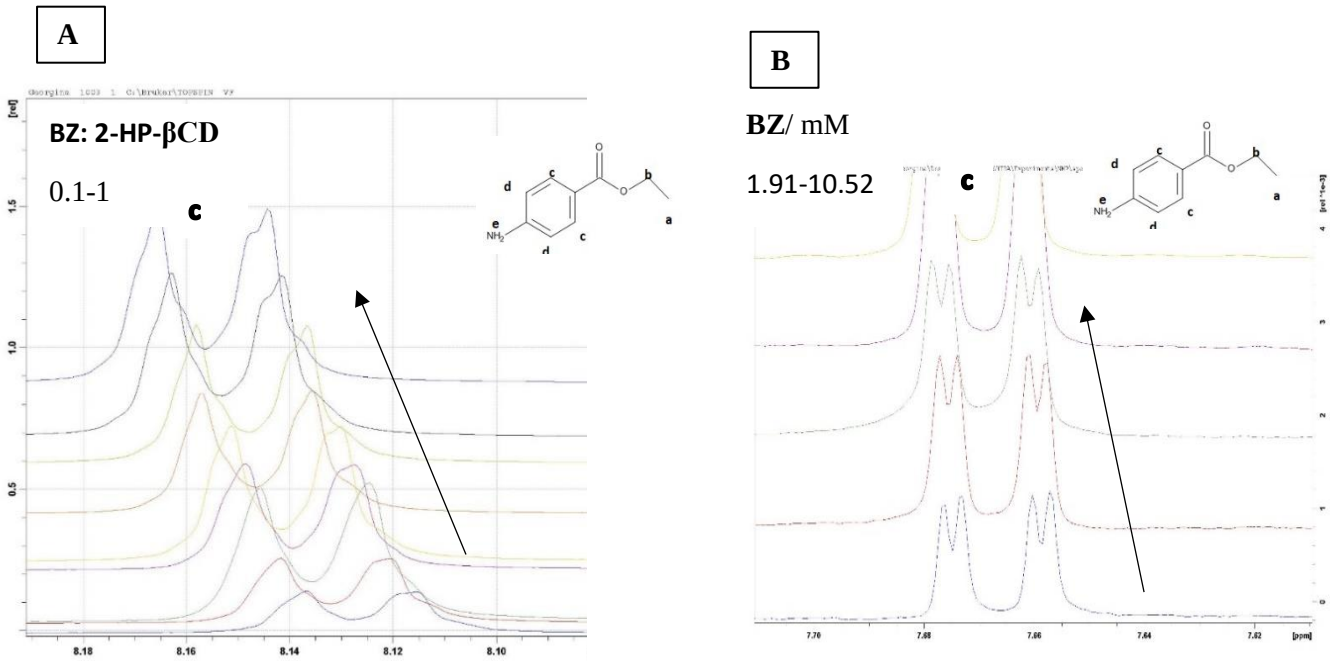

Figure 6: *Change in chemical shift of protons corresponding to the doublet 'c' in the aromatic region on BZ, acquired by 1H NMR, after varying the ratio of (A) 50.85mM BZ: 49.9mM 2-HP-β-CD from 0-1, or (B) increasing the concentration of BZ from 1.91-10.52mM in 50mg/mL β-CDP*

Variation of the drug concentration in a constant concentration of β-CDP also slightly shifted the guest protons downfield. The slightly narrower peaks and larger integral values (Fig. 6) were indicative of increasing free drug in the solution. These trends were additionally

observed for 2AB and 3AB. Altering the β-CDP concentration in constant concentrations of each drug was found to further support the data (broadening peaks, shifting the spectra downfield and reducing integral values). This supported the fluorescence data and suggested a similar interaction for all three compounds with β-CDP.

5.2.2.0 Fluorescence study of the guest in HSA

5.2.2.1 Fluorescence properties of the guest in HSA

The excitation and emission spectra of the compounds: 3AB, 2AB, BZ, MA, TR and AXI have been recorded in water, in the presence of HSA (Chapter 4), and the effect of the protein on the fluorescence properties studied.

When the compound was added to HSA the emission spectra of both the compound and the HSA red shifted. In addition, when compared to that recorded in the absence of the compound, the relative fluorescence intensity of HSA decreased (Chapter 4).

Such decreases in the fluorescence intensity of proteins have been observed. It has been found that proteins contain fluorophores which are shielded from the solvent. In HSA, the specific fluorophore, a single tryptophan residue, contains a rigid indole group, allowing for it to fluoresce. This tryptophan is sensitive to the solvent and thus when its indole group forms hydrogen bonds in polar solvents the emission spectra is red shifted, whilst it is expected to blue shift when 'folding' in an apolar environment. Such effects can occur as the protein is constructed of a 3–dimensional network of amino acids which can break down in a process known as 'unfolding'. The magnitude of such a shift depends on how exposed to the environment the fluorescent amino acid is, and thus the extent of the folding (Lakowicz, 2006). The shifts in the HSA emission spectra were not necessarily similar to those reported

in previous studies. Blue shifts previously observed in the presence of MA or TR (Yue, Chen, Qin, & Yao, 2009; Tayyab, Zaroog, Feroz, Mohamad, & Malek, 2015) were attributed to the less polar environment surrounding the tryptophan residue (Yue et al., 2009). Furthermore, the absence of shifts in the presence of AXI were indicative of little change in the protein structure (Feroz, Mohamad, Lee, Malek, & Tayyab, 2015). Although each of these studies maintained a neutral pH throughout analysis, the difference in shifts, to those in the current study, may occur as a result of the different solvents used for the preparation of the stock solutions (Connors, 1997; Tayyab et al., 2016, 2015).

In addition, the intensity of such protein fluorophores can decrease when they make contact with the quencher and are either returned to their ground state without emitting a fluorophore, or form a non-fluorescent complex. Such effects have previously been observed in studies between HSA and MA (Yue et al., 2009), AXI (Tayyab et al., 2016) and TR (Tayyab et al., 2015).

Alternatively, it may be energetically favourable for the excited state amino acid residue on the HSA to lose an unpaired electron and donate it to an unpaired electron on the ground state guest compound. For such effects to occur the acceptor and donor protons must be within 7nm of each other, and the spectra of the two compounds should overlap (Xu et al., 2017).

The extent of the fluorescence decrease in HSA depends on the distance between the fluorophore and quencher. This information can be derived from Stern-Volmer plots (Lakowicz, 2006).

5.2.2.2 Effect of guest compound on HSA

In the presence of increasing concentrations of HSA the fluorescence intensity was observed to decrease (Fig. 7, Annexe Fig. 18, Table 3).

Monitoring the maximum emission wavelength corresponding to HSA, indicated that as the concentration of compound was increased, the fluorescence intensity of HSA decreased (Fig. 7, Annexe Fig. 18, Table 3). Varying concentrations of HSA exhibited similar effects with each of the compounds. AXI in 0.0011ppb HSA was an exception. Increasing the concentration of AXI increased the emission spectra of HSA slightly. This effect had not been observed in the other concentrations of AXI used. Each HSA and AXI had an emission spectra at 343nm and 394nm, respectively, implying this effect did not occur from an overlap in its spectra, and may instead occur from the formation of an AXI: HSA complex that is more fluorescent than HSA alone. Alternatively, this may indicate that in low concentrations of HSA the quencher may bind to a different site on the HSA. Such effects may occur when the HSA is relocated to a less polar environment (Lakowicz, 2006). Alternatively, the compound may bind to the protein and stabilise it through forming hydrogen bonds and hydrophobic forces, tightening the protein polypeptide chains, causing the helical structure of the protein to fold (Naik, Pawar, Tandel, & J, 2018).

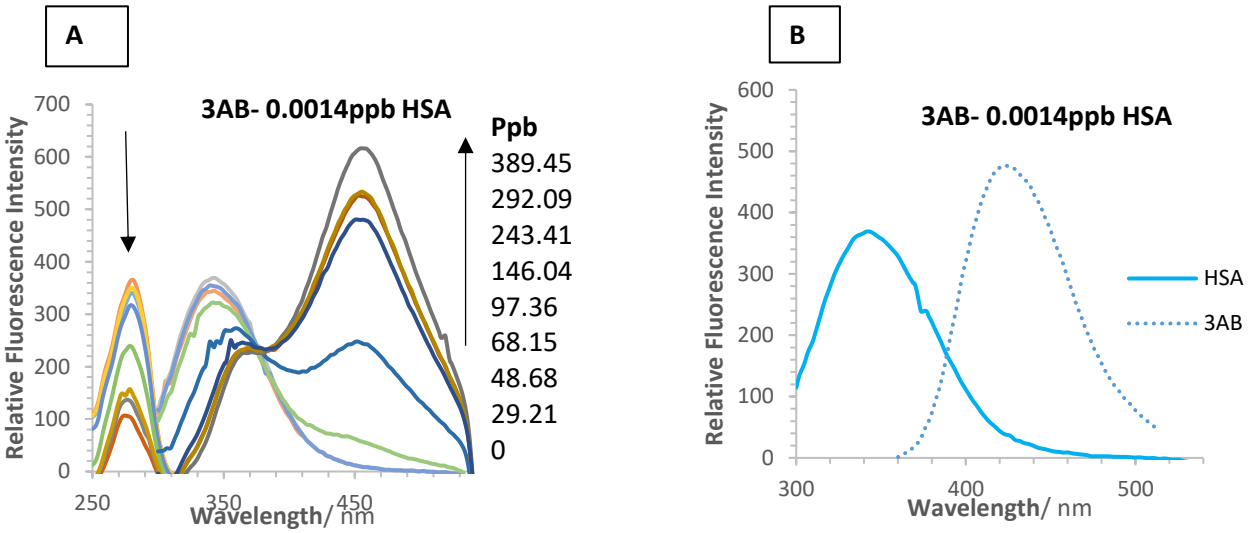

Figure 7: *(A) The effect of increasing concentrations of 3AB on the fluorescence excitation and emission spectra of 0.0014ppb human serum albumin. (B) 21.99ppb 3AB and 0.0014ppb HSA in water*

Isoactinic points were observed in each of the HSA-drug spectra of 3AB, 2AB, BZ and MA, TR, AXI at ≈350nm, ≈368nm, ≈329nm, ≈452nm, ≈370nm and ≈404nm, respectively (Fig. 7, Annexe Fig. 3). Such observations were indicative of the compound in its bound and unbound state at equilibrium, implying complexation (Yue et al., 2009).

5.2.2.3 Interaction of HSA with guest compounds

The decrease in intensity of fluorophores, quenched by other molecules, can be described using Stern-Volmer plots (Lakowicz, 2006). These can be used to determine the sensitivity of a fluorophore for a quencher. Data obtained from the quenching of HSA can therefore be treated using a Stern-Volmer plot (Eq. 10).

$$\frac{F_0}{F} = 1 + K_{SV}[Q] \qquad \textbf{Eq. 10}$$

In which F_0= Fluorescence intensity of HSA in the absence of drug

F= Fluorescence intensity of HSA in the presence of drug

[Q]= concentration of drug

K_{SV} = Stern-Volmer quenching constant

The gradient of the line of best fit corresponds to the Stern-Volmer quenching constant. In the current study this would describe how easily accessible the tryptophan residue (within the HSA) is to each of the studied compounds. The greater the constant, the more easily accessible the compound is (Lakowicz, 2006).

Stern-Volmer plots were constructed by recording the fluorescence quenching of a constant concentration of HSA in increasing concentrations of each of the compounds. To see if the K_{SV} of the compound was influenced by the HSA concentration, various concentrations of HSA were used, and a total of three Stern-Volmer plots constructed for each compound. The specific fluorophore concentrations were selected for their ability to initiate visible fluorescence intensity changes in the presence of the quencher.

The concentrations of the compound used in the Stern-Volmer plots were similar for all compounds but AXI, which required greater concentrations. This observation may allow for the same stock solutions of each compound to be used for their rapid analysis in water, and their quenching effect on HSA. In the presence of 0.0011ppb HSA, AXI was observed to increase the fluorescence intensity of HSA. Such an effect was not observed with this quencher and the other investigated HSA concentrations. Stern-Volmer plots are only used for quenching effects, therefore a Stern-Volmer plot was not constructed for this specific sample and the results were instead fitting using a calibration graph (data in Chapter 6).

All other Stern-Volmer plots appeared to be linear with positive gradients, indicating the fluorescence intensity of HSA was decreased in a concentration dependent manner (Fig. 8, Annexe Fig. 19-24).

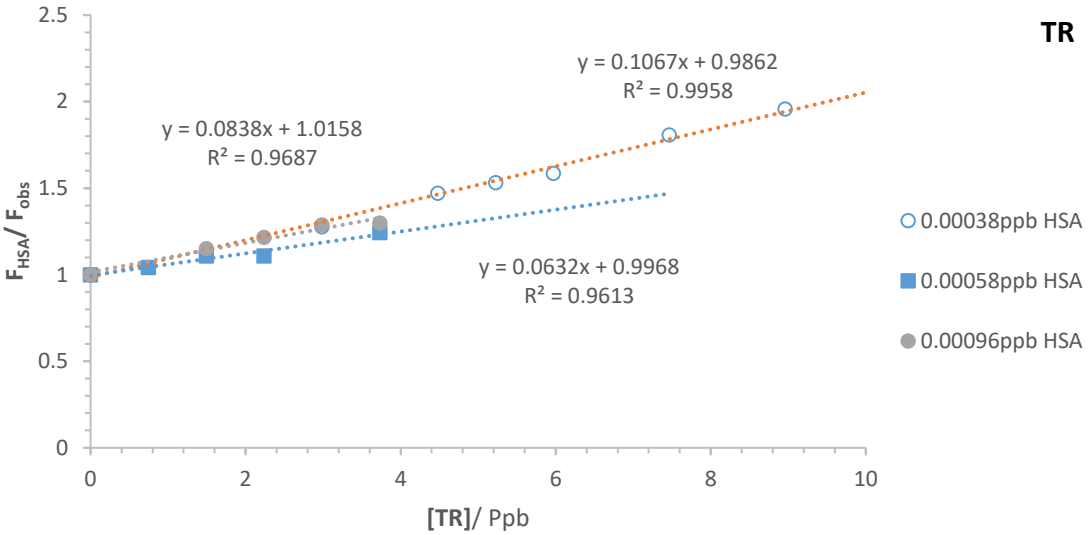

Figure 8: *Average Stern-Volmer plot of 0.00038ppb, 0.00058ppb and 0.00096ppb human serum albumin in increasing concentrations of TR*

The Stern-Volmer constants obtained were ≈1.9 x $10^{-3}M^{-1}$, ≈5.6 x $10^{-3}M^{-1}$, ≈6.3 x $10^{-3}M^{-1}$, ≈3.5 x $10^{-4}M^{-1}$, ≈3.2 x $10^{-5}M^{-1}$ and ≈6.2 x $10^{-4}M^{-1}$, for 3AB, 2AB, BZ, MA, TR and AXI, respectively (Table 3). Lower K_{SV}s determined for TR, when compared to BZ and its isomers, was characteristic of less exposure of the tryptophan residues to the compound. This indicated that quenching using TR was least efficient and may form a weak complex.

Table 3: *Stern-Volmer quenching constants (K_{SV}) observed in for 3AB, 2AB, BZ, MA, TR and AXI in water, in the presence of various concentrations of HSA*

Compound	[HSA]/ Ppb	K_{SV}
3AB	0.0014	0.0056
	0.0038	0.0019
	0.0067	0.0021
2AB	0.00096	0.0046
	0.0048	0.0053
	0.0067	0.0056
BZ	0.000048	0.0025
	0.0014	0.0057
	0.0048	0.0063
MA	0.00048	0.035
	0.0014	0.015
	0.0067	0.018
TR	0.00038	0.32
	0.00058	0.015
	0.00096	0.26
AXI	0.0017	0.062
	0.0023	0.031
	0.0011	3.1

K_{SV} constants were similar for each compound, when in differing concentrations of HSA, with the exception of TR. In the presence of 0.00058ppb HSA lower constants were observed with this compound. Such an effect may indicate that using this smaller ratio of TR: HSA meant that less of the quencher was accessible to the fluorphore (Lakowicz, 2006). This would support the slight increases in the quenching constant that occurred for both TR and AXI in lower concentrations of HSA.

The results were compared to those previously obtained in other studies. Larger Stern-Volmer constants recorded for AXI in earlier studies could be attributed to the much smaller ratio of HSA: AXI that had been used (Tayyab et al., 2016). Although TR and MA had been investigated in the presence of HSA, these studies used different methods (Tayyab et al., 2015) or

equations (Yue et al., 2009) to determine the K_{SV}, preventing these results from being compared to the current ones.

Although the lines of best fit on the Stern-Volmer plots differed, all studied compounds were able to bind to HSA. This may therefore enable their quantification in this protein, as will be outlined in the next chapter.

5.3.0 Conclusion

Using fluorimetry, the complexation between β-CDP and either 3AB, 2AB, BZ, MA, TR or AXI was characterised using the mathematical model previously proposed (Yan Lee, 2016). Integer values reported for the stoichiometries were attributed to partial or multiple binding sites on the β-CDP. Furthermore, pseudo-association constants determined had a strength in the order of BZ>TR>3AB>2AB>MA, respectively, implying various inclusions within the polymer cavity. Multimodal inclusions were hypothesised based on non-integer values for n and m.

Further indication of an inclusion complex between the three isomer compounds and β-CDP was confirmed through NMR analysis. Downfield shifts, broadened peaks and lower integral values in the aromatic protons of 3AB, 2AB and BZ implied their encapsulation and an interaction with β-CDP.

The effect of increasing concentrations of quencher on the fluorescence intensity of HSA was observed and Stern-Volmer plots constructed to provide information on the sensitivity of HSA for each compound. With the exception of 0.0011ppb HSA and AXI, the intensity of HSA was quenched in the presence of increasing quencher concentration. In this specific concentration

of HSA, AXI had the effect of increasing the fluorescence signal. Various K_{SV} values for the other HSA concentrations and compounds used were obtained.

5.4.0 References

Aki, H, Niiya, T., Iwase, Y., & Yamamoto, M. (2001). Multimodal inclusion complexes between barbiturates and 2-hydroxypropyl-beta-cyclodextrin in aqueous solution: isothermal titration microcalorimetry, (13)C NMR spectrometry, and molecular dynamics simulation. *Journal of Pharmaceutical Sciences*, *90*(8), 1186–1197.

Aki, Hatsumi, Niiya, T., Iwase, Y., Kawasaki, Y., Kumai, K., & Kimura, T. (2004). Multimodal inclusion complexes of ampicillin with β-cyclodextrins in aqueous solution. *Thermochimica Acta*, *416*(1–2), 87–92.

Astray, G., Gonzalez-Barreiro, C., Mejuto, J. C., Rial-Otero, R., & Simal-Gándara, J. (2009). A review on the use of cyclodextrins in foods. *Food Hydrocolloids*, *23*(7), 1631–1640.

Baglole, K. N., Boland, P. G., & Wagner, B. D. (2005). Fluorescence enhancement of curcumin upon inclusion into parent and modified cyclodextrins. *Journal of Photochemistry and Photobiology A: Chemistry*, *173*(3), 230–237.

Bortolus, P., Monti, S., Energia, A., & Area, C. N. R. (1996). *Photochemistry in Cyclodextrin Cavities* (Vol. 21).

Cavalli, R., Donalisio, M., Civra, A., Ferruti, P., Ranucci, E., Trotta, F., & Lembo, D. (2009). Enhanced antiviral activity of Acyclovir loaded into β-cyclodextrin-poly(4-acryloylmorpholine) conjugate nanoparticles. *Journal of Controlled Release*, *137*(2), 116–122.

Connors, K. A. (1997). The Stability of Cyclodextrin Complexes in Solution. *Chemical Reviews*, *97*(5), 1325–1358.

di Cagno, M., Terndrup Nielsen, T., Lambertsen Larsen, K., Kuntsche, J., & Bauer-Brandl, A. (2014). β-Cyclodextrin-dextran polymers for the solubilization of poorly soluble drugs. *International Journal of Pharmaceutics*, *468*(1–2), 258–263.

Erdoğar, N., & Bilensoy, E. (2018). Cyclodextrin-Based Nanosystems in Targeted Cancer Therapy. In E. Fourmentin, Sophie, Crini, Grégorio, Lichtfouse (Ed.), *Cyclodextrin Applications in Medicine, Food, Environment and Liquid Crystals* (pp. 59–80).

Fernandes, C. M., Carvalho, R. A., Pereira da Costa, S., & Veiga, F. J. . (2003). Multimodal molecular encapsulation of nicardipine hydrochloride by β-cyclodextrin, hydroxypropyl-β-cyclodextrin and triacetyl-β-cyclodextrin in solution. Structural studies by 1H NMR and ROESY experiments. *European Journal of Pharmaceutical Sciences*, *18*(5), 285–296.

Feroz, S. R., Mohamad, S. B., Lee, G. S., Malek, S. N. A., & Tayyab, S. (2015). Supramolecular interaction of 6-shogaol, a therapeutic agent of Zingiber officinale with human serum albumin as elucidated by spectroscopic, calorimetric and molecular docking methods. *Phytomedicine*, *22*(6), 621–630.

Ferreira, F. da R., Valentim, I. B., Ramones, E. L. C., Trevisan, M. T. S., Olea-Azar, C., Perez-Cruz, F., Goulart, M. O. F. (2013). Antioxidant activity of the mangiferin inclusion complex with β-cyclodextrin. *LWT - Food Science and Technology*, *51*(1), 129–134.

Fülöp, Z., Kurkov, S. V., Nielsen, T. T., Larsen, K. L., & Loftsson, T. (2012). Self-assembly of cyclodextrins: formation of cyclodextrin polymer based nanoparticles. *Journal of Drug Delivery Science and Technology*, *22*(3), 215–221.

Gidwani, B., & Vyas, A. (2014). Synthesis, characterization and application of Epichlorohydrin-β-cyclodextrin polymer. *Colloids and Surfaces B: Biointerfaces*, *114*, 130–137.

Hamai, S. (1999). Inclusion complexes of poly-β-cyclodextrin with 2-anilino-6-naphthalenesulfonic acid, 1-chloronaphthalene, and azulene in aqueous solutions. *Journal of Photochemistry and Photobiology A: Chemistry*, *124*(3), 153–158.

Hernandez-Montelongo, J., Naveas, N., Degoutin, S., Tabary, N., Chai, F., Spampinato, V., Martel, B. (2014). Porous silicon-cyclodextrin based polymer composites for drug delivery applications. *Carbohydrate Polymers*, *110*, 238–252.

Hirayama, F., Utsuki, T., & Uekama, K. (1991). Stoichiometry-dependent photodimerization of tranilast in a γ-cyclodextrin inclusion complex. *Journal of the Chemical Society, Chemical Communications*, *0*(13), 887–888.

Huang, L., He, J., Lu, R., Ge, X., & Guo, J. (2011). Investigation on a host–guest inclusion system by β-cyclodextrin derivative and its analytical application. *Bioorganic & Medicinal Chemistry Letters*, *21*(4), 1113–1117.

Iglesias, E. (2011). Exploring the effect of supramolecular structures of micelles and cyclodextrins on fluorescence emission of local anesthetics. *Photochemical & Photobiological Sciences: Official Journal of the European Photochemistry Association and the European Society for Photobiology*, *10*(4), 531–542.

Junthip, J., Tabary, N., Leclercq, L., & Martel, B. (2015). Cationic β-cyclodextrin polymer applied to a dual cyclodextrin polyelectrolyte multilayer system. *Carbohydrate Polymers*, *126*, 156–167.

Lakowicz, J. R. (2006). *Principles of fluorescence spectroscopy*. Springer.

Letellier, S., Maupas, B., Gramond, J. P., Guyon, F., & Gareil, P. (1995). Determination of the formation constant for the inclusion complex between rutin and methyl-β-cyclodextrin. *Analytica Chimica Acta*, *315*(3), 357–363.

Li, J., Xiao, H., Li, J., & Zhong, Y. (2004). Drug carrier systems based on water-soluble cationic β-cyclodextrin polymers. *International Journal of Pharmaceutics*, *278*(2), 329–342.

Limousin, G., Gaudet, J.-P., Charlet, L., Szenknect, S., Barthès, V., & Krimissa, M. (2007). Sorption isotherms: A review on physical bases, modeling and measurement. *Applied Geochemistry*, *22*(2), 249–275.

Mennini, N., Bragagni, M., Maestrelli, F., & Mura, P. (2014). Physico-chemical characterization in solution and in the solid state of clonazepam complexes with native and chemically-modified cyclodextrins. *Journal of Pharmaceutical and Biomedical Analysis*, *89*, 142–149.

Moulahcene, L., Skiba, M., Senhadji, O., Milon, N., Benamor, M., & Lahiani-Skiba, M. (2015). Inclusion and removal of pharmaceutical residues from aqueous solution using water-insoluble cyclodextrin polymers. *Chemical Engineering Research and Design*, *97*, 145–158.

Murdan, S. (2013). Packaging. In M. E. Aulton & K. M. G. Taylor (Eds.), *Aulton's pharmaceutics : the design and manufacture of medicines* (4th ed.). China: Elsevier Ltd.

Naik, R. S., Pawar, S. K., Tandel, R. D., & J, S. (2018). Insights in to the mechanism of interaction of a thrombin inhibitor, dabigatran etexilate with human serum albumin and influence of β-cyclodextrin on binding: Spectroscopic and computational approach. *Journal of Molecular Liquids*, *251*, 119–127.

Pescitelli, G., Bilia, A. R., Bergonzi, M. C., Vincieri, F. F., & Di Bari, L. (2010). Cyclodextrins as carriers for kavalactones in aqueous media: Spectroscopic characterization of (S)-7,8-dihydrokavain and β-cyclodextrin inclusion complex. *Journal of Pharmaceutical and Biomedical Analysis*, *52*(4), 479–483.

Pinto, L. M. A., Fraceto, L. F., Santana, M. H. A., Pertinhez, T. A., Junior, S. O., & de Paula, E. (2005). Physico-chemical characterization of benzocaine-β-cyclodextrin inclusion complexes. *Journal of Pharmaceutical and Biomedical Analysis*, *39*(5), 956–963.

Sheehan, D. (2009). *Physical biochemistry: principles and applications* (2nd ed.). Retrieved from https://www.wiley.com/en-us/Physical+Biochemistry%3A+Principles+and+Applications%2C+2nd+Edition-p-9780470856031

Szejtli, J. (2005). Past, Present, and Future of Cyclodextrin Research. *Pure and Applied Chemistry*, 70(107), 1825-1845.

Tang, B., Liang, H., Tong, L., & Li, P. (2006). Synthesis of ethylenediamine linked β-cyclodextrin dimer and its analytical application for tranilast determination by spectrofluorimetry. *Bioorganic & Medicinal Chemistry*, *14*(11), 3947–3952.

Tayyab, S., Izzudin, M. M., Kabir, M. Z., Feroz, S. R., Tee, W.-V., Mohamad, S. B., & Alias, Z. (2016). Binding of an anticancer drug, axitinib to human serum albumin: Fluorescence quenching and molecular docking study. *Journal of Photochemistry and Photobiology B: Biology*, *162*, 386–394.

Tayyab, S., Zaroog, M. S., Feroz, S. R., Mohamad, S. B., & Malek, S. N. A. (2015). Exploring the interaction between the antiallergic drug, tranilast and human serum albumin: Insights from calorimetric, spectroscopic and modeling studies. *International Journal of Pharmaceutics*, *491*(1–2), 352–358.

Tejashri, G., Amrita, B., & Darshana, J. (2013). Cyclodextrin based nanosponges for pharmaceutical use: A review. *Acta Pharmaceutica*, *63*(3), 335–358.

Upadhyay, S., & Kumar, G. (2009). NMR and molecular modelling studies on the interaction of fluconazole with β-cyclodextrin. *Chemistry Central Journal*, *3*(1), 1-9.

Utsuki, T., Hirayama, F., & Uekama, K. (1993). Different photodimerization behaviour of tranilast in α-, β- and γ-cyclodextrin complexes: cavity-size and stoichiometry dependence. *J. Chem. Soc., Perkin Trans. 2*, *0*(1), 109–114.

Voicescu, M., & Bandula, R. (2015). 3,6-diHydroxyflavone/bovine serum albumin interaction in cyclodextrin medium: Absorption and emission monitoring. *Spectrochimica Acta Part A: Molecular and Biomolecular Spectroscopy*, *138*, 628–636.

Xu, L., Hu, Y.-X., Li, Y.-C., Zhang, L., Ai, H.-X., Liu, H.-S., Sang, Y.-L. (2017). Study on the interaction of tussilagone with human serum albumin (HSA) by spectroscopic and molecular docking techniques. *Journal of Molecular Structure*, *1149*, 645–654.

Yan Lee, L. (2016). *Study Of The Photodegradation And Photostability Of Anti-Cancer Drugs In Different Media Towards The Development Of Both New Actinometers And Liquid Formulations* (De Montfort University). Retrieved from https://www.dora.dmu.ac.uk/bitstream/handle/2086/12188/Lok Yan%27s Thesis.pdf?sequence=1&isAllowed=y

Yang, X., Zhao, Y., Chen, Y., Liao, X., Gao, C., Xiao, D., Yang, B. (2013). Host–guest inclusion system of mangiferin with β-cyclodextrin and its derivatives. *Materials Science and Engineering: C*, *33*(4), 2386–2391.

Yousef, F. O., Zughul, M. B., & Badwan, A. A. (2007). The modes of complexation of benzimidazole with aqueous β-cyclodextrin explored by phase solubility, potentiometric titration, 1H-NMR and molecular modeling studies. *Journal of Inclusion Phenomena and Macrocyclic Chemistry*, *57*(1–4), 519–523.

Yue, Y., Chen, X., Qin, J., & Yao, X. (2009). Characterization of the mangiferin–human serum albumin complex by spectroscopic and molecular modeling approaches. *Journal of Pharmaceutical and Biomedical Analysis*, *49*(3), 753–759.

Chapter 6:

Development, evaluation and application of novel quantification methods

Chapter 6: Development, evaluation and application of novel quantification methods

6.1.0 Introduction

6.1.1 Introduction

To improve the ability to detect the compounds selected for this study in biofluids and surface waters, two novel methods have been proposed. These methods aim to monitor the fluorescence spectra of the compounds in the presence of host molecules (β-CDP or HSA). Both methods have the potential to easily and rapidly provide quantitative determination of each compound.

The initial method has proposed employing β-CDP to enable low concentrations of each compound to be analysed in buffered water and canal water. This study was based on the greater fluorimetric response of compounds that had previously been observed in the presence of cyclodextrin (Huang, He, Lu, Ge, & Guo, 2011), along with the superior complexing properties of its polymeric derivatives (Fülöp, Kurkov, Nielsen, Larsen, & Loftsson, 2012). In such β-CDPs, evidence of a greater fluorescence intensity has previously been observed, when compared to that in monomers (Song et al., 2018). These effects were expected to occur as the polymeric derivative possessed several binding sites, allowing for multiple drug molecules to be complexed (Fülöp et al., 2012). A relationship between the fluorescence intensity of the complex, and the strength of the complex was additionally confirmed. Through the formation of these drug-β-CDP inclusion complexes, it was expected that the increase in fluorescence intensity could be utilised for the detection of the compounds. The accuracy and precision of the results was therefore evaluated, as it was expected that the method could enhance the amount of compound able to be detected.

The second method explores using the decrease in fluorescence intensity of HSA and Stern-Volmer plots, to determine the concentration of compounds. As far as we are aware the literature does not provide an example of such a method.

6.2.0 Results

6.2.1.0 Analytical parameters in water, canal water and β-CD polymers

It was stated in Chapters 4-5 that the fluorescence intensity signal of the selected compounds was increased in the presence of β-CDP. Furthermore, the stoichiometries and pseudo-association constants of the complexes formed were calculated.

To ensure precise analysis throughout the studies, calibration graphs were constructed in triplicate in both water and canal water, and in the absence and presence of β-CDP (Table 1, Annexe Fig. 8-9, Table 1-2). In the media the various graphs were linear, in the absence of β-CDP, from as low as 13ppt, to as high as 58ppb, although this range was considerably reduced (≈1.34-8.93ppb) in the presence of excess β-CDP (Table 1). Expanded linearity ranges of 2AB, BZ, MA and TR were observed when water was used as a solvent, rather than canal water. This indicated that the relationship between the fluorescence intensity and concentration of the compounds occurred over a greater range when in a neutral pH environment, than in canal water. High regression coefficients and gradient Relative Standard Deviations (RSDs) demonstrated the accuracy and precision of the method, and low standard deviations showed it was repeatable (HMS, 2017). These results demonstrated that the contaminants within the matrix had a negligible effect that did not alter quantification in the real sample.

Table 1: *Calibration results of 3AB, 2AB, BZ, MA, TR and AXI in water (W) and canal water (C), in the absence and presence of 25mg/mL, 12mg/mL, 12mg/mL, 4mg/mL, 12mg/mL and 15mg/mL β-CDP, respectively (β-CDP in water, Cβ-CDP in canal water), n=number of calibration points, r=regression coefficient*

Compound	Medium	Calibration				
		Slope	Intercept	n	Linearity range/ ppb	r
3AB	W	0.083	3.30	7	0.16-48.68	0.997
	CW	0.047	-0.0025	6	5.46-34.09	0.995
	β-CDP	0.79	2.59	6	0.65-3.03	0.996
	Cβ-CDP	8.17	7.15	6	0.65-3.25	0.997
2AB	W	6.69	1.40	7	0.013-8.19	0.999
	CW	6.68	1.21	7	0.013-8.19	0.999
	β-CDP	44.40	3.67	6	0.013-0.98	0.997
	Cβ-CDP	43.33	10.71	6	0.013-0.98	0.998
BZ	W	0.29	4.50	7	0.97-57.99	0.998
	CW	0.30	-1.05	7	1.61-48.37	0.997
	β-CDP	9.33	0.81	7	0.13-4.84	0.999
	Cβ-CDP	8.32	2.32	7	0.19-1.42	0.999
MA	W	0.48	1.02	7	0.10-2.52	0.998
	CW	0.51	0.51	7	0.10-2.52	0.998
	β-CDP	4.13	5.80	7	0.10-2.52	0.998
	Cβ-CDP	3.77	4.81	6	0.20-2.07	0.997
TR	W	0.093	2.38	7	0.75-14.93	0.994
	CW	0.10	2.25	6	0.75-6.47	0.990
	β-CDP	1.27	8.90	6	0.20-3.98	0.998
	Cβ-CDP	1.72	26.79	6	0.17-2.86	0.993
AXI	W	2.47	-6.38	6	0.30-3.01	0.996
	CW	0.92	-1.62	6	2.14-57.16	0.981
	β-CDP	2.57	50.62	6	0.15-1.21	0.997
	Cβ-CDP	0.42	83.35	6	1.34-8.93	0.992

6.2.1.2 Recovery parameters

In both water and canal water, good recoveries of the compounds (less than 15%) were recorded in triplicate (Table 2). Using three concentrations from across the linearity range, average recoveries of 92-108% were also obtained in the presence of β-CDP. This indicates the reliability of the method, and its precision for analysing all the analyte concentrations (Table 2).

Table 2: *Recovery of 3AB, 2AB, BZ, MA, TR and AXI in approximately 25mg/mL, 12mg /mL, 12mg/mL, 4mg/mL, 12mg/mL and 15mg/mL β-CDP, respectively, in water and canal water (+C_{Add}/ ppb=concentration added, ≠C_{Det}/ ppb=average concentration detected,*%$_{REC}$= average percentage recovery)*

Compound	**Water**			**Canal water**		
	+C_{Add}/ ppb	**≠C_{Det}/ ppb**	***%$_{REC}$**	**+C_{Add}/ ppb**	**≠C_{Det}/ ppb**	***%$_{REC}$**
3AB	0.65	0.66	102.19	0.65	0.58	90.05
	1.62	1.52	93.64	1.95	1.87	96.06
	2.60	2.47	95.06	3.25	3.08	95.02
2AB	0.41	0.39	97.11	0.013	0.013	97.52
	0.98	1.02	104.91	0.4	0.49	99.61
	0.098	0.092	93.20	0.82	0.85	104.47
BZ	0.29	0.28	96.86	0.19	0.21	108.89
	1.93	1.79	92.70	1.93	1.90	96.36
	4.84	4.56	94.23	3.87	3.71	95.92
MA	0.50	0.50	95.19	0.20	0.21	101.32
	1.51	1.59	107.29	1.01	1.10	108.50
	2.52	2.52	99.91	2.02	2.14	106.29
TR	0.22	0.23	100.53	0.37	0.40	106.82
	0.49	1.58	106.00	1.49	1.56	104.56
	3.73	3.85	103.02	2.99	2.87	96.15
AXI	0.90	0.89	96.59	1.34	1.27	94.84
	0.60	0.58	95.31	8.04	8.39	104.34
	1.21	1.14	94.28	10.72	10.23	95.46

6.2.1.3 Robustness

The robustness of the method was ensured by either employing a different fluorimeter, or varying the excitation and emission wavelengths used (±2-5nm). Using the AXI calibration graph equation from the previous study (Yan Lee, 2016), the average recoveries and associated % Relative Standard Deviations (RSDs) were determined in triplicate (Table 3, Annexe Table 6). Results obtained for either modification (recoveries ±15%) indicated the method was robust, and quantification of the compounds was not influenced by the changes made.

Table 3: *Recovery and statistical results of 3AB, 2AB, BZ, MA, TR and AXI obtained in water on another fluorimeter (+C_{Add}/ ppb=concentration added, ≠C_{Det}/ ppb=average concentration detected,*%$_{REC}$= average percentage recovery, SD=standard deviation, RSD=relative standard deviation)*

Compound	+C_{Add}/ ppb	≠C_{Det}/ ppb	*%$_{REC}$	SD	RSD
3AB	9.74	9.39	96.43	0	0
	29.21	26.49	90.69	0.76	7.76
	38.95	41.99	107.81	1.51	3.88
2AB	0.098	0.10	104.15	0.0042	4.15
	0.49	0.52	106.33	0.028	5.33
	0.88	0.94	106.58	0.096	10.14
BZ	3.87	4.19	108.28	0.17	3.97
	11.61	11.52	99.26	0.93	8.04
	17.42	18.86	108.28	0.58	3.06
TR	14.80	7.92	106.03	0.54	6.81
	29.59	15.95	106.83	0.91	5.70
	5.92	2.84	95.15	0.15	5.26
AXI	8.04	7.66	95.32	0	0
	9.32	10.25	109.93	0	0
	8.68	10.25	98.19	0	0

6.2.1.4 Effect of pH

To ensure the best detection of the samples, the pH of buffered water (pH≈7) was altered from pH=1.43 to 11.55, and the change in fluorescence intensity of 9.73ppb 3AB, 12.28ppb 2AB, 9.67ppb BZ, 7.47ppb TR and 40.19ppb AXI investigated. Increasing the pH of 3AB, 2AB and AXI increased the fluorescence intensity, up to pH≈6, 4 and 5, respectively. Solvents with an alkalinity greater than pH≈10 decreased the intensity. A change in pH from pH=1.43 to 11.55 had little effect on the fluorescence response of BZ, indicating a poor influence of the medium pH on the intensity of this compound. The most significant effect of pH was observed for TR, in which the greatest intensity was observed at pH=2.06-3.13, depleting from pH=4.34-6.08, before increasing very slightly when the medium was made more basic (Fig. 1).

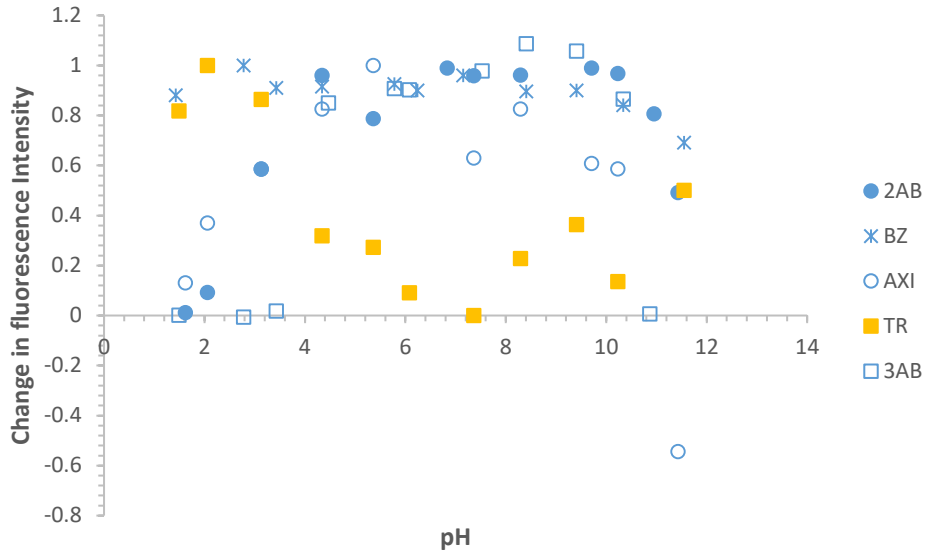

Figure 1: *Effect of pH on the maximum fluorescence intensity of 9.73ppb 3AB, 12.28ppb 2AB, 9.67ppb BZ, 7.47ppb TR and 40.19ppb AXI*

Reproducible results were obtained and a maximum pH observed at a neutral pH for all observed compounds but TR (Fig. 1). This exhibited a greatest intensity at pH≈3. Media of neutral pH (pH=7) was used for all compounds with the exception of TR. This employed pH=4. The pH of the canal water directly from the source was measured as pH≈6.13, before dilution in water pH=7. This implied all the compounds analysed, with the exception of TR, could be detected in environments mimicking biofluids and surface waters, with minimal sample preparation, making the technique cost effective and rapid.

6.2.2.0 Analysis of HSA containing samples

6.2.2.1 Methodology for the analysis of HSA containing samples

Processes that decrease the fluorescence intensity of fluorophores can occur from various interactions between the fluorophore and additional compounds. Regarding proteins, interactions with other compounds can occur from either collisional (Grigoryan, Grigoryan, & Ghazaryan, 2013) or static quenching (Yue, Chen, Qin, & Yao, 2009). Collisional quenching

occurs when the excited state fluorophore comes into contact with a quencher, causing the fluorophore to return to its ground state without emitting a photon. In contrast, static quenching occurs when the quencher and fluorophore form a non-fluorescent ground state complex.

Such processes alter the fluorescence intensity of the fluorophore, and can be fitted to the Stern-Volmer plots previously mentioned (Chapter 4)(Eq. 1). These plots describe the relationship between the fluorescence intensity of a fluorophore in the presence and absence of various concentrations of a quencher.

$$\frac{F_0}{F} = 1 + K_{SV}[Q] \qquad \textbf{Eq. 1}$$

F_0= Fluorescence intensity of HSA in the absence of the quencher

F= Fluorescence intensity of HSA in the presence of the quencher

[Q]= concentration of the quencher

K_{SV}= Stern-Volmer quenching constant

Assuming that the fluorophores are of equal accessibility to the quencher, linear Stern-Volmer plots would be expected. This is because both the number of collisions and complexes formed are proportional to the concentration of quencher.

Differentiation between the quenching types can be achieved by measuring the fluorescence lifetime, or the effect of temperature on the gradients of the Stern-Volmer plots (K_{SV}). An increase in temperature is likely to increase the rate of diffusion, resulting in more collisions and thus a higher quenching constant. Furthermore, depopulation of the excited state of the fluorophore is expected to decrease the fluorescence lifetime in such collisional processes. In

static quenching, however, the excited state fluorophore is not influenced by the quencher, and so the fluorescence lifetimes are unchanged. Higher temperatures might, however, affect the protein/ quencher complexes, causing them to dissociate.

The number of collisions that can occur in collisional quenching processes is influenced by the quencher diffusion rate. K_{SV} is therefore equal to the multiple of the fluorescence lifetime of the unquenched molecule (τ) and the bimolecular quenching constant of the reaction (k_q).

Previous chapters (4-5) have demonstrated that the fluorimetric spectrum of HSA both decreases and red shifts in the presence of the quencher, and its fluorophore is sensitive to the solvent (Chapter 4).

Table 4: *Stern-Volmer quenching constants (K_{SV}) observed for 3AB, 2AB, BZ, MA, TR and AXI in water, in the presence of various concentrations of HSA, the shift in the emission spectra of HSA; n= number of calibration points and k_q= the bimolecular quenching constant. Fluorescence lifetime of unquenched HSA (τ)= 2.8ns*

Compound	**[HSA]/ ppb**	**K_{SV}/ M^{-1}**	**k_q/ x 10^7 $M^{-1}s^{-1}$**	**n**	**Shift observed/ nm**
3AB	0.0014	0.0056	0.20	10	23
	0.0038	0.0019	0.068	6	
	0.0067	0.0021	0.075	6	
2AB	0.00096	0.0046	0.16	7	1
	0.0048	0.0053	0.19	7	
	0.0067	0.0056	0.20	6	
BZ	0.000048	0.0025	0.089	6	Unobserved
	0.0014	0.0057	0.20	6	
	0.0048	0.0063	0.23	7	
MA	0.00048	0.035	1.3	5	1
	0.0014	0.015	0.54	5	
	0.0067	0.018	0.64	6	
TR	0.00038	0.32	11.43	7	13
	0.00058	0.015	0.54	5	
	0.00096	0.26	9.3	5	
AXI	0.0017	0.062	2.2	5	1
	0.0023	0.031	1.1	5	
	0.0011	N/A			

Data from the quenching of HSA in the presence of increasing concentrations of each quencher compound were fitted to Stern-Volmer plots. To assess whether the quenching process was collisional or static, the values of K_{SV} were studied in more detail. The bimolecular quenching constant limit for a diffusion-controlled quenching process is 1 x 10^{10} $M^{-1}s^{-1}$ (Nan, Hao, Ye, Feng, & Sun, 2019; Lakowicz, 2006), and the previously measured fluorescence lifetime of tryptophan in water was 2.8ns (tryptophan being the main fluorophore in HSA).

As can be observed (Table 4) the Stern-Volmer constants (gradient of linear line) did not exceed 0.32 M^{-1}. The bimolecular quenching constants determined from the data (Table 4) were therefore no higher than 10^8 $M^{-1}s^{-1}$. This would therefore not rule out a collisional quenching process (Lakowicz, 2006).

In addition, the absorbance spectra of the compounds was observed. An overlap between the absorbance spectra of each compound and the emission spectra of HSA, has been observed in earlier studies with HSA, and was indicative of radiationless energy transfer, and a static quenching process (Lakowicz, 2006). In addition, it was also noticed that high values of K_{SV} were determined for AXI, MA and TR. This might indicate that these complexes were stronger than those formed with the other compounds.

All of these data represent a good method to prove HSA/ drug association.

It has previously been observed that LODs of 1.7ppb perampanel could be detected in human serum. Using capillary electrophoresis, the compounds were then able to be separated (Tůma et al., 2018). In addition, it has been observed that, when interacted, emission spectra, characteristic of each HSA and MA, were visible. As the concentration of MA was increased the peak of each the HSA and MA decreased and increased, respectively (Yue et al., 2009).

Based on the fact that when the interacted compounds were successfully separated the concentration of quencher could be quantified, and the fact that two peaks were observed by fluorimetry, an idea was constructed. Our working hypothesis proposes that as Stern-Volmer plots relate the concentration of quencher to fluorescence intensity of fluorophore, they could be used to quantify an unknown concentration of quencher (the drug associated to the protein).

The fluorescence intensity of a known concentration of HSA was therefore measured, in the absence and presence of increasing compound concentrations. The equation of the line of best fit from each linear plot was then used to determine F_0/F. In a known concentration of HSA, once its fluorescence intensity had been collected, the concentration of the quencher could then be determined.

6.2.2.2 Analytical parameters of HSA containing samples

Using 5-10 concentrations (n) of each guest compound, the constructed Stern-Volmer plots were analytically assessed for their ability to detect the compounds. It was observed (Table 5, Annexe Table 4) that the average linearity range of each 3AB, 2AB, BZ, MA and AXI, in the presence of HSA, spanned over a broad range of concentrations, particularly apparent for the three isomeric compounds. Different concentrations of fluorophore were observed to have different quenching constants, with RSDs less than 8%. The effect of fluorophore concentration is not, however, something often addressed. In addition, it does not feature in the Stern-Volmer equation, implying the quenching extent is fluorophore-concentration independent (Lakowicz, 2006). Although the observation had been commented on, the results of the study were considered with caution as no reasons, other than increased

sensitivity of the fluorophore, were given for this effect (Vaughns, 2007). The quenching of various concentrations of HSA by each compound was therefore investigated.

High regression coefficients in each HSA concentration used, demonstrated that the method was accurate. Intercept values of 1, or close to 1, indicated each compound conformed to the Stern-Volmer equation (Castanho & Prieto, 1998).

As previously mentioned (Chapter 5), an increase in the fluorescence intensity of 0.0011ppb HSA was observed in the presence of AXI. The difference between the emission wavelengths of each compound excluded the possibility of an overlap in its spectra, and was therefore attributed to the formation of an AXI: HSA complex that is more fluorescent than HSA alone. AXI hence may not be a quencher of HSA. Therefore, on this basis a calibration graph was constructed to quantify this particular complex. Regression coefficients and linearity ranges obtained (for AXI in 0.0011ppb HSA), of which were similar to those in the Stern-Volmer plots, evidenced its accuracy and implied the use of each plot to quantify the compounds. Through use of the individual Stern-Volmer equations each equation was applied and studied in more detail (Table 5, Annexe Table 4).

Table 5: *Calibration results of 3AB, 2AB, BZ, MA, TR and AXI in water, in the presence of various concentrations of HSA; RSD= Relative Standard Deviation, r=correlation coefficient (applied data from Table 4)*

Compound	Calibration					
	[HSA]/ ppb	Slope/ x $10^8 M^{-1}$	Intercept	Linearity range/ ppb	r	RSD/ %
3AB	0.0014	0.0056	0.90	74.64-389.45	0.989	1.70
	0.0038	0.0019	0.96	97.36-486.82	0.992	3.30
	0.0067	0.0021	1.00	64.91-292.09	0.997	1.42
2AB	0.00096	0.0046	1.00	49.12-212.86	0.990	7.29
	0.0048	0.0053	0.98	20.47-147.36	0.995	4.96
	0.0067	0.0056	1.00	24.56-122.80	0.997	4.20
BZ	0.000048	0.0025	1.00	32.25-193.50	0.988	4.74
	0.0014	0.0057	0.95	24.19-225.75	0.986	2.17
	0.0048	0.0063	0.95	48.37-290.24	0.994	0.50
MA	0.00048	0.035	1.06	1.14-20.45	0.985	1.01
	0.0014	0.015	1.00	5.11-23.86	0.992	3.91
	0.0067	0.018	1.00	2.88-18.31	0.995	3.95
TR	0.00038	0.32	1.00	2.74-9.21	0.995	2.86
	0.00058	0.015	1.00	1.00-4.98	0.944	8.39
	0.00096	0.26	1.03	1.00-3.73	0.950	3.28
AXI	0.0017	0.062	1.00	4.29-15.01	0.982	3.43
	0.0023	0.031	1.13	3.22-16.08	0.890	2.18
	0.0011	3.1	103.79	10.72-27.69	0.918	2.67

Average recoveries obtained (less than 15%) (Annexe Table 5) for a range of compound concentrations in each of the three HSA solutions used in the study, indicated the method was both suitable and reliable for the detection of the selected compounds.

6.2.3.0 Limits of detection and quantification

To assess each method for its sensitivity and ability to quantify pharmaceutical preparations of drug (Elokely, Eldawy, Elkersh, & El-Moselhy, 2011), the detection limits of the compounds in the various media were evaluated.

With the exception of AXI, lower detection limits of the compounds were observed in the presence of canal water, than in water (Table 6). This medium had previously been determined to have a lower pH and different polarity to that of water (Chapter 4). This may play a role in the improved detection and suggest that slight protonation of the compounds may alter the fluorescence intensity, or influence the lifetime of the species (Lakowicz, 2006). As a result of such an observation, adjustment of the acidity or polarity of the drug matrix may enable enhancement of the detection limits of the compounds to their fullest.

Table 6: *Limit of detection and limit of quantification of 3AB, 2AB, BZ, MA, TR and AXI in water (W) and canal water (C), in the absence and presence of ≈25mg/mL, 12mg/mL, 12mg/mL, 4mg/mL, 12mg/mL and 15mg/mL, respectively (β-CDP in water, Cβ-CDP in canal water), and in the specified concentrations of HSA*

Compound	Medium	Detection limit/ ppb	Quantitation limit/ ppb
3AB	W	1.88	5.70
	C	1.54	4.67
	β-CDP	0.033	0.10
	Cβ-CDP	0.026	0.078
	0.0014 HSA	7.54	22.84
	0.0038 HSA	10.36	31.41
	0.0067 HSA	2.85	8.63
2AB	W	0.011	0.033
	C	0.0066	0.020
	β-CDP	0.0067	0.020
	Cβ-CDP	0.0085	0.026
	0.00096 HSA	5.25	15.90
	0.0048 HSA	1.84	5.59
	0.0067 HSA	3.18	9.63
BZ	W	0.50	1.53
	C	0.16	0.50
	β-CDP	0.023	0.071
	Cβ-CDP	0.050	0.15
	0.00048 HSA	4.75	14.38
	0.0014 HSA	4.16	12.60
	0.0048 HSA	3.74	11.33
MA	W	0.061	0.18
	C	0.034	0.10
	β-CDP	0.047	0.14
	Cβ-CDP	0.084	0.25
	0.0014 HSA	1.99	6.04
	0.00048 HSA	1.40	4.23
	0.0067 HSA	1.32	3.99
TR	W	0.45	1.37
	C	0.089	0.27

	β-CDP	0.43	1.30
	Cβ-CDP	0.0030	0.0092
	0.00038 HSA	0.37	1.12
	0.00058 HSA	0.19	0.58
	0.00096 HSA	0.33	1.01
AXI (3 hours)	W	0.062	0.19
	C	2.38	7.22
	β-CDP	0.17	0.52
	Cβ-CDP	0.91	2.75
AXI HSA	0.0017 HSA	1.01	3.13
	0.0023 HSA	2.70	8.19
AXI (HSA calibration)	0.0011 HSA	31.57	95.67

In the presence of β-CDP, the detection limits of 3AB, BZ and TR were enhanced in both canal water and water, up to 59.2, 21.7 and 29.7 times, respectively. Although not as substantial, β-CDP elevated the intensity of 2AB and MA in water 1.6 times and 1.3 times, respectively, and that of AXI in canal water 2.6 times.

In the presence of HSA, each of the compounds were able to be detected. Increasing the concentration of HSA produced a greater fluorescence signal for BZ and MA and thus, lower detection limits of the drug could be determined. It was, however, observed that lower LODs of both TR and AXI were able to be detected in the presence of the protein, than in its absence.

6.2.4.0 Advantages and limitations of the developed methods

The first method utilised β-CDP to enhance the detection of all studied compounds, up to 59 times. Results from the current study were compared to fluorimetric results from previous studies with β-CD monomers. In previous studies 3.2ppb TR was able to be detected in the presence of ethylenediamine linked β-cyclodextrin dimer (Tang, Liang, Tong, & Li, 2006), and 30ppb BZ was detected by chemiluminescence, gaining little, if any, fluorescence improvements from β-cyclodextrin (X. R. Zhang, Baeyens, Der Weken, Calokerinos, & Imai, 1995). Concentrations of all of these compounds (<1ppb) were able to be detected with β-CDP in the current study.

There were, however, studies in which no better detection to that observed with monomeric cyclodextrins was achieved with β-CDP. 0.0096ppb MA had previously been detected using ethyl substituted β-cyclodextrin (Huang et al., 2011), 3.5 times lower than results from the current study. Such an observation would support results from previous studies, suggesting that each compound was included within the cyclodextrin cavity to form the most energetically stable complex (Perez, Jaime, & Sanchez-Ruiz, 1995). Aside from MA, all compounds studied had improved detection limits in the presence of β-CDP and water, when compared to those in its absence. The lowest concentrations of MA could be detected in canal water, in the absence of β-CDP, implying its intensity was influenced by the solvent. Although improvements in the fluorescence intensity of MA, and a complex were still observed, these were lower than those of the other compounds. It was for this reason that it was not considered cost beneficial to carry out all validation studies for this compound.

An interaction between the compounds and HSA had previously been evidenced for MA, TR and AXI (Tayyab et al., 2016; Tayyab, Zaroog, Feroz, Mohamad, & Malek, 2015; Yue et al., 2009), decreasing the fluorescence intensity of the compounds. This decrease was attributed to a static quenching process for MA and AXI, as a decrease in binding strength was observed at elevated temperatures, however, no comment on the detection of the compounds was made (Yue et al., 2009).

The latter method using HSA enabled each of the investigated compounds to be determined, quantifying concentrations as low as 0.58ppb. It was observed that the LODs of TR were lower than those previously obtained in plasma and urine (200ppb and 2000ppb, respectively using HPLC)(Slobodzian, Hsieh, & Bayne, 1985), human plasma (500ppb through HPLC)(Tadano, Yuhki, Aoki, Miyazaki, & Arita, 1985), rat plasma and brain tissue (LLOQ of 53.50ppb using LC-

MS/MS)(Yang et al., 2018). In addition, LODs were lower for MA than had previously been detected in rat plasma (557ppb through HPLC coupled to MS/MS)(Mehta, Shah, Lohidasan, & Mahadik, 2015).

The current method did not necessarily improve detection of the compounds in biological samples. Lower concentrations had previously been detected in rainbow trout fillet tissue for BZ using RP-HPLC (6ppb)(Meinertz, Stehly, Hubert, & Bernardy, 1999), and in rat serum (7.1ppb in by UPLC-ES-MS/MS)(Hou et al., 2010), and lower LODs were achieved for MA using HPLC coupled to MS/MS (5.74ppb in rat plasma)(Sheng et al., 2014) or HPLC (1ppb in rat plasma or eyes)(Hou et al., 2010)(0.0004ppb and 0.0001ppb in rat blood and eyes, respectively)(H. Zhang et al., 2010)(0.0005ppb in rat blood)(Lai, Lin, Lin, & Tsai, 2003). Our method did, however, have the advantages of rapidity and simplicity, and relatively good performance.

6.3.0 Conclusion

The previously proposed fluorimetric method for the determination of 3AB, 2AB, BZ, MA, TR and AXI in water and canal water, in both the presence and absence of β-CDP was validated as linear, accurate and robust under the conditions outlined. All compounds were evaluated for successful detection in β-CDP when subject to various quality control procedures.

Although not true of all the compounds, the compounds often had superior detection limits in this β-CDP to the other cyclodextrins previously investigated. In addition, the greatest enhancement in detection was able to be achieved for the majority of compounds when using a pH similar to that of biofluids and surface waters.

Furthermore, a method was able to be proposed and tested for the detection of the drugs in HSA, in which Stern-Volmer quenching plots were utilised. This proved to be a novel way in which to detect the compounds studied in HSA, with successful detection being achieved. Lower detection limits were obtained for TR and MA, than those previously reported in biofluids, and in the presence of HSA the compounds were able to be detected (≤10ppb).

Both methods were found to be accurate and robust, with the ability to detect low concentrations of the drugs in both canal water and water, in the presence and absence of β-CDP, and to detect concentrations of the compounds in the presence of HSA.

6.4.0 References

Castanho, M. A., & Prieto, M. J. (1998). Fluorescence quenching data interpretation in biological systems. The use of microscopic models for data analysis and interpretation of complex systems. *Biochimica et Biophysica Acta*, *1373*(1), 1–16.

Elokely, K. M., Eldawy, M. A., Elkersh, M. A., & El-Moselhy, T. F. (2011). Fluorescence Spectrometric Determination of Drugs Containing α-Methylene Sulfone/Sulfonamide Functional Groups Using N-Methylnicotinamide Chloride as a Fluorogenic Agent. *International Journal of Analytical Chemistry*, *2011*, 1–9.

Fülöp, Z., Kurkov, S. V., Nielsen, T. T., Larsen, K. L., & Loftsson, T. (2012). Self-assembly of cyclodextrins: formation of cyclodextrin polymer based nanoparticles. *Journal of Drug Delivery Science and Technology*, *22*(3), 215–221.

Grigoryan, K., Grigoryan, K. R., & Ghazaryan, A. G. (2013). Quenching Mechanism of Human Serum Albumin Fluorescence by Gangleron. *Proceedings of the Yerevan State University. Chemistry and Biology*, *2013*(2), 6–10.HMS (Ed.). (2017). Physical Tests. In *Fluorescence Spectroscopy* (pp. 1–7). Retrieved from https://hmc.usp.org/sites/default/files/documents/HMC/GCs-Pdfs/c853.pdf

Hou, Y., Fan, S., Zhang, H., Gu, Y., Yu, X., & Li, B. (2010). Pharmacokinetic study of mangiferin in rat plasma and retina using high-performance liquid chromatography. *Molecular Vision*, *16*, 1659–1668.

Huang, L., He, J., Lu, R., Ge, X., & Guo, J. (2011). Investigation on a host–guest inclusion system by β-cyclodextrin derivative and its analytical application. *Bioorganic & Medicinal Chemistry Letters*, *21*(4), 1113–1117.

Lai, L., Lin, L.-C., Lin, J.-H., & Tsai, T.-H. (2003). Pharmacokinetic study of free mangiferin in rats by microdialysis coupled with microbore high-performance liquid chromatography and tandem mass spectrometry. *Journal of Chromatography. A*, *987*(1–2), 367–374.

Lakowicz, J. R. (2006). *Principles of fluorescence spectroscopy*. Springer.

Mehta, P., Shah, R., Lohidasan, S., & Mahadik, K. R. (2015). Pharmacokinetic profile of phytoconstituent(s) isolated from medicinal plants—A comprehensive review. *Journal of Traditional and Complementary Medicine*, *5*(4), 207–227.

Meinertz, J. R., Stehly, G. R., Hubert, T. D., & Bernardy, J. A. (1999). Liquid chromatographic determination of benzocaine and N-acetylbenzocaine in the edible fillet tissue from rainbow trout. *Journal of Chromatography A*, *855*(1), 255–260.

Nan, Z., Hao, C., Ye, X., Feng, Y., & Sun, R. (2019). Interaction of graphene oxide with bovine serum albumin: A fluorescence quenching study. *Spectrochimica Acta Part A: Molecular and Biomolecular Spectroscopy*, *210*, 348–354.

Perez, F., Jaime, C., & Sanchez-Ruiz, X. (1995). MM2 Calculations on Cyclodextrins:Multimodal Inclusion Complexes. *The Journal of Organic Chemistry*, *60*(12), 3840–3845.

Sheng, N., Zhi, X., Yuan, L., Zhang, Z., Jia, P., Zhang, X., Wang, X. (2014). Pharmacokinetic and excretion study of three secoiridoid glycosides and three flavonoid glycosides in rat by LC–MS/MS after oral administration of the Swertia pseudochinensis extract. *Journal of Chromatography B*, *967*, 75–83.

Slobodzian, D. K., Hsieh, J. Y., & Bayne, W. F. (1985). Simultaneous determination of tranilast and metabolites in plasma and urine using high-performance liquid chromatography. *Journal of Chromatography*, *345*(2), 345–354.

Song, C., Yang, X., Wang, K., Wang, Q., Liu, J., Huang, J., Liu, W. (2018). Sensitive detection of T4 polynucleotide kinase activity based on β-cyclodextrin polymer enhanced fluorescence combined with exonuclease reaction. *Talanta*, *180*(2018), 271–276.

Tadano, K., Yuhki, Y., Aoki, I., Miyazaki, K., & Arita, T. (1985). High-performance liquid chromatographic determination of tranilast in plasma. *Journal of Chromatography*, *341*(1), 228–231.

Tang, B., Liang, H., Tong, L., & Li, P. (2006). Synthesis of ethylenediamine linked β-cyclodextrin dimer and its analytical application for tranilast determination by spectrofluorimetry. *Bioorganic & Medicinal Chemistry*, *14*(11), 3947–3952.

Tayyab, S., Izzudin, M. M., Kabir, M. Z., Feroz, S. R., Tee, W.-V., Mohamad, S. B., & Alias, Z. (2016). Binding of an anticancer drug, axitinib to human serum albumin: Fluorescence quenching and molecular docking study. *Journal of Photochemistry and Photobiology B: Biology*, *162*, 386–394.

Tayyab, S., Zaroog, M. S., Feroz, S. R., Mohamad, S. B., & Malek, S. N. A. (2015). Exploring the interaction between the antiallergic drug, tranilast and human serum albumin: Insights from calorimetric, spectroscopic and modeling studies. *International Journal of Pharmaceutics*, *491*(1–2), 352–358.

Tůma, P., Bursová, M., Sommerová, B., Horsley, R., Čabala, R., & Hložek, T. (2018). Novel electrophoretic acetonitrile-based stacking for sensitive monitoring of the antiepileptic drug perampanel in human serum. *Journal of Pharmaceutical and Biomedical Analysis*, *160*, 368–373.

Vaughns, C. (2007). *Stern-Volmer Quenching of Conjugated Polymers: A Study of Fluorophore Concentration* (Georgia Institute of Technology). Retrieved from https://smartech.gatech.edu/bitstream/handle/1853/19941/vaughns_christopher_f_200712_ro.pdf

Yan Lee, L. (2016). *Study Of The Photodegradation And Photostability Of Anti-Cancer Drugs In Different Media Towards The Development Of Both New Actinometers And Liquid Formulations* (De Montfort University). Retrieved from https://www.dora.dmu.ac.uk/bitstream/handle/2086/12188/Lok Yan%27s Thesis.pdf?sequence=1&isAllowed=y

Yang, W., Sabi-mouka, E. M. B., Wang, L., Shu, C., Wang, Y., Ding, J., & Ding, L. (2018). Determination of tranilast in bio-samples by LC–MS/MS: Application to a pharmacokinetic and brain tissue distribution study in rats. *Journal of Pharmaceutical and Biomedical Analysis*, *147*, 479–484.

Yue, Y., Chen, X., Qin, J., & Yao, X. (2009). Characterization of the mangiferin–human serum albumin complex by spectroscopic and molecular modeling approaches. *Journal of Pharmaceutical and Biomedical Analysis*, *49*(3), 753–759.

Zhang, H., Hou, Y., Liu, Y., Yu, X., Li, B., & Cui, H. (2010). Determination of Mangiferin in Rat Eyes and Pharmacokinetic Study in Plasma After Oral Administration of Mangiferin-Hydroxypropyl-Beta-Cyclodextrin Inclusion. *Journal of Ocular Pharmacology and Therapeutics*, *26*(4), 319–324.

Zhang, X. R., Baeyens, W. R. G., Der Weken, G. V., Calokerinos, A. C., & Imai, K. (1995). Chemiluminescence determination of some local anaesthetics. *Analytica Chimica Acta*, *303*(1), 137–142.

Chapter 7:

Photokinetic study of TR in ethanol

Chapter 7: Photokinetic study of TR in ethanol

7.1.0 Introduction

7.1.1 Introduction

Tranilast (TR) (N-(3,4-dimethoxycinnamoyl) anthranilic acid) is a poorly soluble (Darakhshan & Pour, 2015) anti-allergic drug, used to treat bronchial asthma, atopic rhinitis and atopic dermatitis. It has been found to photodegrade under UV-A/ B irradiation (Kawabata, Yamamoto, Debari, Onoue, & Yamada, 2010) and fluorescent light (Naohide Hori et al., 1999) to form reversible *cis*-isomer and irreversible dimer products (Hirayama, Utsuki, & Uekama, 1991).

The degradation of the *trans*-isomer in aqueous solution has previously been quantified, forming 6.2% *cis*-isomer, and 62.5% dimer products (Naohide Hori et al., 1999). In studies measuring its degradation rate, the data was treated using zero-order kinetics (Utsuki, Hirayama, & Uekama, 1993).

Our group has previously reported a new method for the elucidation of photokinetics, which has been used and applied to describe unimolecular AB(1Φ) and reversible AB(2Φ) photodegradation reactions. The model can be used to determine the quantum yields of the photoreaction and overcomes the limitations of thermal reaction orders (Maafi & Lee, 2015a). The aim of the current study is to investigate the dependency of quantum yields on irradiation wavelength and demonstrate the potential use of TR in actinometry.

7.1.2.0 The Mathematical framework

7.1.2.1 Φ-order kinetics for non-isosbestic irradiation

As mentioned (Chapter 1), the use of zero-, first- and second- order cannot accurately describe photochemical reactions. The recently proposed approach, based on Φ-order kinetics, can therefore be used to describe the time evolution of the concentration of the species through one of the related quantities, such as the medium absorbance. Φ-order kinetics can be applied when the medium is exposed to non-isosbestic and monochromatic irradiation at a constant temperature. This model overcomes issues such as multiple interpretations of data, allows for the quantum yields to be determined, can uniquely characterise photokinetic data and can allow for the drug compound to be utilised as an actinometer.

The model equations for Φ-order kinetics which describe the photoreversible transformation of the native species (A) to its photoproduct (B) can be characterised by the forward ($\Phi_{AB}^{\lambda_{irr}}$) and reverse ($\Phi_{BA}^{\lambda_{irr}}$) quantum yields. Species A should be continuously irradiated with a monochromatic beam (where the non-isosbestic wavelength is $I_{\lambda_{irr}}$). Both species A and B should absorb different amounts of incident light ($P_{\lambda irr}$) and therefore have different absorptivities (ε), of which neither are equal to zero ($\varepsilon_A^{\lambda_{irr}} \neq \varepsilon_A^{\lambda_{irr}} \neq 0$).

Eq. 1 can be applied when the absorbance of the medium has been measured at the observation wavelength, as opposed to the irradiation wavelength. $I_{\lambda_{irr}}$ is the excitation light across the medium, whereas $I_{\lambda_{obs}}$ is the optical path length of the light within the sample. Such values may therefore differ to one another.

The coefficients: $A_{tot}^{\frac{\lambda_{irr}}{\lambda_{obs}}}(t)$, $A_{tot}^{\frac{\lambda_{irr}}{\lambda_{obs}}}(0)$, $A_{tot}^{\frac{\lambda_{irr}}{\lambda_{obs}}}(\infty)$, $A_{tot}^{\frac{\lambda_{irr}}{\lambda_{irr}}}(0)$, $A_{tot}^{\frac{\lambda_{irr}}{\lambda_{irr}}}(\infty)$ are therefore the total absorbances of the medium (at $I_{\lambda_{obs}}$) at: reaction time (t), at the initial time (0) and the photostationary state (pss (t=∞)). At a given irradiation wavelength the reaction is monitored at either a specific observed wavelength ($\lambda_{irr}/\lambda_{obs}$) or the same wavelength ($\lambda_{irr}/\lambda_{irr}$). It is assumed that no by-products are formed:

$$A_{tot}^{\frac{\lambda_{irr}}{\lambda_{obs}}}(t) = A_{tot}^{\frac{\lambda_{irr}}{\lambda_{obs}}}(\infty) + \frac{A_A^{\frac{\lambda_{irr}}{\lambda_{obs}}}(0) - A_{tot}^{\frac{\lambda_{irr}}{\lambda_{obs}}}(\infty)}{A_A^{\frac{\lambda_{irr}}{\lambda_{irr}}}(0) - A_{tot}^{\frac{\lambda_{irr}}{\lambda_{irr}}}(\infty)} \times \frac{I_{\lambda_{obs}}}{I_{\lambda_{irr}}} \times log\left[1 + \left(10^{\left[\left(A_A^{\frac{\lambda irr}{\lambda irr}}(0) - A_{tot}^{\frac{\lambda irr}{\lambda irr}}(\infty)\right) \times \frac{I_{\lambda irr}}{I_{\lambda obs}}\right]} - 1\right) \times e^{-k_{A\rightleftharpoons B}^{\frac{\lambda_{irr}}{}} \times t}\right]$$

Eq. 1

The exponential factor, $k_{A\rightleftharpoons B}^{\lambda_{irr}}$, representing the overall rate-constant can be analytically represented by:

$$k_{A\rightleftharpoons B}^{\lambda_{irr}} = \left(\Phi_{A\rightarrow B}^{\lambda_{irr}} \times \varepsilon_A^{\lambda_{irr}} + \Phi_{B\rightarrow A}^{\lambda_{irr}} \times \varepsilon_B^{\lambda_{irr}}\right) \times I_{\lambda_{irr}} \times F_{\lambda_{irr}}(\infty) \times P_{\lambda_{irr}} = \beta_{\lambda_{irr}} \times P_{\lambda_{irr}}$$

Eq. 2

Where $\Phi_{A\rightarrow B}^{\lambda_{irr}}$and $\Phi_{B\rightarrow A}^{\lambda_{irr}}$ are the forward and reverse quantum yields of the reaction photochemical stages at the specific irradiation wavelength ($I_{\lambda_{irr}}$), $P_{\lambda_{irr}}$is the radiant power (in einstein dm^{-3}), $\beta_{\lambda_{irr}}$is a proportionality factor between the overall rate-constant and the radiant power, and $F_{\lambda_{irr}}(\infty)$ is the time-independent photokinetic factor which can be expressed as:

$$F_{\infty}^{\lambda_{irr}} = \frac{1-10^{-\left(A_{tot}^{\frac{\lambda_{irr}}{\lambda_{irr}}}(\infty) \times (I_{\lambda_{irr}}/I_{\lambda_{obs}})\right)}}{\left(A_{tot}^{\frac{\lambda_{irr}}{\lambda_{irr}}}(\infty) \times (I_{\lambda_{irr}}/I_{\lambda_{obs}})\right)}$$

Eq. 3

7.1.2.2 Elucidation method of TR photoreversible reaction

The three unknown parameters (photochemical forward and reverse quantum yields and absorption spectrum of product B) cannot be determined using the data obtained from Eq. 1. An elucidation method can therefore be accomplished in three stages.

Firstly, the photodegradation reaction under monochromatic irradiation, at a non-isosbestic wavelength, can be monitored at a specific wavelength by HPLC. The concentration of the photoproduct can be determined from: $C_B(\infty) = C(\infty) - C_A(\infty)$.

The absorption spectrum of the photoproduct ($\varepsilon_B^{\lambda_{irr}}$) can then be reconstructed using the following equation:

$$\varepsilon_B^{\lambda_{irr}} = \frac{A_{tot}^{\frac{\lambda_{irr}}{\lambda_{obs}}}(\infty) - C_A(\infty) \times \varepsilon_A^{\lambda_{irr}} \times I_{\lambda_{obs}}}{C(0) - C_A(\infty) \times I_{\lambda_{obs}}} \qquad \textbf{Eq. 4}$$

If $\varepsilon_B^{\lambda_{irr}}$ is deduced, the reaction quantum yields at any irradiation wavelength (and thus the absolute values of $\Phi_{A\to B}^{\lambda_{irr}}$ and $\Phi_{B\to A}^{\lambda_{irr}}$ at any non-isosbestic or isosbestic wavelengths) can be determined. $\Phi_{A\to B}^{\lambda_{irr}}$ can be established using:

$$\Phi_{A\to B}^{\lambda_{irr}} = \frac{\upsilon_{0(cld.)}^{\lambda_{irr}/\lambda_{obs}}}{(\varepsilon_B^{\lambda_{obs}} - \varepsilon_A^{\lambda_{obs}}) \times I_{\lambda_{irr}} \times P_{\lambda_{irr}} \times F_0^{\lambda_{irr}} \times C_0} \qquad \textbf{Eq. 5}$$

Using the initial velocity ($\upsilon_0^{\lambda_{irr}/\lambda_{obs}}$) as obtained from:

$$\upsilon_0^{\lambda_{irr}/\lambda_{obs}} = \frac{A_{tot}^{\frac{\lambda_{irr}}{\lambda_{obs}}}(0) - A_{tot}^{\frac{\lambda_{irr}}{\lambda_{obs}}}(\infty)}{A_{tot}^{\frac{\lambda_{irr}}{\lambda_{irr}}}(0) - A_{tot}^{\frac{\lambda_{irr}}{\lambda_{irr}}}(\infty)} \times \frac{K_{A\rightleftharpoons B(mod.)}^{\lambda_{irr}}}{Ln(10) \times I_{\lambda_{irr}}/I_{\lambda_{obs}}} \left(10^{(A_{tot}^{\frac{\lambda_{irr}}{\lambda_{irr}}}(\infty) - A_{tot}^{\frac{\lambda_{irr}}{\lambda_{irr}}}(0) \times (I_{\lambda_{irr}}/I_{\lambda_{obs}})} - 1 \right) \qquad \textbf{Eq. 6}$$

By fitting the HPLC data to the concentration profiles $K_{A\rightleftharpoons B}^{\lambda_{irr}}$ can be determined, overcoming the requirement for an isosbestic irradiation wavelength to be used. This value can be used to determine the final unknown, $\Phi_{B\rightarrow A}^{\lambda_{irr}}$

$$\Phi_{B\rightarrow A}^{\lambda_{irr}} = \frac{1}{\varepsilon_B^{\lambda_{irr}}}\left(\frac{k_{A\rightleftharpoons B}^{\lambda_{irr}}}{I_{\lambda_{irr}} \times P_{\lambda_{irr}} \times F_{\lambda_{irr}(\infty)}}\right) - \Phi_{A\rightarrow B}^{\lambda_{irr}} \times \varepsilon_A^{\lambda_{irr}} \qquad \textbf{Eq. 7}$$

The equilibrium constant $K_{A\rightleftharpoons B}^{\lambda_{irr}}$ for such non-isosbestic irradiations is equal to the ratio of the quantum yield values at $I_{\lambda_{irr}}$:

$$K_{A\rightleftharpoons B}^{\lambda_{irr}} = \frac{C_B(\infty)}{C_A(\infty)} = \frac{\Phi_{A\rightarrow B}^{\lambda_{irr}} \times \varepsilon_A^{\lambda_{irr}}}{\Phi_{B\rightarrow A}^{\lambda_{irr}} \times \varepsilon_B^{\lambda_{irr}}} \qquad \textbf{Eq. 8}$$

The quantum yields and absorption coefficients at any irradiation can then be used to determine the $K_{A\rightleftharpoons B}^{\lambda_{irr}}$ of the reaction for the selected irradiation wavelengths.

The value of $K_{A\rightleftharpoons B}^{\lambda_{irr}}$ is independent of the initial concentration of the species. Lower concentrations than those used for the HPLC experiment can therefore be used for spectroscopic measurements.

7.2.0 Results

7.2.1 Photodegradation of TR in ethanol

The electronic absorption spectrum of TR in ethanol can be categorised by broad absorption spectrum with two main absorption regions from 200-250nm and 260-400nm. No absorbance of the compound or its photoproducts was observed outside the UV region. The main maximum peaks are at 336nm and 200nm, with the former having a higher absorbance intensity.

Upon UV light exposure of the compound in ethanolic solution, decreases in the 260-400nm absorption region were observed, along with an increase in the region 200-230nm. The presence of isosbetic points indicates the reaction proceeds smoothly (Fig. 1).

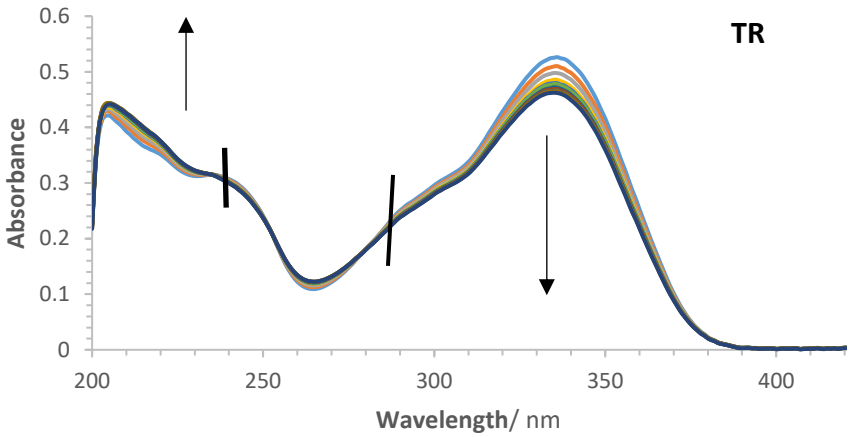

Figure 1: *Evolution of the electronic absorption spectra of 1.53 x 10^{-5}M TR, in ethanol, subjected to a continuous irradiation with a 330nm monochromatic beam, respectively. The arrows indicate the direction of the evolution of absorption maxima during photoreaction. The arrows and vertical lines represent the direction of the absorbance change, and the isosbestic points, respectively*

As can be observed, the photodegradation rate of the first stage of the TR conversion *(trans* ⇌ *cis*) is greater than that of the second stage (Fig. 2). Closer observation of the first stage of the process indicated that after ≈1,500 seconds a plateau in the absorbance change was reached. Such an observation would indicate that this *trans* ⇌ *cis* conversion had finished before a second photoreaction began. The variation in photodegradation rate between these two processes, and the fact that the second photoreaction process was slower than that of the first stage, and did not reach a plateau, would indicate that for more reliable determination of the $k_{A\rightleftharpoons B}^{\lambda_{irr}}$ values, only the first section of the photodegradation should be considered (*trans* ⇌ *cis*)(Maafi & Lee, 2015b).

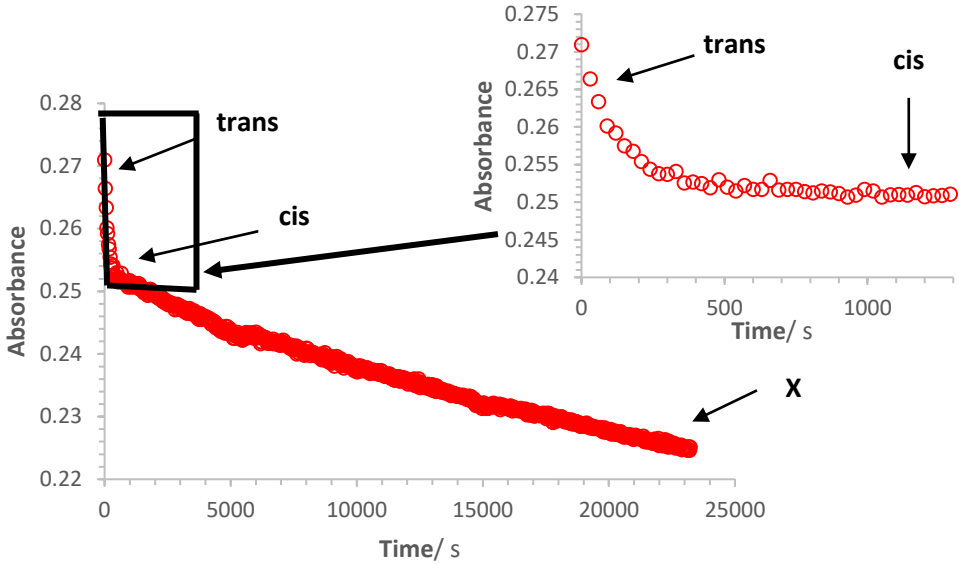

Figure 2: *Effect of irradiation on the photodegradation traces of TR (1.53 x 10^{-5}M), in ethanol, subjected to continuous irradiation with a 330nm monochromatic beam*

Such observations would suggest various π→π* electronic transitions in the aromatic ring. As can be observed (Fig. 2) the time it took for TR to photodegrade was >25,000s.

$$trans \underset{\Phi_{BA}^{\lambda_{irr}}}{\overset{\Phi_{AB}^{\lambda_{irr}}}{\rightleftarrows}} cis \longrightarrow X \qquad \textbf{Eq. 12}$$

7.2.2 Modelling of TR photodegradation kinetics

Ethanolic solutions of TR were exposed to different irradiation wavelengths from various regions of its absorption spectra (245nm, 265nm, 290nm, 300nm, 310nm, 320nm, 330nm, 340nm, 350nm) and the photodegradation kinetics were studied. The variation in the absorbance was recorded at a specific observation wavelength. Successful fitting of the experimental traces to the Φ-order kinetics model confirmed it was a good description of the data (Fig. 3)

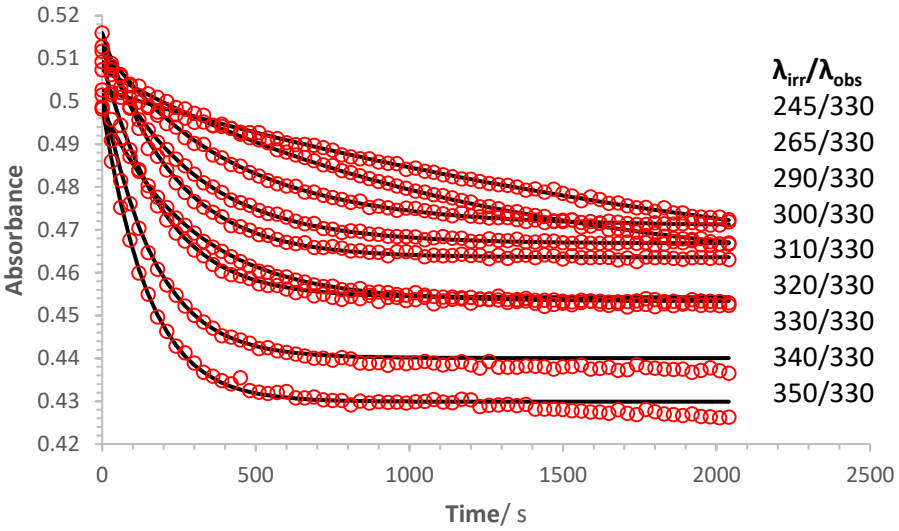

Figure 3: *Photokinetic profiles of TR in ethanol (1.53 x 10^{-5}M) obtained at different irradiation wavelengths (λ_{irr}=245, 265, 290, 300, 310, 320, 330, 340 and 350nm) and observed at λ_{obs}=330. The circles represent experimental data, whereas the solid lines represent the fitting of the traces with Eq. 1*

Degradation of TR was more rapid at longer wavelengths, in the range 320nm-350nm, than at shorter wavelengths (Table 1).

Such an observation could indicate that the photodegradation of TR spans the UV-A spectral range. There did not appear to be a relationship between the determined $k_{A\rightleftharpoons B}^{\lambda_{irr}}$ values and the $P_{\lambda irr}$ values, each independent of the other (Table 1). Such an observation would demonstrate that the rate of TR degradation was irradiation wavelength-specific and

conforms to the Φ-order kinetics model. This demonstrates the advantage of using Φ-order kinetics over classical thermal reaction equations, and thus that the same experiment performed in different conditions, or using a different concentration of compound, would give different results. This would cause difficulties if using thermal reaction orders.

Table 1: *Overall rate-constants, spectroscopic and kinetic parameters of TR for a set of monochromatic irradiation wavelengths in ethanol at 22°C*

λ_{irr}/nm	$A_{tot}^{\lambda_{irr}/330}(0)$	$P_{\lambda_{irr}}$ x 10^7/ Einstein s^{-1} dm^{-3})	$A_{tot}^{\lambda_{irr}\lambda_{irr}}(\infty)$	$K_{A\rightleftharpoons B}^{\lambda_{irr}}$/$s^{-1}$
350	0.50	9.11	0.341	0.0074
340	0.50	6.68	0.436	0.0065
330	0.51	5.33	0.454	0.0042
320	0.52	4.62	0.399	0.0046
310	0.50	4.03	0.313	0.0035
300	0.51	4.20	0.283	0.0035
290	0.51	3.08	0.241	0.0025
280	0.54	3.63	0.192	0.0017
265	0.51	5.19	0.145	0.00082
245	0.50	4.17	0.318	0.00042

7.2.3 HPLC monitoring of TR photodegradation kinetics

HPLC monitoring of the monochromatic wavelength of TR at 330nm showed the presence of the parent compound and one photoproduct (Annexe Fig. 25). The concentration profiles of these isomers determined in the specific conditions indicated that at the photostationary state (Pss) ≈73% of the compound remained (*trans*-TR), whereas the remainder had been converted to the *cis*-isomer (Fig. 4).

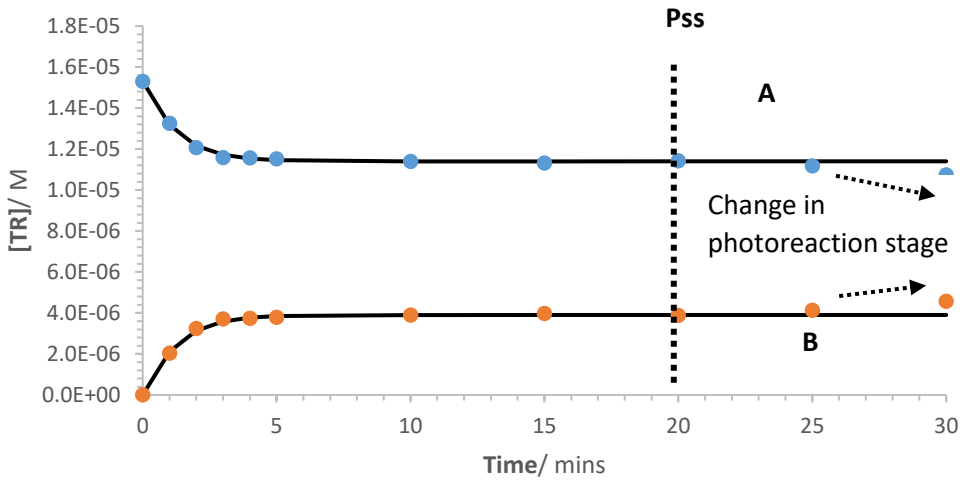

Figure 4: *(A) Evolution of TR concentration (1.53 x 10^{-5}M) over the period of photodegradation and (B) the formation of its photoproduct. The reaction was monitored by HPLC under continuous irradiation from a monochromatic beam at 330nm ($P_{\lambda_{330}}$=5.33 x 10^{-7} einstein s^{-1} dm^3)*

The HPLC data was successfully fitted to the first-order equation for a photoreversible reaction (Eq. 1), and the rate of the overall photodegradation $k_{A\rightleftharpoons B}^{\lambda_{irr}}$ was acquired as the fitting parameters (Eqs. 5-7). This would therefore allow for the forward and reverse quantum yields at the non-isosbestic wavelength to be determined (Table 2). The plateau observed in the HPLC data (between the *trans* and *cis* isomers) occurred at the same stage as in the absorbance traces (25*60=1500s), further supporting the absorption results and providing further evidence of multiple photoreactions. Such an observation would account for the changes observed in the absorption spectra (Fig. 1).

7.2.4 Elucidation of absorption spectra

Eq. 4 could then be used to acquire the value of $\varepsilon_B^{\lambda_{irr}}$. By applying Eq. 4 to TR, and using the spectrum of the medium at pss (∞), data from the HPLC experiment, and the value of the equilibrium constant, $k_{A\rightleftharpoons B}^{\lambda_{irr}}$, the full spectrum of the photoproduct could be reconstructed. The electronic absorption spectra of the two isomers overlap (*E-, Z-*). The absorption coefficient of the *Z*-isomer was lower in the regions 270-400nm, and 240nm-250nm, and higher from 200-230nm and 250-280nm than that of the *E*-isomer (Fig. 5).

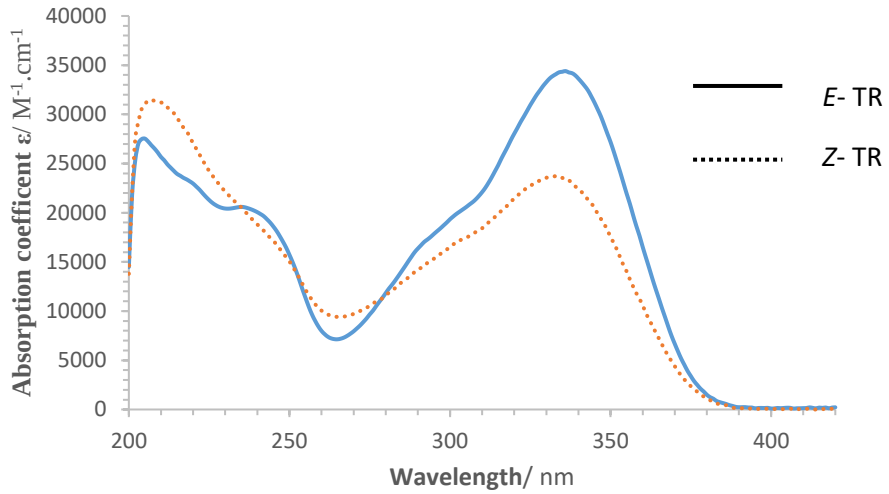

Figure 5: *Electronic absorption spectra (absorption coefficient units) of E-(native) and Z-(photoproduct) TR*

7.2.5 TR photodegradation quantum yields

From knowledge of the photoproduct absorption coefficients, the absolute values of the quantum yields for both the *cis* and *trans* isomer phototransformations can be obtained for various wavelengths, using Eqs. 5 and 6 (Table 2). It can be observed that the quantum yield for the A→B transformation of TR increases with increasing irradiation wavelength (Table 2) and is less sensitive to wavelengths from 290-350nm. These values were consistently lower than those for the reverse reaction, in which 7 times increase in the quantum yields were

obtained from 290-350nm. The greatest variation in $\Phi_{A\rightarrow B}^{\lambda irr}$ was observed from 245nm-290nm, in which the values of $\Phi_{A\rightarrow B}^{\lambda irr}$ increased 5.5 times (Table 2). The results would suggest that the *cis*→*trans* quantum yields were 2 times less efficient than that of the *trans*→*cis*.

Table 2: *Quantum yields, overall rate –constant, proportionality factor and radiant power values for TR photodegradation reactions under various monochromatic irradiation wavelengths*

λ_{irr}(nm)	$P_{\lambda_{irr}}$x 10^7/ Einstein s^{-1} dm^{-3}	$\frac{^{\lambda}irr}{A_{tot}^{\lambda_{irr}}}(\infty)$	$k_{A\rightleftharpoons B}^{\lambda irr}$	$\upsilon_0^{\lambda_{irr}/\lambda_{330}}$ x 10^5/ s^{-1}	$\varepsilon_A^{\lambda_{irr}}$/ M^{-1}	$\varepsilon_B^{\lambda_{irr}}$/ M^{-1}	$F_{\lambda irr}(0)$	$\Phi_{A\rightarrow B}^{\lambda irr}$	$\Phi_{B\rightarrow A}^{\lambda irr}$
245	0.326	0.405	0.00045	-0.38	18596.81	17135.70	1.19	0.0080 ± 0.30	0.017 ± 0.65
265	0.131	0.507	0.0011	1.40	7136.29	9408.13	1.73	0.026 ± 0.015	0.044 ± 0.025
290	0.247	0.432	0.0029	-1.93	16357.73	14277.49	1.37	0.044 ± 0.26	0.19 ± 1.10
300	0.295	0.330	0.0038	-4.38	19333.85	16543.82	1.26	0.050 ± 0.11	0.15 ± 0.34
310	0.330	0.295	0.0039	-6.21	22091.30	18415.90	1.18	0.054 ± 0.073	0.15 ± 0.21
320	0.432	0.247	0.0048	-14,63	28027.83	21412.0	1.00	0.055 ± 0.13	0.16 ± 0.36
330	0.51	0.193	0.0055	-26.72	33273.85	23552.46	0.89	0.057 ± 0.27	0.15 ± 0.73
340	6.68	0.131	0.0065	-39.23	3334.25	22365.76	0.89	0.058 ± 0.039	0.13 ± 0.075
350	9.11	0.326	0.0078	-43.27	27192.99	17539.61	1.04	0.058 ± 0.13	0.12 ± 0.27

In addition, there is a linear correlation between the irradiation wavelengths and the ratio of quantum yields ($\Phi_{B\to A}^{\lambda irr}/\Phi_{A\to B}^{\lambda irr}$). Such an observation would not support the quantum yield ratio predicted by Kasha's rule, which states that the quantum yield is not dependent on the wavelength. This has previously been confirmed by our group (Maafi & Lee, 2015b), and would evidence the necessity for monochromatic light to be used for more accurate determination of quantum yields.

The evolution of the quantum yields with irradiation wavelengths (Eq. 13 and 14) can be decribed by a sigmoid pattern to represent the forward quantum yield values, and a triangular pattern to represent those of the reverse (Fig. 6):

$$\Phi_{A\to B}^{\lambda irr} = 0.0055 + \frac{0.052}{1+12\times e^{-0.1(\lambda_{irr}-254)}} \qquad \textbf{Eq. 13}$$

$$\Phi_{B\to A}^{\lambda 265-290} = 0.0057 \times \lambda_{irr} - 1.4618 \qquad \textbf{Eq. 14}$$

$$\Phi_{B\to A}^{\lambda 290-350} = 0.0011 \times \lambda_{irr} - 0.5055$$

This can allow for the values of the quantum yield to be determined at any irradiation wavelength, using the fewest experimental results. The linear relationship between the determined quantum yield and the calculated experiment (Fig. 6), confirmed the

effectiveness of the technique for the determination of the quantum yields at wavelengths from 254-350nm, through use of the appropriate equation (Eq. 13-14, Fig. 6).

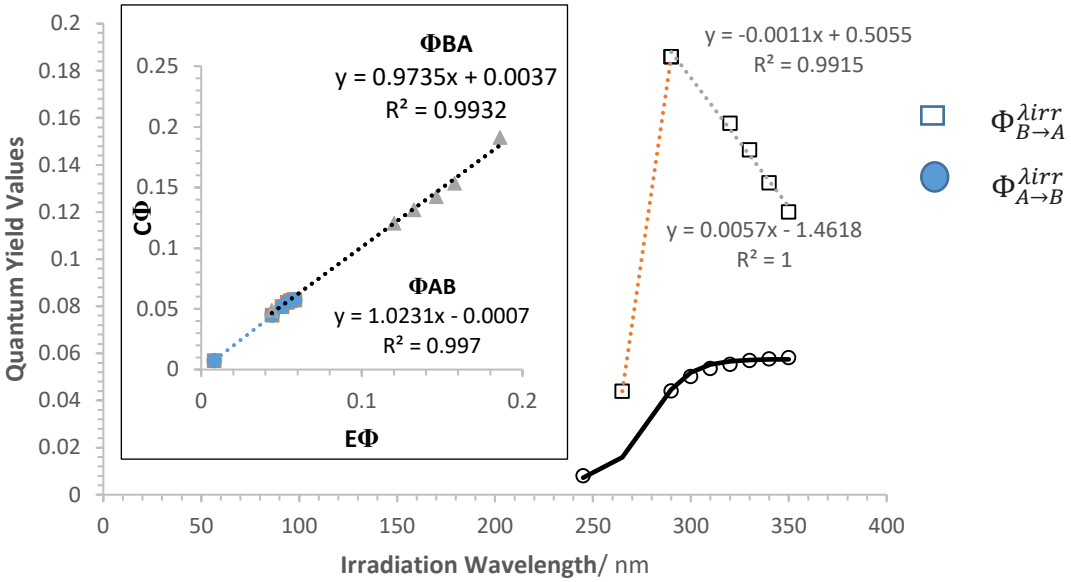

Figure 6: *Sigmoid and triangular patterns (Eq. 13-14) obeyed by the experimental quantum yield values ($\Phi_{A\to B}^{\lambda irr}$ and $\Phi_{B\to A}^{\lambda irr}$), using values of TR and its photoproduct measured for various irradiation wavelengths. Inset: Relationship between the experimental quantum yields (EΦ) and calculated quantum yields (CΦ) of $\Phi_{A\to B}^{\lambda irr}$ and $\Phi_{B\to A}^{\lambda irr}$*

7.2.6 TR actinometry

It has been stated that for photostability testing quinine hydrochloride can be used as an actinometer, however it is limited as it is not thermally stable, and is rarely used to investigate photodegradation processes in solution. Through the use of Φ-order kinetics, however, drug compounds may be used as actinometers.

The potential for TR to be used as an actinometer was assessed by measuring the photoreactivity of the species at different wavelengths (Table 1).

The value of $\beta_{\lambda irr}$ was calculated from Eq. 2 and plotted graphically to obtain a sigmoid shape (Fig. 7), using the following formula:

$$\beta_{\lambda irr} = 882040 \times \left(\frac{1}{86.70735}\right) \times e^{-\left(\frac{\lambda_{irr}-326.5}{2394.32}\right)} \qquad \textbf{Eq. 15}$$

Furthermore, the actinometry equations can be applied to determine the radiant power of TR, from an unknown light source, within this wavelength range:

$$P_{\lambda irr} = \frac{k_{A \rightleftharpoons B}^{\lambda irr}}{\beta_{\lambda irr}} \qquad \textbf{Eq. 16}$$

If the variation in absorbance is observed at 330nm and fitted to Eq. 1 then the value of $k_{A \rightleftharpoons B}^{\lambda irr}$ can be determined. This will allow for $\beta_{\lambda irr}$ to be calculated, and thus the deduction of $P_{\lambda irr}$.

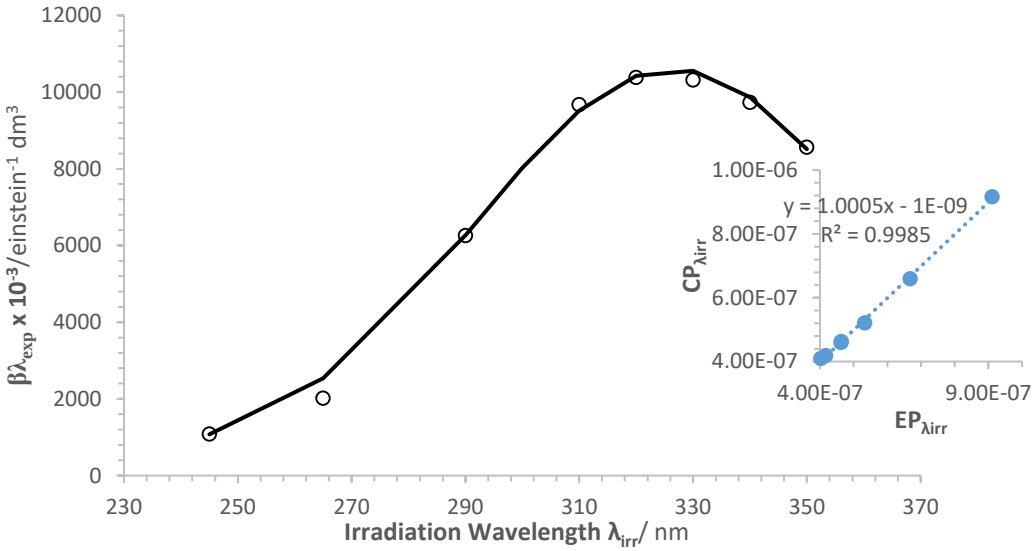

Figure 7: *Relationship between $\beta_{\lambda irr}$ with irradiation wavelength, $\beta_{\lambda irr}$ is expressed in einstein^{-1}dm^3. Inset: Linear relationship between experimental radiant power ($EP_{\lambda irr}$) and calculated radiant power ($CP_{\lambda irr}$)*

The success and reliability of TR as an actinometer was evidenced by a good linear correlation between both the experimental and calculated power values (Fig. 7).

7.2.7 Effect of TR concentration

Various concentrations of TR in ethanol from within the linearity range were selected (2.06 x 10^{-5}-3.86 x 10^{-6}M) to investigate their effect on the photodegradation rate of TR. Each solution was subject to a particular irradiation wavelength (λ_{irr}=330nm), and the wavelength monitored at λ_{obs}=330nm, maintaining a constant radiant power. The kinetic profiles and overall rate-constants are presented in Table 3.

Table 3: *Initial concentration, overall rate-constants, absorbance at the photostationary phase and photokinetic factor of TR photodegradation measured at 330nm*

$C_{TR}(0)$ x 10^{-5}/ M	$A_{\infty}^{\frac{\lambda_{irr}}{\lambda_{obs}}}(t)$	$F_{\infty}^{\lambda irr}$	$k_{TR}^{\lambda_{irr}}$ / s^{-1}	% degradation
2.06	0.542	1.32	0.0072	16.24
1.53	0.412	1.49	0.0076	36.30
1.38	0.374	1.54	0.0078	42.17
1.15	0.312	1.64	0.0080	51.72
0.918	0.256	1.74	0.0082	60.41
0.84	0.251	1.75	0.0083	61.28
0.77	0.225	1.80	0.0084	65.27
0.61	0.173	1.90	0.0086	73.31
0.54	0.155	1.94	0.0087	76.06
0.38	0.107	2.04	0.0090	83.52

The data was well fitted to the Φ-order equation, and it was observed that there was 16% degradation over two minutes when higher concentrations of TR were used (2.06 x 10^{-5}M), when compared to the 83%, in the presence of 3.83 x 10^{-6}M TR.

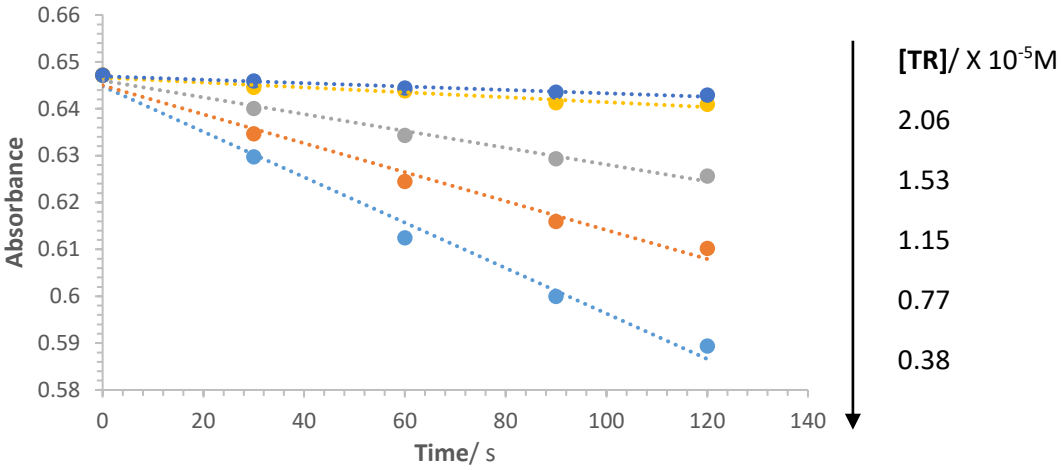

Figure 8: *Effect of increasing TR concentrations on the photodegradation traces of TR in ethanol when irradiated at 330nm and observed at 330nm*

According to Eq. 3 the reduction in photodegradation rate is related to the photokinetic factor, as this photokinetic factor is influenced by the absorbance of the species.

Linear relationships between $k_{A\rightleftharpoons B}^{\lambda_{irr}}$ and $F_{Pp}^{\lambda irr}$ were established with an intercept close to zero and high correlation coefficient (Fig. 9). Such an observation would indicate that the photoreaction is concentration dependent and thus zero- and first-order reaction mechanisms are unsuitable and unreliable for the treatment of photodegradation kinetic data of this compound.

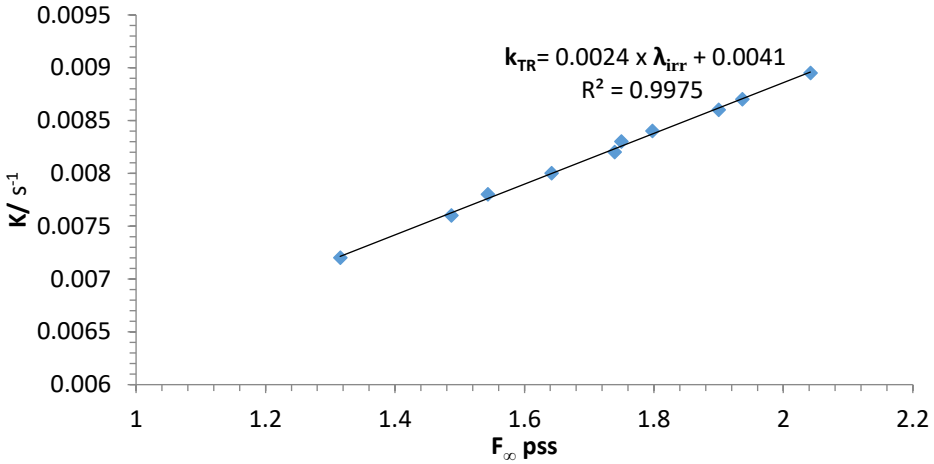

Figure 9: *Linear relationship between TR concentration and overall rate-constant of photodegradation and photokinetic factor $F_{Pp}^{\lambda irr}$, when irradiating various concentrations (3.83 x 10^{-6}M-2.06 x 10^{-5}M) at 330nm and observing at 330nm*

7.3.0 Conclusion

The kinetic data of TR under non-isosbestic irradiation was able to be described by Φ-order kinetics. The method allowed for determination of the quantum yield and the application of TR in actinometry, allowing for reliable data to be gathered on the photodegradation reaction. In addition, it outlined the importance of the factor of $\beta_{\lambda irr}$ to describe the photoreactivity of drugs, and that use of Φ-order kinetics over zero-, first- and second- order kinetics had the advantage of reliability.

The strategy of considering the kinetics in two stages has proven to be useful. The fitting of the first stage to Eq. 1 alone indicated that the above choice was correct. It additionally provided proof that the cis⇌trans mechanism obeyed Φ-order kinetics.

The elucidation of the kinetics after showed that the quantum yields of the forward reactions are different from those of the reverse ones. Both are wavelength dependent. The strategy facilitated the modelling factor of $\beta_{\lambda irr}$ that can be used for actinometry, and the effect of concentration.

7.4.0 References

Darakhshan, S., & Pour, A. B. (2015). Tranilast: A review of its therapeutic applications. *Pharmacological Research*, *91*, 15–28.

Hirayama, F., Utsuki, T., & Uekama, K. (1991). Stoichiometry-dependent photodimerization of tranilast in a γ-cyclodextrin inclusion complex. *Journal of the Chemical Society, Chemical Communications*, *0*(13),887–888.

Maafi, M., & Lee, L.-Y. (2015a). Determination of Dacarbazine Φ-Order Photokinetics, Quantum Yields, and Potential for Actinometry. *Journal of Pharmaceutical Sciences*, *104*(10), 3501–3509.

Maafi, M., & Lee, L. Y. (2015b). Actinometric and Φ-order photodegradation properties of anti-cancer Sunitinib. *Journal of Pharmaceutical and Biomedical Analysis*, *110*, 34–41.

Naohide Hori, M. F., Kazuhiko Ikegami, Den-ichi Momose, Noriyasu Saito, and, & Mitsuo Matsumoto. (1999). Effect of UV-Absorbing Agents on Photodegradation of Tranilast in Oily Gels. *Chemical Pharmaceutical Bulletin*, *47*(12), 1713–1716.

Utsuki, T., Hirayama, F., & Uekama, K. (1993). Different photodimerization behaviour of tranilast in α-, β- and γ-cyclodextrin complexes: cavity-size and stoichiometry dependence. *Journal of the Chemical Society, Perkin Transactions 2*, *2*(1), 109–114.

Chapter 8:

Photokinetic studies, using HSA And β-CDP, on two photounstable compounds in buffer

Chapter 8: Photokinetic studies, using HSA and β-CDP, on two photounstable molecules in buffer

8.1.0 Introduction

8.1.1 Introduction

In previous studies TR and AXI have been found to be photounstable (Hirayama, Utsuki, & Uekama, 1991; Yan Lee, 2016). In addition, many drugs are photounstable in blood, influencing their detection and correct administration (Nilsson, 2010). Such effects can occur when compounds bind to a protein, as the amount of free drug available to undergo photodegradation is reduced (Iain Love, Graeme T. Smith, 2013). Such an effect can be influenced by both the matrix and the drug compound (Corey M. Ohnmacht, 2013). The European Medicines Agency has therefore declared that the compound in the blood matrix should be stable immediately after sampling (Achim Freisleben et al., 2011). If such degradation processes can be slowed the stability of the compound can be improved, allowing for it to be kept for a longer period of time, in the case that further tests are required (Dixon, Mbeunkui, & Wiegel, 2015).

Cyclodextrins have been used to provide stability against photodegradation as they are capable of including compounds within their cavity, affecting the molecular rotation of the compound (Iglesias-García, Brandariz, & Iglesias, 2010). If the group of the compound involved in the photodegradation process is included, the rotations of the double bond (involved in the photodegradation process) are restricted, limiting the space in which the compound can undergo changes. This has the effect of reducing the rate at which the photoreaction occurs (Bortolus, Monti, Energia, & Area, 1996).

Photostability studies on TR and AXI have previously been carried out in cyclodextrins. It has been observed that in the presence of β-CDP greater stability of AXI was achieved than through use of the β-CD monomer, however, this study did not investigate the rate constants of the degradation (Yan Lee, 2016). In addition TR has been studied in the presence of γ-cyclodextrin (Hirayama et al., 1991; Utsuki, Hirayama, & Uekama, 1993), and the rate of both the isomerisation and dimerization of the compound slowed (Utsuki et al., 1993). Although in the latter study a relationship between the rate of compound degradation and the concentration of cyclodextrin was established, β-CDP was not employed. Furthermore, there are fewer studies which use HSA to provide photostability. The use of HSA for photostability has been previously utilised for folic acid, in which it was observed that tryptophan in HSA was found to be able to act as a photosensitizer, reducing the amount of photoproduct formed (Vorobey, Steindal, Off, Vorobey, & Moan, 2006).

The current study therefore aims to investigate the photokinetic behaviours of AXI and TR in the presence of various concentrations of HSA or β-CDP, and apply the Φ-order kinetic model, developed by our group, to the data to determine the individual rate constants.

8.1.2 Φ-order kinetic model

The rate at which the concentration of a compound is altered can provide information on the quantity of its active ingredient remaining when the target site is reached. This can provide information on the amount of drug that should be initially administered. The rates at which such a photochemical reaction proceeds are dependent upon a number of factors. Theoretical and experimental methods currently used for determining the kinetics of photochemical reactions do not take all influencing factors into consideration (Ibhadon, Arabatzis, Falaras, & Tsoukleris, 2007), often using the same Arrhenius equations applied to thermodynamic

studies in order to determine the rate-constants (Montazerozohori, Nasr-Esfahani, & Joohari, 2012).

These methods are limited as they take temperature effects into consideration (Montazerozohori et al., 2012), but not other factors influencing the rate of photodegradation (Ibhadon et al., 2007). A Φ-order kinetic model has been proposed by our group. This model accounts for factors known to influence the rate of photochemical reactions, allowing for reaction rates to be characterised and data obtained in different conditions to be compared. This is expected to improve the accuracy and precision of photochemical kinetic results.

The photokinetic traces of a compound can be obtained by irradiating the photounstable compound and monitoring its UV-absorption spectra. This data can then be fitted to the Φ-order kinetic model by plotting the irradiation time against the absorbance determined by using the following equation:

$$A_{tot}^{\lambda_{\overline{\lambda_{obs}}}^{irr}}(t) = A_{tot}^{\lambda_{\overline{\lambda_{obs}}}^{irr}}(\infty) + \frac{A_{tot}^{\lambda_{\overline{\lambda_{obs}}}^{irr}}(0) - A_{tot}^{\lambda_{\overline{\lambda_{obs}}}^{irr}}(\infty)}{A_{tot}^{\lambda_{\overline{\lambda_{obs}}}^{irr}}(0) - A_{tot}^{\lambda_{\overline{\lambda_{obs}}}^{irr}}(\infty)} \times \frac{I_{\lambda_{obs}}}{I_{\lambda_{irr}}} \times log\left[1 + \left(10^{\left[\left(A_{tot}^{\frac{\lambda irr}{\lambda obs}}(0) - A_{tot}^{\frac{\lambda irr}{\lambda obs}}(\infty)\right) \times \frac{I_{\lambda obs}}{I_{\lambda irr}}\right]} - 1\right) \times e^{-k^{\frac{\lambda_{irr}}{\lambda_{obs}}} \times t}\right]$$ **Eq. 1**

In this equation $A_{tot}^{\lambda_{irr}}(0)$ and $A_{tot}^{\lambda_{irr}}(\infty)$ indicate the total absorbance of the reaction solution before irradiation, and at specific time (t), when an equilibrium between the parent and photoproduct has been reached. The wavelength at which the sample is irradiated and observed is represented by λ_{irr} and λ_{obs}, respectively, and the light pathlength is represented

by $I_{\lambda_{irr}}$ and $I_{\lambda_{obs}}$, respectively. By fitting the Φ-order kinetic model to the experimental data, the rate constant $k_{A\rightleftharpoons B}^{\lambda_{irr}}$ can be determined. Full elucidation on the acquisition of this model can be found in previous papers (W. Maafi & Maafi, 2013).

8.2.0 Results

8.2.1 Effect of light on the absorbance spectrum of the compounds

The photoproducts of TR and AXI have previously been attributed to a *cis*-isomer and dimer (*(2) International Application Published Under the Patent Cooperation Treaty (PCT)*, 2012; Naohide Hori et al., 1999; Sparidans, Iusuf, Schinkel, Schellens, & Beijnen, 2009). Both photoproducts of TR had been confirmed using GC-MS, the dimer having a higher m/z (Kakegawa, Mitsou, Matsumoto, Satoh, Akagi, 1985). In addition, LC/MS/MS had also been used to confirm AXI formed a *cis*-isomer (Sparidans et al., 2009), and the formation of a dimer was evidenced by comparisons with compounds containing AXI (*(2) International Application Published Under the Patent Cooperation Treaty (PCT)*, 2012). In the literature a *cis*-isomer is formed when the π double bonds of a *trans*-isomer are destroyed. This allows the σ-bond to rotate and reform (Barlow & Mountford, 2014).

As the compounds were ascertained to have a low solubility in water (Nagai & Ito, 2014; Yan Lee, 2016) they were prepared in 10%/2.5% (v/v) ethanol: water (TR, AXI, respectively). After irradiation for a day (≈7 hours), the electronic absorption spectra recorded for each TR and AXI was broad, with maximum absorption peaks situated at ≈330nm and ≈360nm, respectively. No absorbance of the compounds was observed outside the UV region.

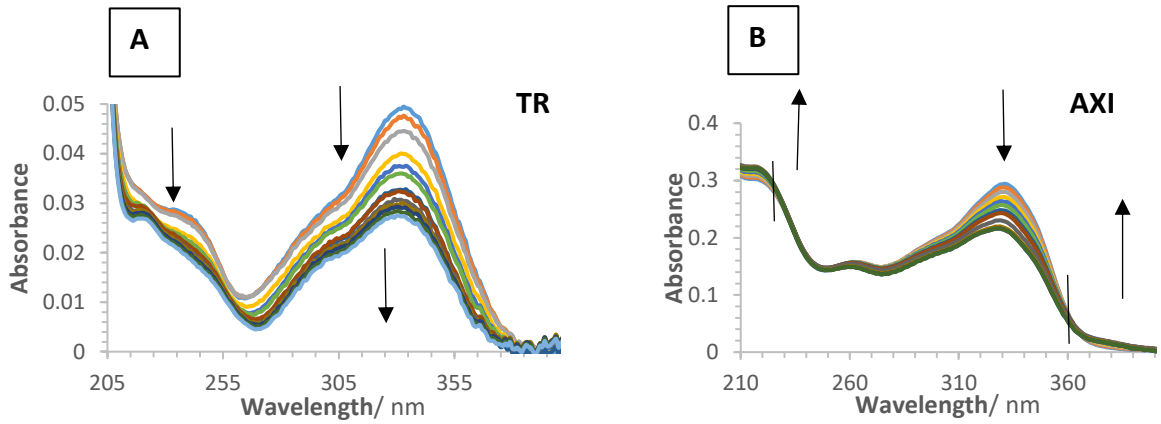

Figure 1: *Evolution of the electronic absorption spectra of (A) 1.5 x 10^{-6}M TR, and (B) 1.24 x 10^{-5}M AXI in buffer pH=7, subjected to continuous irradiation with a (A) 350nm and (B) 330nm monochromatic beam, respectively (total irradiation time of 5.4 x 10^{3}Ms at a radiant power of P_{350}/ P_{330}= Einstein $s^{-1}dm^{-3}$) The arrows indicate the direction of the evolution of absorption maxima during photoreaction. Isosbetic points at (B) 230nm and 360nm (solid lines)*

Using light of a specific energy, continuous irradiation of the compounds decreased the maximum absorption spectra of TR and AXI in the regions of ≈280-370nm, and ≈270nm-350nm, respectively. The shape of the photoproducts and TR overlapped and no other features were observed. Weak increases in the spectra of AXI at ≈330nm and ≈380nm, and quasi-isosbetic points at ≈330nm ≈360nm were observed. No additional features were observed (Fig. 1). The changes in the specific peaks represented by arrows, and the isosbetic points, illustrated by solid lines (Fig. 1), would imply a one-step reaction (Mauser & Gauglitz, 1998). Each compound took >6,000s to degrade in these conditions, forming a photoproduct which absorbed at different wavelengths to that of the parent compound, and absorbed a

smaller quantity of light at its characteristic λ_{max}. Such a degradation had previously been reported for TR and AXI (Utsuki et al., 1993; Yan Lee, 2016) in pH=7 and ethanol, respectively. Although the behaviour of AXI was similar to that previously observed by our research group (Yan Lee, 2016), the absorption in the earlier study was greater at ≈380nm and ≈230nm. This may indicate a greater ratio of a particular photoproduct was being formed, as can occur when the environment of the compound is altered, as this can influence the recombination of the compound to form its photoproducts (Bortolus et al., 1996).

8.2.2 AB_3 (3Φ) order kinetics of TR and AXI in water pH=7

Graphical representation of the compounds in the presence and absence of a macromolecule show that in the absence of a macromolecule each compound degraded exponentially and then linearly (Fig. 2), indicative of more than one photodegradation process and different reaction rates of each stage. The region between the exponential and linear phase represented the 'photostationary phase'. In such a region it is expected that formation of the photoproduct occurs at the same rate as the degradation of the reactant compound.

For such photoreactions a model has been proposed by our group (M. Maafi & Maafi, 2016). The specific model allows for experimental trace data obtained for species involved in consecutive photoreactions to be described as it considers the various photodegradation processes (Fig. 2).

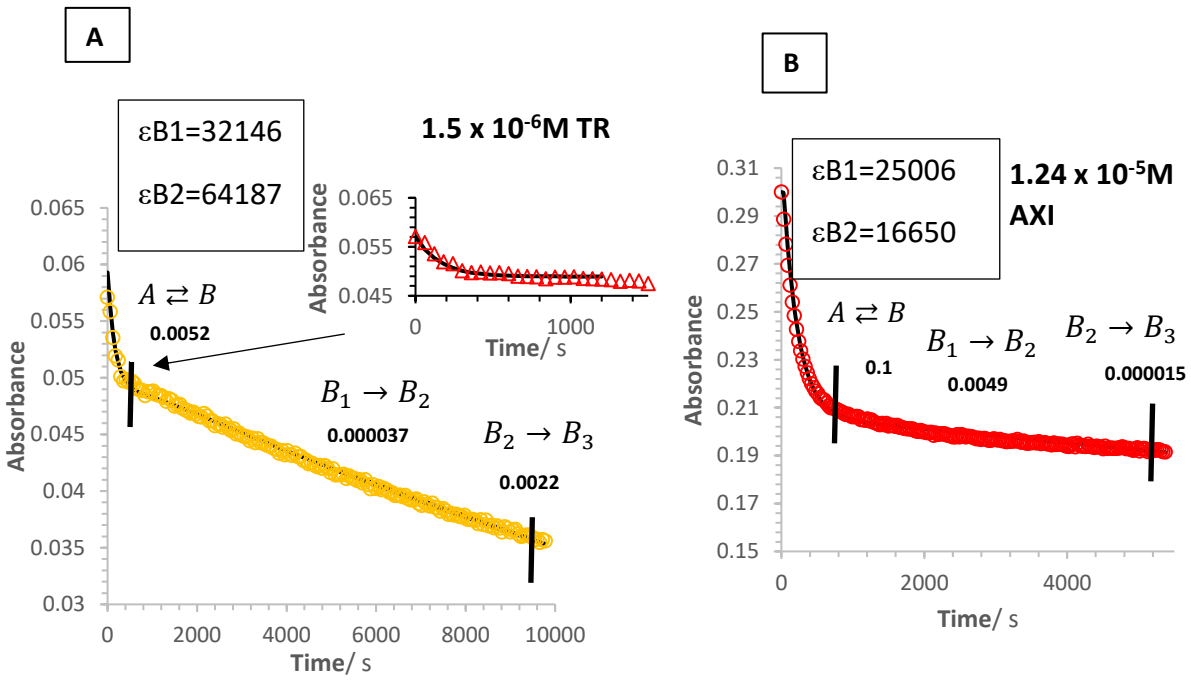

Figure 2: *Effect of irradiation on the photodegradation traces (circles) of (A) TR (1.5 x 10^{-6}M), and (B) AXI in buffer pH=7 (1.24 x 10^{-5}M), subjected to continuous irradiation with a (A) 350nm/ (B) 330nm monochromatic beam (total irradiation time of 4.0 x 10^{3}Ms at a radiant power of P_{350}/P_{330} = Einstein $s^{-1}dm^{-3}$), fitted to the AB_3 (3Φ) order kinetics model (solid lines), example of photostationary phase outlined (solid lines), processes, rate constants and ε values used for the fitting*

After continuous irradiation for ≈6,000s neither compound reached a plateau, indicating their photoreactions continued indefinitely. This prevented the concentration of the second photodegradant, and thus the absorption coefficient at the end of the photoreaction from being determined, preventing accurate fitting to the AB_3 (3Φ) order equation.

By substituting a value for the end of the photoreaction into the equation, only a loose fitting to the proposed AB_3 (3Φ) order kinetics model could be obtained. Successful fitting of the

data to this model supported the hypothesis that multiple photoreactions were occurring, allowing for the estimated values of the theoretical individual rate constants, εB1 and εB2, to be determined (Fig. 2).

The photodegradation rate of AXI was found to be greater for the $B_1 \rightarrow B_2$ phototransformation process than that of the $B_2 \rightarrow B_3$ process, whereas opposite trends were observed for TR. As the $A \rightarrow B$ process was faster than that of $B_1 \rightarrow B_2$ or $B_2 \rightarrow B_3$ for both photoreactions, and followed an exponential trend, it may indicate an $A \rightleftarrows B$ reversible reaction (Yan Lee, 2016). We therefore propose to consider and discuss the different stages of the photoreaction separately.

Conditions used for the photoreaction of AXI, including, solvent, host molecule, irradiated wavelength and observation wavelength, differed between the current study and the earlier study by our group, preventing the rate-constants from being compared, however the photodegradation of AXI in this earlier study, was investigated in detail (Yan Lee, 2016). In addition (Chapter 7) a higher $k_{A \rightleftharpoons B}^{\lambda_{irr}}$ was obtained for TR in ethanol, than that in buffer, when all other conditions were held constant. Such an observation would indicate that the photodegradation rate of this compound was lower in buffer than in ethanol.

To determine the specific photoproducts that could be identified for TR, LC/MS was carried out on both unirradiated and irradiated samples. In the unirradiated sample the presence of one chromatogram and a molecular ion [M+H$^+$] at an *m/z* ratio of 328.3 corresponded to the molecular mass of TR. After irradiation two peaks (2,3)(Fig. 3) were observed, each with a

molecular ion [M+H$^+$] at an *m/z* ratio of 328.3, confirming the presence of two isomeric compounds (Fig. 3).

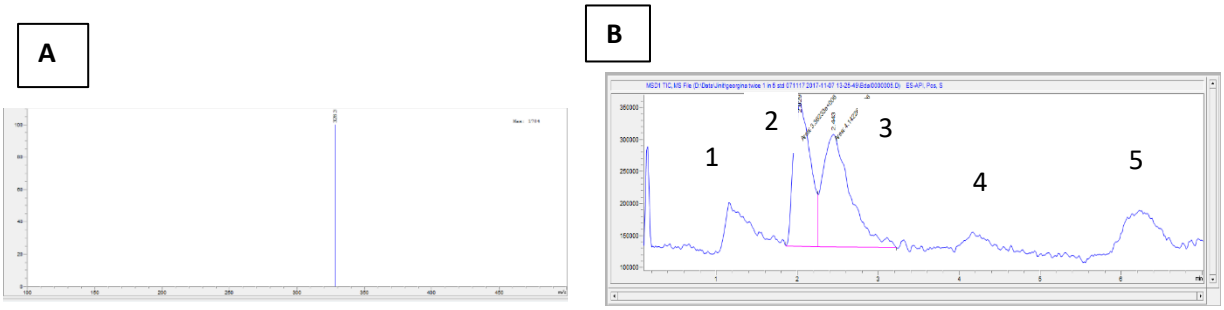

Figure 3: *6.11 x 10^{-4}M TR (A) irradiated SIM mass spectrum [M+H$^+$] and (B) total ion count chromatogram full scan*

8.2.3 Effect of HSA and β-CDP on the photostability of the compounds

Each of the compounds had previously been found to complex with, or bind to β-CDP or HSA. The photostability of the compounds in the presence of each of these macromolecules was therefore assessed to determine the influence of the macromolecule concentration on the photodegradation rate.

The macromolecules themselves were firstly subject to light irradiation to ensure they were photostable, and absorbed at a different wavelength to the compound. The lack of absorbance spectra changes after ≈4 hours continuous irradiation of each molecule confirmed they were both photostable. The electronic absorption spectra of HSA was characterised by two absorption regions at ≈220 and ≈260-300nm, and that of β-CDP had a maximum absorption peak at 250nm. As thus, neither macromolecule absorbed in the absorption region of the species enough to influence the analysis of the compounds.

When irradiated at their maximum absorbance wavelength, each compound in the presence of either macromolecule exhibited similar behaviours (Fig. 4).

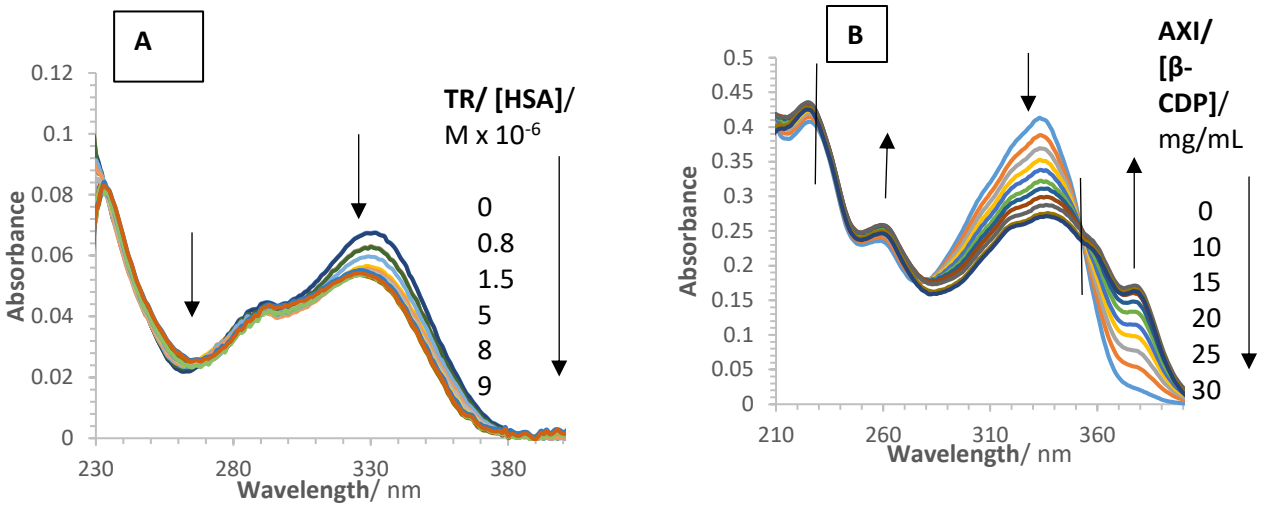

Figure 4: *Evolution of the electronic absorption spectra of (A) 1.5 x 10^{-6}M TR and (B) 1.24 x 10^{-5}M AXI in buffer pH=7 in various concentrations of HSA ((A) 1.14 × 10^{-5}-1.24 × 10^{-4}M/ (b) 8.0 x 10^{-7}M-9.92 x 10^{-5}M) and β-CDP (0-30mg/mL), subjected to a continuous irradiation with a (A) 350nm/ (B) 330nm monochromatic beam (total irradiation time of 4.0 x 10^{3}Ms at a radiant power of P_{350}/P_{330} = Einstein $s^{-1}dm^{-3}$). The arrows indicate the direction of the evolution of absorption maxima during photoreaction. Isosbetic points at 230nm and 360nm (solid lines)*

No changes in the shape of the maximum absorption spectra of the compound were observed throughout irradiation, implying the compounds had a similar degradation process in both the presence and absence of each macromolecule.

In the presence of a macromolecule, greater absorbances in AXI at ≈380nm resulted in a significantly clearer isosbestic point at ≈360nm. These would indicate a larger proportion of this specific photoproduct was formed. In addition, the change in absorbance was the same for either compound when in the presence of a macromolecule, as that in its absence, undergoing absorbance decreases at 350nm and 330nm for TR and AXI, respectively. Such trends had previously been observed for AXI in β-CDP (Yan Lee, 2016).

In addition, the differences between the rate of degradation in the presence and absence of each macromolecule were compared and it observed that the trends were similar, however, in the presence of a macromolecule a $B_2 \rightarrow B_3$ conversion process was not clearly evident for either compound (Fig. 5). This observation would indicate that when using this concentration of macromolecule all, or almost all of the compound molecules were complexed with β-CDP, and thus the photoproducts were being formed less rapidly.

Increasing the concentration of macromolecule gradually decreased the overall rate at which TR photodegraded (Fig. 5), however, this relationship was unclear for AXI (Fig. 5). For more reliable treatment of the data the section of the data indicative of an $A \rightleftarrows B$ reversible reaction was fitted to the Φ–order kinetics model (Eq. 1).

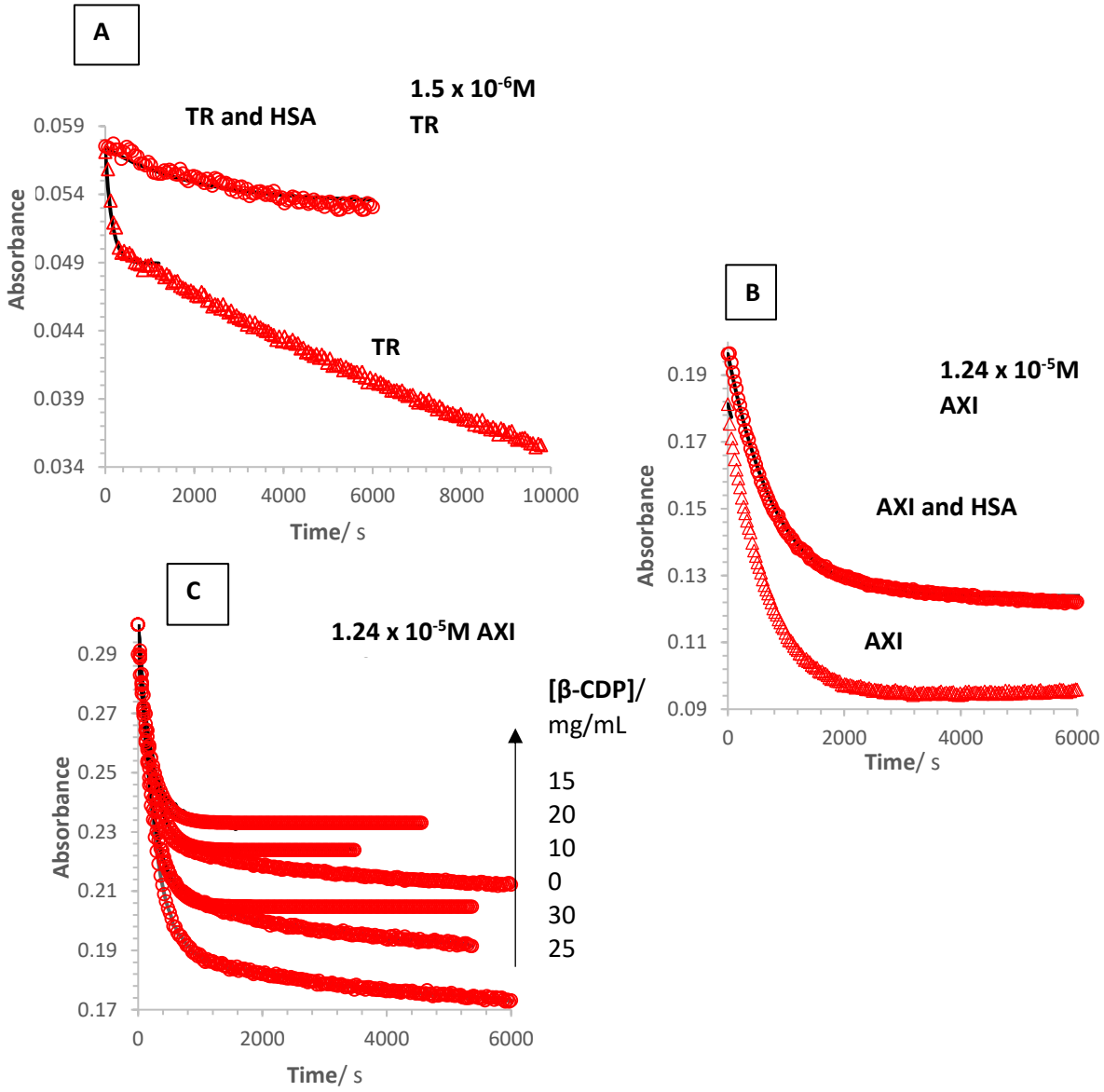

Figure 5: *Effect of irradiation on the photodegradation traces (circles) of (A) TR (1.5 x 10^{-6}M), and (B) AXI in buffer pH=7 (1.24 x 10^{-5}M) (triangles), and (A) TR and (B) AXI in the presence of HSA ((A)1.14 × 10^{-5}M/(B) 9.92 x 10^{-5}M), and (C) AXI in the presence of β-CDP (0-30mg/mL) (circles), subjected to continuous irradiation with a (A) 350nm/ (B) 330nm monochromatic beam (total irradiation time of 4.0 x 10^{3}Ms at a radiant power of P_{350}/P_{330} = Einstein $s^{-1}dm^{-3}$), with the data up until the first photostationary phase fitted to the Φ–order kinetics model (solid lines)*

8.2.4 Effect of HSA and β-CDP on the photokinetic rate constants of the compounds

Similar absorption spectra observed for both the parent compounds and their photoproducts enabled the Φ–order kinetic model to be applied at a non-isosbestic wavelength, at which both the parent and its photodegradant could absorb. This would allow the specific benefits of the method to be exploited.

Input of the conditions the experiment was carried out in, initial absorbance reading, final absorbance reading, and time, enabled the data to be fitted to this semi-empirical model (Eq. 1)(Fig. 6). An appropriate rate-constant was inputted into the equation and adjusted accordingly.

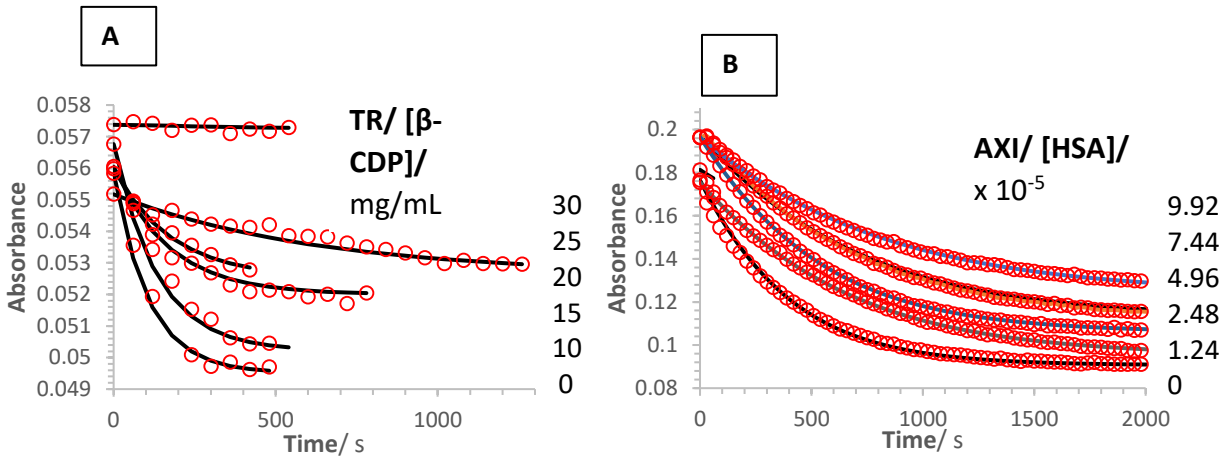

Figure 6: *Effect of increasing HSA concentration (B) 8.0 x 10^{-7}M-9.92 x 10^{-5}M and β-CDP (A) 0-30mg/mL, on the photodegradation traces (circles) of (A) 1.5 x 10^{-6}M TR and (B) 1.24 x 10^{-5}M AXI in buffer pH=7, subjected to continuous irradiation with a (A) 350nm/(B) 330nm monochromatic beam (total irradiation time of 4.0 x 10^{3}Ms at a radiant power of P_{350}/P_{330}= Einstein $s^{-1}dm^{-3}$), and fitted to the Φ–order kinetics model (solid lines)*

The theoretical absorbance from the Φ-order kinetics model (Eq. 1) and the experimental absorbance were almost identical at the specified irradiation and observation wavelengths (Fig. 6), implying a reversible reaction (Yan Lee, 2016). The value of $k_{A\rightleftharpoons B}^{\lambda_{irr}}$ obtained to achieve

such a fitting would provide an indication of the gradient of the curves, and thus be representative of the reaction rate. Successful fitting using data from all the macromolecule concentrations studied enabled the rate-constants of the individual reactions occurring to be compared (Table 1).

Table 1: *TR and AXI overall reaction rates and photoreaction reduction percentages in various concentrations of HSA and β-CDP*

Compound	**Concentration of host molecule/ mg/mL**	$A^{\lambda_{irr}}_{\overline{HSA}\,\overline{\beta CDP}}(0)$	$k^{\lambda_{irr}}_{TR/AXI}$ **/s^{-1}**	$P_{\lambda irr}$ **(Einstein s^{-1} dm^{-3})**	$\frac{k^{\lambda_{irr}}_{TR/AXI}(A^{\lambda_{irr}}_{HSA/\beta CDP}=0)}{k^{\lambda_{irr}}_{TR/AXI}/(A^{\lambda_{irr}}_{HSA/\beta CDP}\neq 0)}$	**% k Reduced**
HSA						
TR	0	0.0571	0.0065	0.426	1	0
	0.012	0.0646	0.006	0.43	1.08	7.69
	0.023	0.0593	0.0057	0.429	1.14	12.31
	0.075	0.0582	0.0042	0.425	1.55	35.38
	0.12	0.0575	0.0027	0.426	2.41	58.46
	0.14	0.0587	0.002	0.425	3.25	69.23
	0.16	0.0578	0.0012	0.428	5.42	81.54
	0.19	0.0574	0.0005	0.427	13	92.31
AXI	0	0.181	0.003	0.428	1	0
	0.19	0.166	0.0026	0.43	0.84	-19.57
	0.37	0.197	0.0022	0.425	1.21	17.39
	0.75	0.197	0.0022	0.428	1.04	4.35
	0.12	0.197	0.0017	0.425	1.28	21.74
	1.49	0.196	0.0035	0.426	1.64	39.13
β-CDP						
TR	0	0.0536	0.0093	0.428	1	0
	10	0.0568	0.0075	0.425	1.44	30.77
	15	0.0560	0.0059	0.426	1.86	46.15
	20	0.0560	0.0056	0.427	2.5	60
	25	0.0552	0.0016	0.426	4.06	75.38
	30	0.0573	0.00022	0.425	29.55	96.62
AXI	0	0.3	0.0053	0.428	1	0
	10	0.3	0.005	0.43	1.06	5.66
	15	0.290	0.0049	0.425	1.51	33.96
	20	0.3	0.0048	0.428	1.10	9.43
	25	0.3	0.0047	0.425	1.13	11.32
	30	0.3	0.0046	0.426	1.15	13.21

Lower rate-constants obtained using greater concentrations of macromolecule and fitted to the Φ–order kinetics, confirmed each macromolecule was affecting the photodegradation rate (Table 1). Comparison of the rate-constants obtained in the presence of various concentrations of macromolecule, with those in its absence, allowed for the percentage reduction in rate constant to be ascertained. The addition of the highest investigated concentration of each macromolecule reduced the rate-constant of each compound by similar amounts, ≈90% and ≈35% for TR and AXI respectively. Similar reductions in the rate-constants were observed in either of the macromolecules. Such an effect may indicate each macromolecule was capable of photoprotecting these compounds in the specific conditions, and that more photoprotection was provided for TR than AXI.

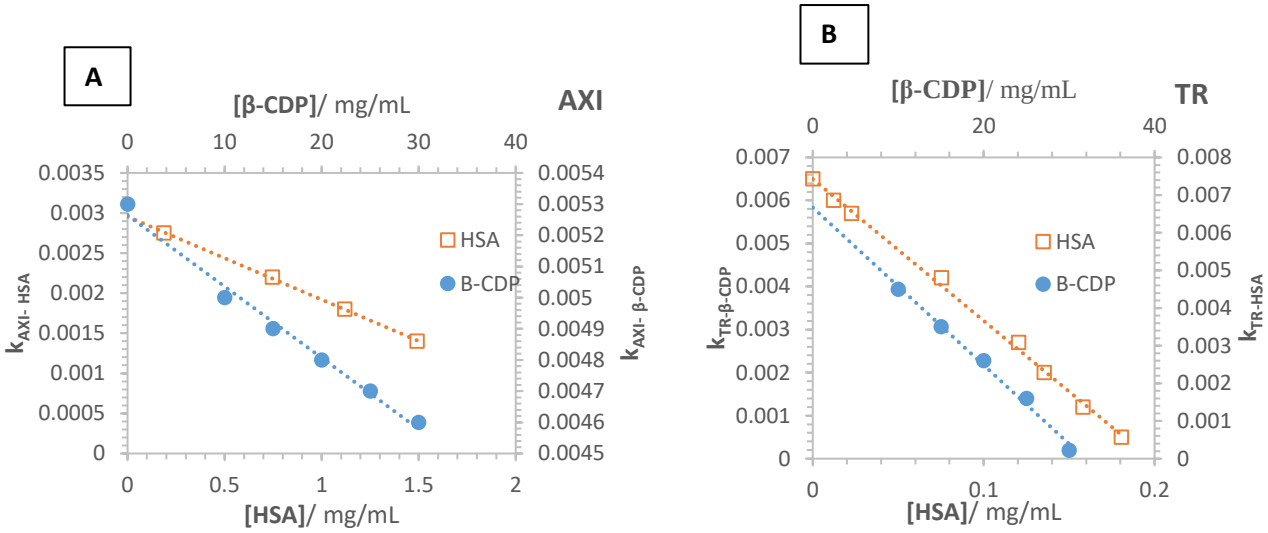

Figure 7: *Linear relationships between various HSA (squares) or β-CDP (circles) concentrations (A) 1.14 × 10^{-5}-1.24 × 10^{-4}M/ (B) 8.0 x 10^{-7}M-9.92 x 10^{-5}M, and 0-30mg/mL, respectively, on the overall kinetic rate-constant of TR or AXI transformation. Data taken from Table 1. $\lambda_{irr}/\lambda_{obs}$ = (A) 350/350, (B) 330/330, for TR and AXI, respectively*

Plots of the rate-constant against various concentrations of macromolecule were linear (Fig. 7), with high correlation coefficients. The plots could therefore provide an indication of the rate-constant for a given concentration of host compound in these conditions.

Significant differences in the linear gradients of the plots for each compound, in the presence of increasing concentration of macromolecule, indicated the reduction in the rate-constants was proportional to the concentration of the macromolecule (Fig. 7). The gradients were steeper in β-CDP than in HSA. Such an observation would suggest that in the studied concentrations of macromolecule, β-CDP could reduce the rate-constant more rapidly than HSA.

This could therefore be considered a new method for identifying the occurrence of a HSA/ drug complex. It would be an interesting application of photokinetics to proteins and β-CDP.

Through the formation of more stable compounds, and knowledge of the photokinetic rate constants, it is expected that the method could provide enhanced stability of the compounds in the bloodstream, allowing for accurate dosing, and thus allow for smaller concentrations of the drug to be administered. In addition, it would be expected to improve quantification of the compounds, allowing for them to be detected after a longer period of time, and with more accuracy.

8.2.5 Effect of HSA and β-CDP on the linear degradation phase of the compounds

As previously stated (8.2.2) the AB_3 (3Φ) order kinetics model could not reliably describe the data. The section of the photokinetic trace data which was not fitted to the Φ-order kinetics model appeared to be linear. Lines of best fit, with high correlation coefficients, could therefore be constructed, passing through the traces, and the gradient used to estimate the rate of this stage of the photoreaction.

An example of the concentration of the host on the traces and reaction rate is given (Fig. 8).

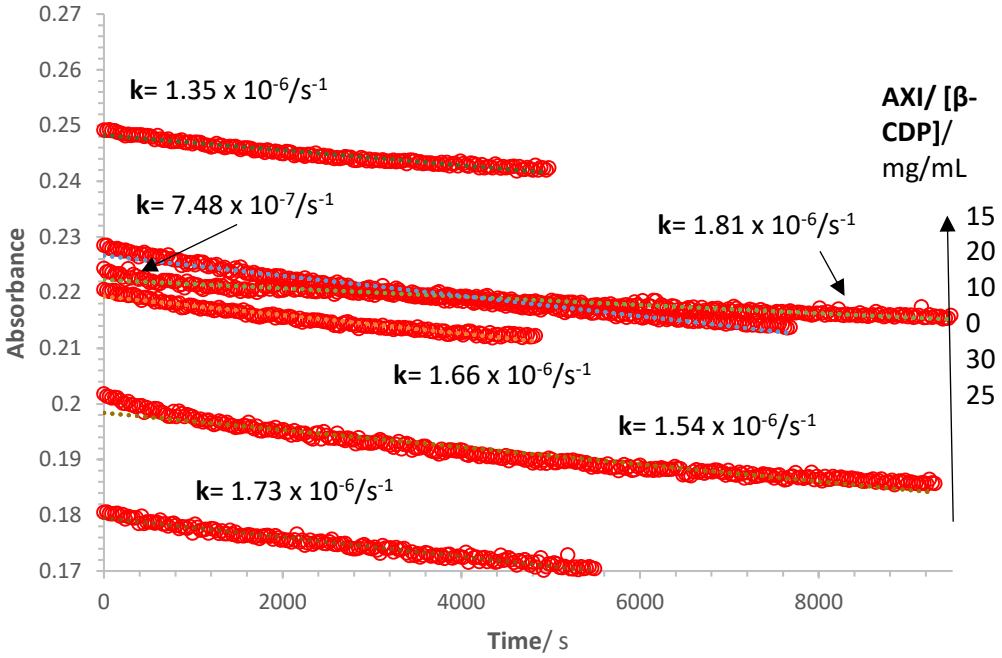

Figure 8: *Effect of increasing β-CDP concentration (0-30mg/mL) on the photodegradation traces of AXI (1.24 x 10^{-5}M) in aqueous solution, fitted to the linear relationships, and the effect of the concentration on the individual rate constants*

It can be observed (Fig. 8) that for this specific phase of the photoreaction there was a poor relationship between the rate-constant and the concentration of the macromolecule. Such an effect could imply that the macromolecule concentration did not necessarily influence the rate of this specific stage of the photoreaction.

Different methods were used to determine the rate-constant of the two phases of photodegradation, and the phases had different trendline shapes. As a consequence results obtained from only a single phase could be compared.

Nonetheless, the effects may occur from movement restriction of the compound, or potentially the presence of tryptophan, reducing the amount of photoproduct formed.

8.3.0 Conclusion

The results indicate that both compounds could photodegrade exponentially and then linearly, indicating the formation of two or more photoproducts. The lack of plateau observed in the absorbance reading after >6,000s continuous irradiation only allowed an estimated fitting to the AB_3 (3Φ) order kinetics. Fitting of the first 'phase' of the traces to the Φ–order kinetics model for an $A \rightleftarrows B$ reversible reaction, however, was achieved.

In the presence of either HSA or β-CDP, similar effects on the degradation trends of the compounds were observed, as in its absence, obeying Φ–order kinetics. Comparisons of the rate-constants obtained using the various concentrations of macromolecule suggested that the rate of the reaction was progressively reduced as the concentration of macromolecule increased.

Such results were indicative that the macromolecules were able to provide photostability to the compounds.

8.4.0 References

(2) International Application Published Under the Patent Cooperation Treaty (PCT). (2012). Retrieved from https://patentimages.storage.googleapis.com/b0/a3/96/b1151b8c6043ab/WO2013046133A1.pdf

Achim Freisleben, Margarete BrudnyKlöppel, H. M., Ronald de Vries, Marcel de Zwart, &, & Philip Timmerman. (2011). Blood stability testing: European Bioanalysis Forum view on current challenges for regulated bioanalysis. *White Paper*, *3*(12), 1333–1336.

Barlow, D. (David), & Mountford, D. (2014). *Chemistry of drugs*. Retrieved from https://www.worldcat.org/title/chemistry-of-drugs/oclc/889893972

Bortolus, P., Monti, S., Energia, A., & Area, C. N. R. (1996). *Photochemistry in Cyclodextrin Cavities* (Vol. 21).

Corey M. Ohnmacht. (2013). LC-MS Bioanalysis of Photosensitive and Oxidatively Labile Compounds. In W. Li, J. Zhang, & F. L. S. Tse (Eds.), *Handbook of LC-MS bioanalysis : best practices, experimental protocols, and regulations* (pp. 491–505).

Dixon, R. B., Mbeunkui, F., & Wiegel, J. V. (2015). Stability study of opioids and benzodiazepines in urine samples by liquid chromatography tandem mass spectrometry. *Journal of Analytical Science and Technology*, *6*(17), 1-10.

Hirayama, F., Utsuki, T., & Uekama, K. (1991). Stoichiometry-dependent photodimerization of tranilast in a γ-cyclodextrin inclusion complex. *Journal of the Chemical Society, Chemical Communications*, *0*(13), 887–888.

Iain Love, Graeme T. Smith, and H. M. H. (2013). Assessment of Whole Blood Stability and Blood/Plasma Distribution of Drugs. In W. Li, J. Zhang, & F. L. S. Tse (Eds.), *Handbook of LC-MS bioanalysis : best practices, experimental protocols, and regulations* (pp. 129–139).

Ibhadon, A. O., Arabatzis, I. M., Falaras, P., & Tsoukleris, D. (2007). The design and photoreaction kinetic modeling of a gas-phase titania foam packed bed reactor. *Chemical Engineering Journal*, *133*, 317–323.

Iglesias-García, I., Brandariz, I., & Iglesias, E. (2010). Fluorescence study of tetracaine–cyclodextrin inclusion complexes. *Supramolecular Chemistry*, *22*(4), 228–236.

Kakegawa, Mitsou, Matsumoto, Satoh, Akagi, T. (1985). Hyaluronidase-inhibitory and anti-allergic activities of the photo-irradiated products of tranilast. *Chemical & Pharmaceutical Bulletin*, *33*(9), 3738–3744.

Maafi, M., & Maafi, W. (2016). Modelling and elucidation of the kinetics of multiple 2 consecutive photoreactions AB 4 (4Φ) with Φ-order kinetics. Application to the photodegradation of riboflavin. *Journal of Pharmaceutical Sciences*, *105*(12), 3537–3548.

Maafi, W., & Maafi, M. (2013). Modelling nifedipine photodegradation, photostability and actinometric properties. *International Journal of Pharmaceutics*, *456*(1), 153–164.

Mauser, H. (Heinz), & Gauglitz, G. (Günter). (1998). *Photokinetics : theoretical fundamentals and applications*. Retrieved from https://books.google.co.uk/books?id=hw81gL9Ac-IC&pg=PA264&lpg=PA264&dq=quasi+isosbestic+point&source=bl&ots=VIRkhPalch&sig=UcKfhFN2JyAjlfHN1oX2S5EkCso&hl=en&sa=X&ved=2ahUKEwiAgpPbtt7fAhWyunEKHYqGBHcQ6AEwCXoECAcQAQ#v=onepage&q=quasi isosbestic point&f=

Montazerozohori, M., Nasr-Esfahani, M., & Joohari, S. (2012). Photocatalytic degradation of an organic dye in some aqueous buffer solutions using nano titanium dioxide: A kinetic study. *Environment Protection Engineering*, *38*(3), 45–55.

Nagai, N., & Ito, Y. (2014). Therapeutic Effects of Gel Ointments Containing Tranilast Nanoparticles on Paw Edema in Adjuvant-Induced Arthritis Rats. *Biological and Pharmaceutical Bulletin*, *37*(1), 96–104.

Naohide Hori, M. F., Kazuhiko Ikegami, Den-ichi Momose, Noriyasu Saito, and, & Mitsuo Matsumoto. (1999). Effect of UV-Absorbing Agents on Photodegradation of Tranilast in Oily Gels. *Chemical Pharmaceutical Bulletin*, *47*(12), 1713–1716.

Nilsson, G. (2010). *Stability of zopiclone in whole blood Studies from a forensic perspective* (Linköping University). Retrieved from https://www.diva-portal.org/smash/get/diva2:349342/FULLTEXT01.pdf

Sparidans, R. W., Iusuf, D., Schinkel, A. H., Schellens, J. H. M., & Beijnen, J. H. (2009). Liquid chromatography-tandem mass spectrometric assay for the light sensitive tyrosine kinase inhibitor axitinib in human plasma. *Journal of Chromatography B*, *877*, 4090–4096.

Utsuki, T., Hirayama, F., & Uekama, K. (1993). Different photodimerization behaviour of tranilast in α-, β- and γ-cyclodextrin complexes: cavity-size and stoichiometry dependence. *Journal of the Chemical Society, Perkin Transactions. 2*, *0*(1), 109–114.

Vorobey, P., Steindal, A. E., Off, M. K., Vorobey, A., & Moan, J. (2006). Influence of Human Serum Albumin on Photodegradation of Folic Acid in Solution. *Photochemistry and Photobiology*, *82*(3), 817-822.

Yan Lee, L. (2016). *Study Of The Photodegradation And Photostability Of Anti-Cancer Drugs In Different Media Towards The Development Of Both New Actinometers And Liquid Formulations* (De Montfort University). Retrieved from https://www.dora.dmu.ac.uk/bitstream/handle/2086/12188/Lok Yan%27s Thesis.pdf?sequence=1&isAllowed=y

Chapter 9:

Conclusion

Chapter 9: Conclusion

9.1 Conclusions

Poor detection of pharmaceuticals in biofluids and surface waters can have costly or hazardous consequences as decisions are made based on such results. There is therefore the necessity for a reliable, rapid and sensitive technique. Currently available methods tend to be either costly and time-consuming or unreliable and often challenging as the drug compounds may interact with species in the sample media or environment. Such effects as light and the presence of proteins can have effects, influencing the drug compounds, causing their structure to change and affecting their spectral properties. There is a lack of techniques able to accurately determine concentrations of drug compounds in serum samples, that has the requirements for routine analysis. Furthermore, there are no specific methods for reliably assessing the kinetics of drugs that are photounstable and thus difficult to detect, current methods often treating the data using zero-, first- and second-order equations. Such equations do not account for factors influencing the extent of the photoreaction. Therefore there may be multiple interpretations of the data.

To allow for improved detection, and to enhance the spectral signal of 3AB, 2AB, BZ, MA, TR and AXI, β-CDP was added to each compound in both neutral and canal water samples. The shift and an increase in the fluorescence spectra in both media demonstrated the successful complexation of each compound with β-CDP.

The increases in signal were characterised by determining the stoichiometry and inclusion complex of each compound, to provide information on the complex binding strength, and the number of guest molecules each β-CDP unit was capable of complexing. The unknown

molecular weight of β-CDP was overcome by utilising a recently proposed mathematical equation. Such a method enabled the determination of both the inclusion complex and stoichiometry.

Poor detection in serum samples was able to be overcome through the development of a novel, easy to implement method. The technique addressed the obstacles of spectral changes and allowed for the detection of all compounds, when in the presence of the protein constituting the majority of serum, HSA.

The two proposed fluorimetric methods for the determination of the six compounds was evaluated and found to be reliable and accurate for routine analysis of the compounds in both canal water and HSA.

The photokinetic traces of TR and AXI were both able to form three photoproducts, the first part of which was able to be described by the newly proposed Φ-order equation for unimolecular and photoreversible reactions, obeying an A⇌B mechanism when subjected to non-isosbestic irradiation. Along with previous studies, this implies both TR and AXI could be described by Φ-order kinetics.

The use of the Φ-order equation was applied for the determination of the quantum yield of TR to indicate its photoreactivity. Application of the equations enabled the development of drug actinometers and the proposed method was able to demonstrate that both the quantum yield and β_{irr} were wavelength dependent, a factor not taken into account when interpreting photokinetic data.

The photostability of each TR and AXI was then ascertained in the presence of HSA and in β-CDP, and the data was well fitted to the Φ-order equation. The model was able to

demonstrate that the photodegradation rate of either compound was reduced when presented with either HSA or β-CDP. This reduction provided evidence that not only were the compounds stabilised against photodegradation, but that when interacted with either macromolecule they continued to obey Φ-order kinetics.

Common problems encountered when detecting pharmaceuticals in biofluids and surface waters were addressed in the study. Results from each method indicated the benefit for the methods to be used for future pharmaceutical samples in biofluids and surface waters.

9.2 Further studies

Although the study was only carried out with six compounds, there is the potential for further work in all three areas of this work.

The use of β-CDP to facilitate compound detection in canal water could be extended to other compounds and other surface waters, and may even be applied to compounds in media, such as less complex biofluids.

Studying the effect of temperature on the compound-β-CDP inclusion complexes could indicate the temperature at which a most stable complex is formed, and that at which it begins to dissociate. Through observing the lifetime of the species it may be possible to obtain information on the effect of β-CDP on the non-radiative energy loss processes competing with fluorescence.

The method developed to enable quantification of the compounds in HSA could not only be conducted using other compounds, to determine whether the method was only restricted to the six compounds investigated, but could be investigated with other fluorescent proteins to see if the method could be extended to these.

In addition, further information on the binding of the compound to HSA may be achieved by studying the effect of temperature and fluorescent lifetime of the species on the Stern-Volmer plot, as this can provide information on the quenching mechanism and thus provide an indication as to the interactions that may exist between the compound and protein. By studying the effect of HSA binding site markers, such as Ketoprofen and Warfarin, on the fluorescence of the compounds it could be determined which binding site each compound has a preference for, which may be useful for determining whether thereis competition between compounds for a particular binding site, altering the concentration of free drug.

The photodegradation of photounstable compounds, other than TR and AXI, may be investigated and be able to be modelled using Φ-order kinetics, and it could be investigated whether β-CDP or HSA are able to enhance photostability of compounds other than those used in this study, and whether other proteins, which may be present in biofluids or other pharmaceutical-containing commonly analysed samples, are able to provide photostabilising effects to compounds.

Furthermore, the study could be expanded, and other instrumentation used to collect additional data. Optimised ROESY NMR data could be used to determine the mode and stability of compound-β-CDP complex, and SEM and IR could be used to provide information on how the compound is complexed and the interactions that may be involved.

Annexe

Annexe

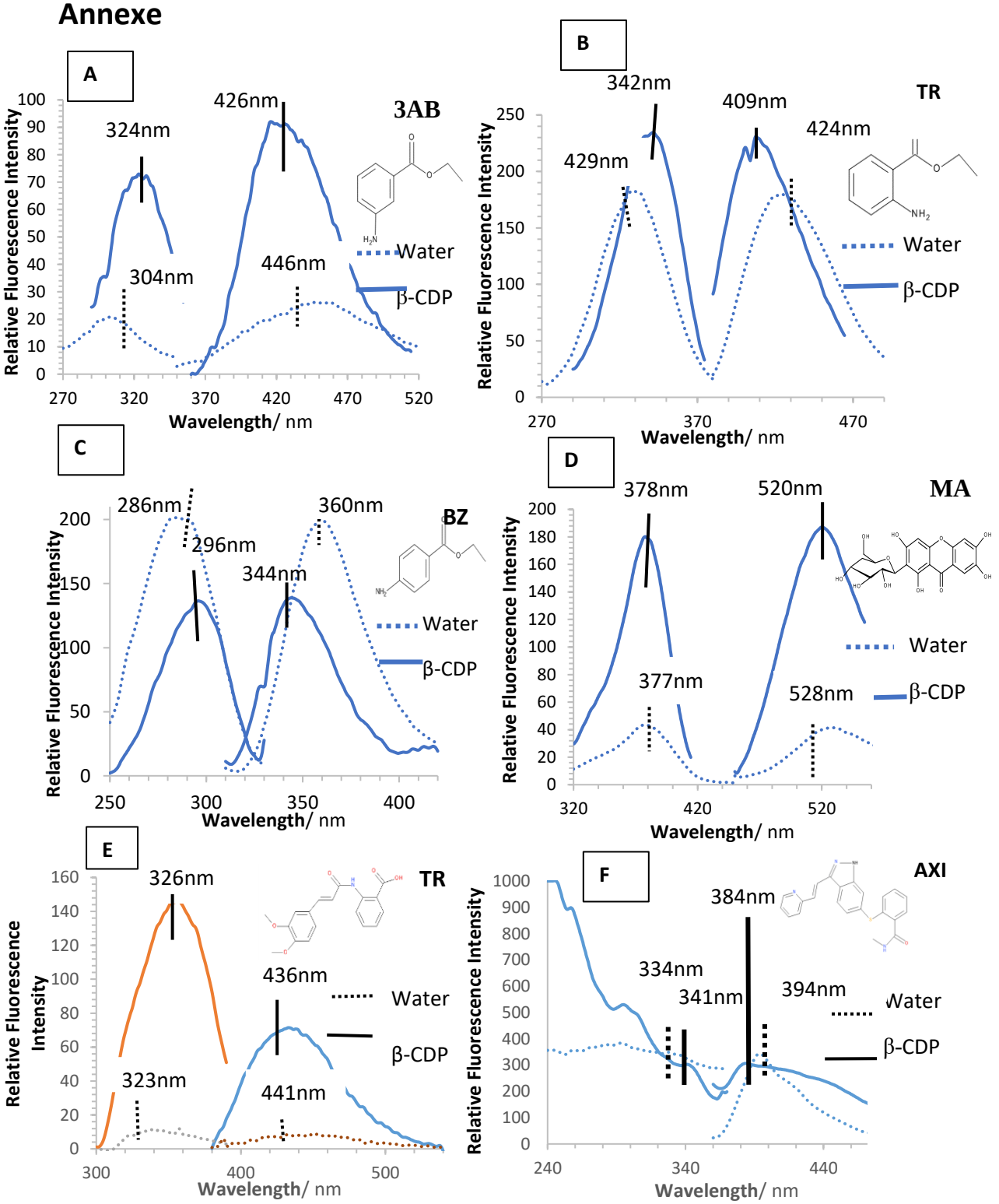

Figure 1: Excitation and emission spectra of 24.33ppb (A) 3AB, (B) 0.41ppb 2AB, (C) 38.74ppb BZ, (D) 2.02ppb MA, (E) 1.49ppb TR and (F) 3.01ppb AXI in water (Water)(dashed lines), and (A) 0.65ppb 3AB, (B) 0.33ppb 2AB, (C) 0.97ppb BZ, (D) 1.01ppb MA, (E) 1.49ppb TR and (F) 3.01ppb AXI in (A) 25.20mg/mL, (B) 12.0mg/mL, (C) 4.32mg/mL, (D) 12.17mg/mL, (E) 11.98mg/mL and (F) 15.08mg/mL β-CDP, respectively (β-CDP)(plain lines), at room temperature, the maximum spectra of which are labelled

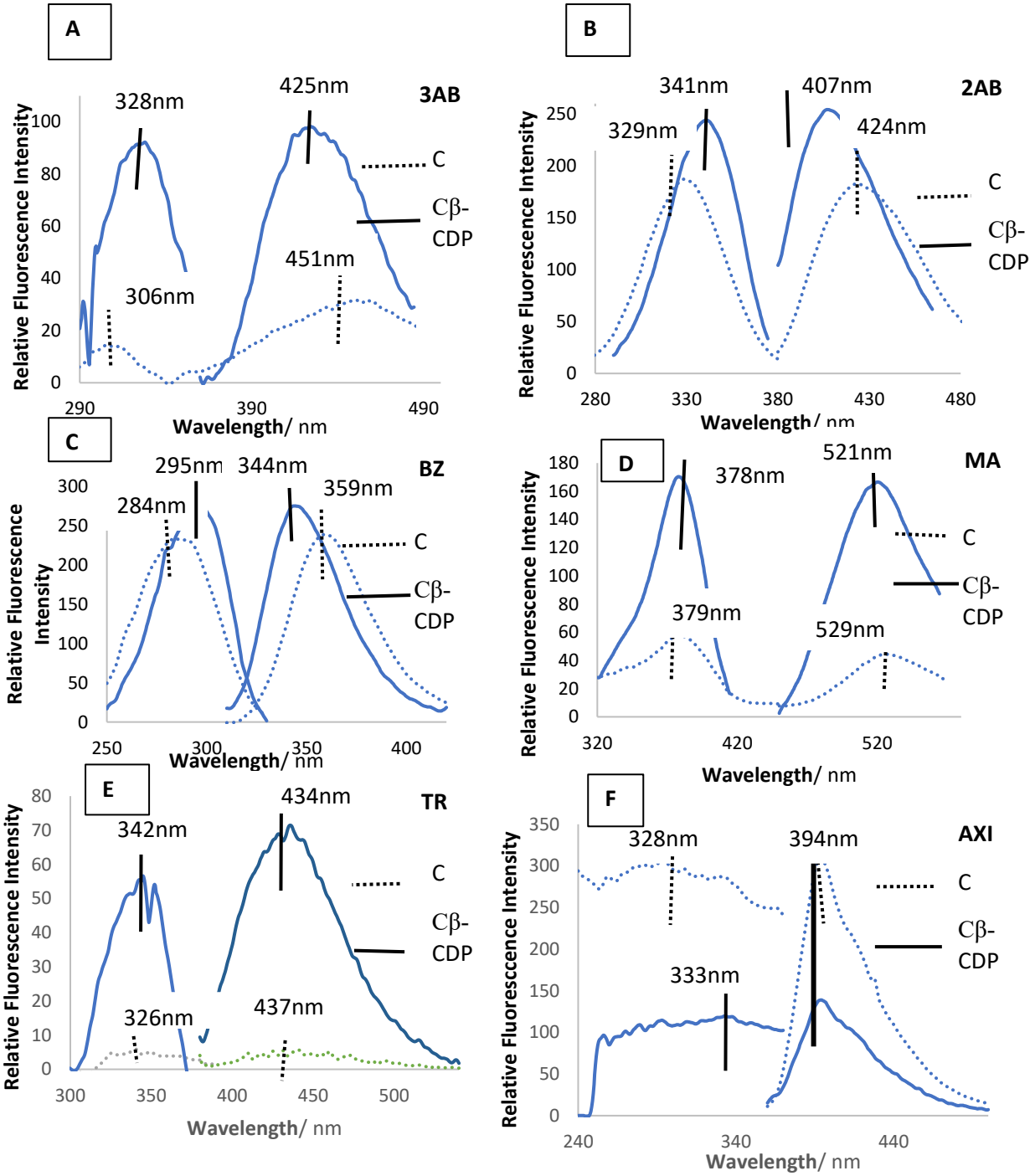

Figure 2: Excitation and emission spectra of (A) 29.24ppb 3AB, (B) 1.64ppb 2AB, (C) 48.37ppb BZ, (D) 2.02ppb MA, (E) 0.75ppb TR and (F) 2.41ppb AXI in canal water (C)(dashed lines), (A) 0.65ppb 3AB, (B) 0.33ppb 2AB, (C) 1.93ppb BZ, (D) 1.01ppb MA, (E) 0.75ppb TR and (F) 1.21ppb AXI in (A) 25.13mg/mL, (B) 12.03mg/mL, (C) 4.09mg/mL, (D) 12.01mg/mL, (E) 11.98mg/mL and (F) 15.02mg/mL β-CDP(Cβ-CDP)(plain lines), respectively, at room temperature, the maximum spectra of which are labelled

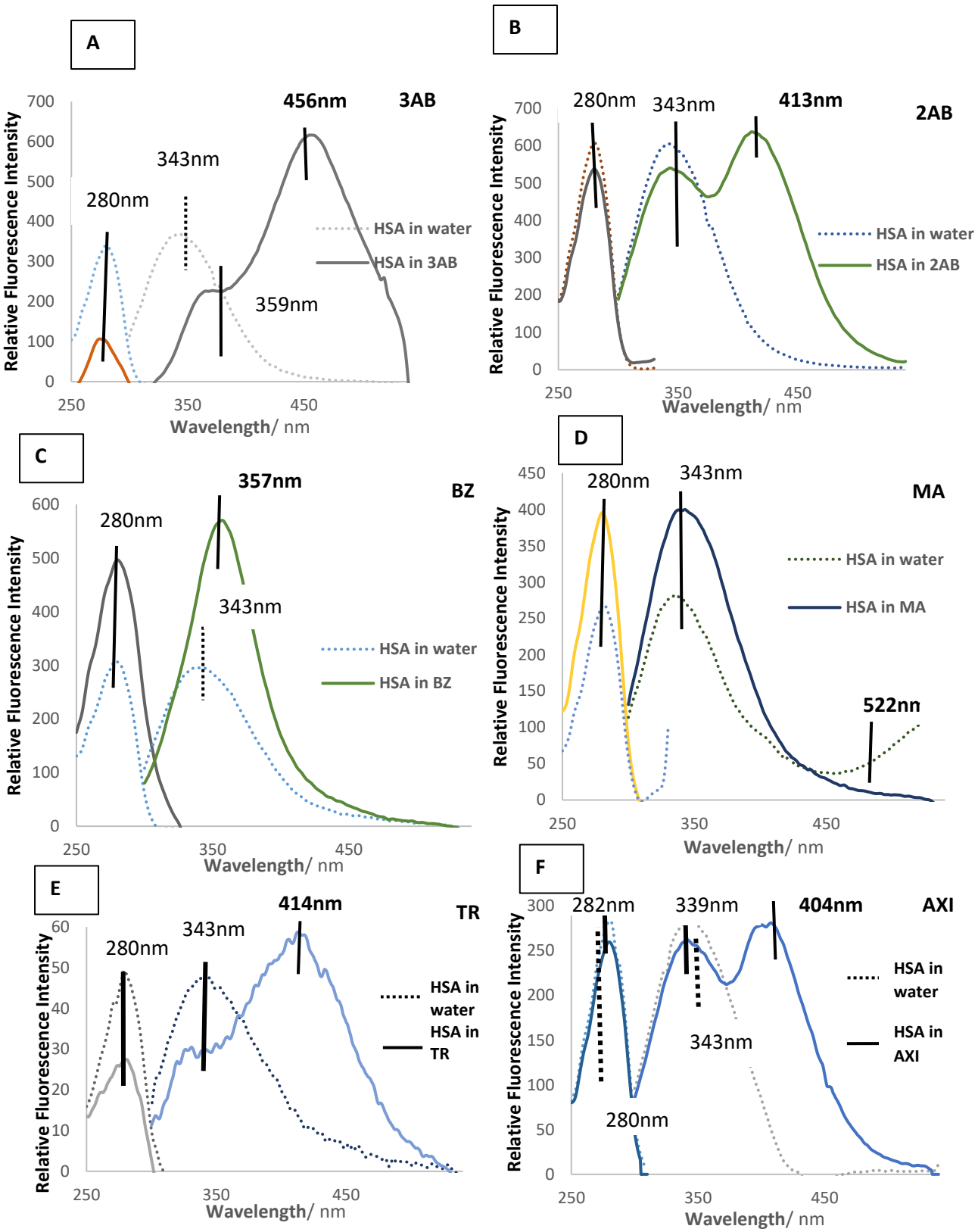

Figure 3: Excitation and emission spectra of (A) 0.0014ppb, (B) 0.0048ppb, (C) 0.0014ppb, (D) 0.0014ppb, (E) 0.0038ppb and (F) 0.0017ppb HSA in water (dashed lines), and (A) 38.95ppb 3AB in 0.0014ppb HSA, (B) 24.56ppb 2AB in 0.0048ppb HSA, (C) 24.19ppb BZ in 0.0014ppb HSA, (D) 28.97ppb MA in 0.0014ppb HSA, (E) 7.47ppb TR in 0.0038ppb HSA and (F) 3.01ppb AXI in 0.0017ppb HSA (plain lines), at room temperature, the maximum spectra of HSA is labelled, along with the maximum emission spectra of the drugs (included in bold)

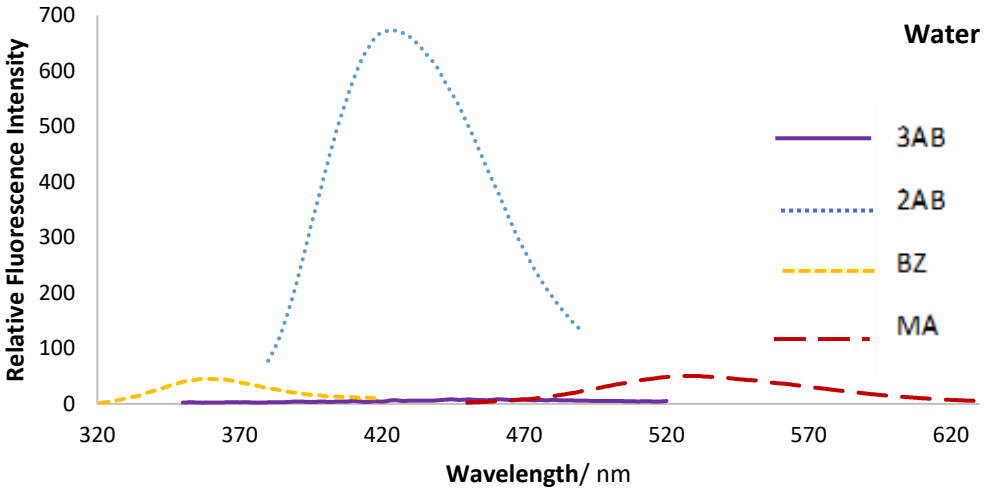

Figure 4: Comparison of the emission spectra of 5.7ppb 3AB, 5.73ppb 2AB, 9.67ppb BZ and 2.52ppb MA in water

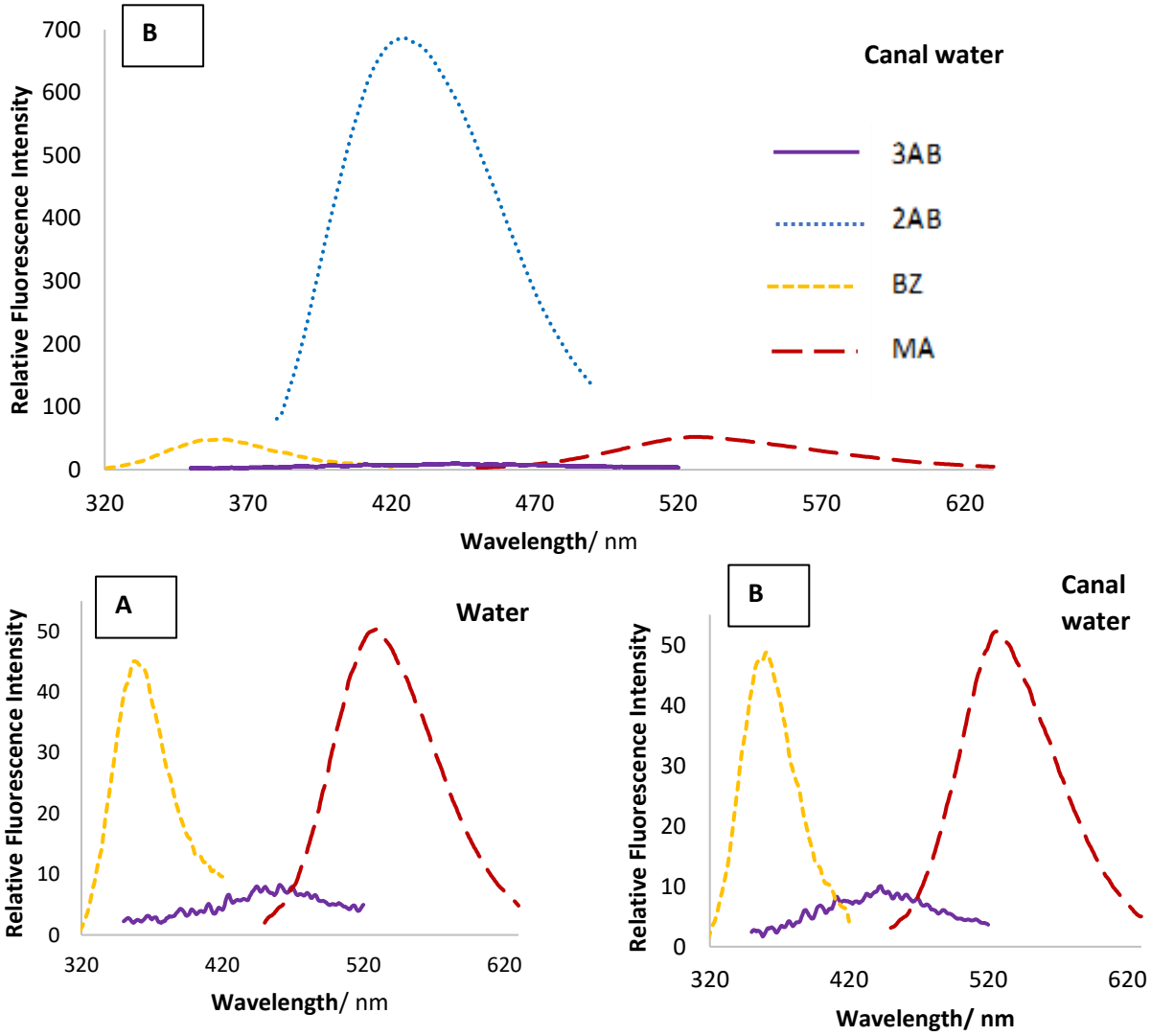

Figure 5: Comparison of the emission spectra of 5.7ppb 3AB, 5.73ppb 2AB, 9.67ppb BZ and 2.52ppb MA in (A) water and (B) canal water

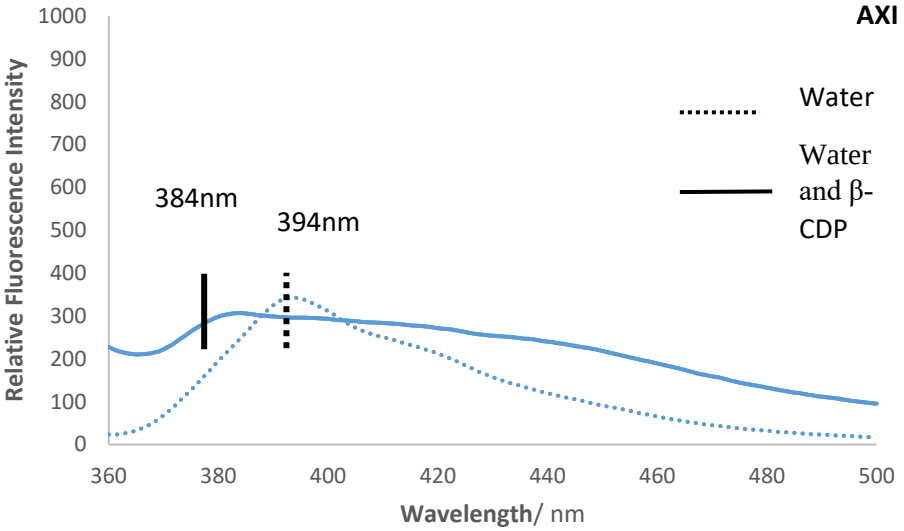

Figure 6: Excitation and emission spectra of 3.01ppb AXI in water and ethanol (98/2)(dashed lines), and 3.01ppb AXI in 15.08mg/mL β-CDP, respectively (plain lines), at room temperature, the maximum spectra of which are labelled

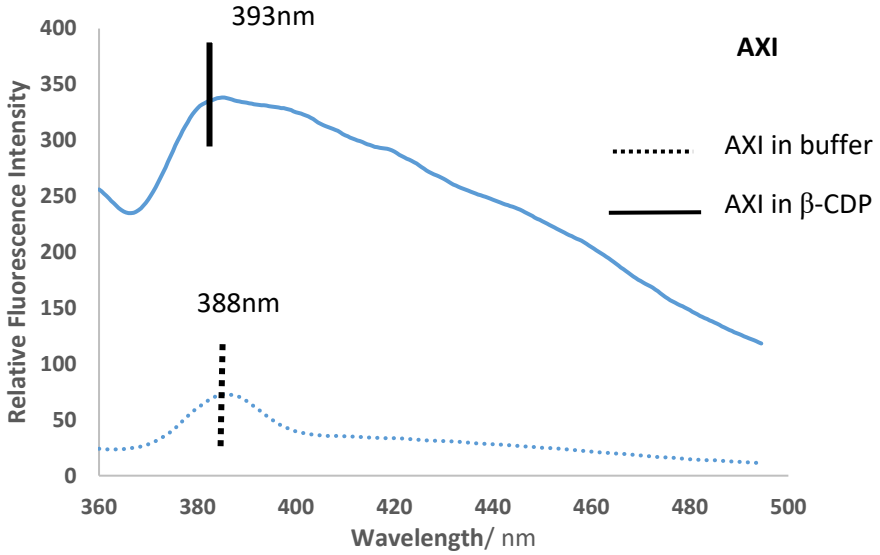

Figure 7: Emission spectra of 2.41ppb AXI in water: ethanol solution after 3 hours, and 2.41ppb AXI in water: ethanol solution and 15.22mg/mL β-CDP water: ethanol solution after 3 hours

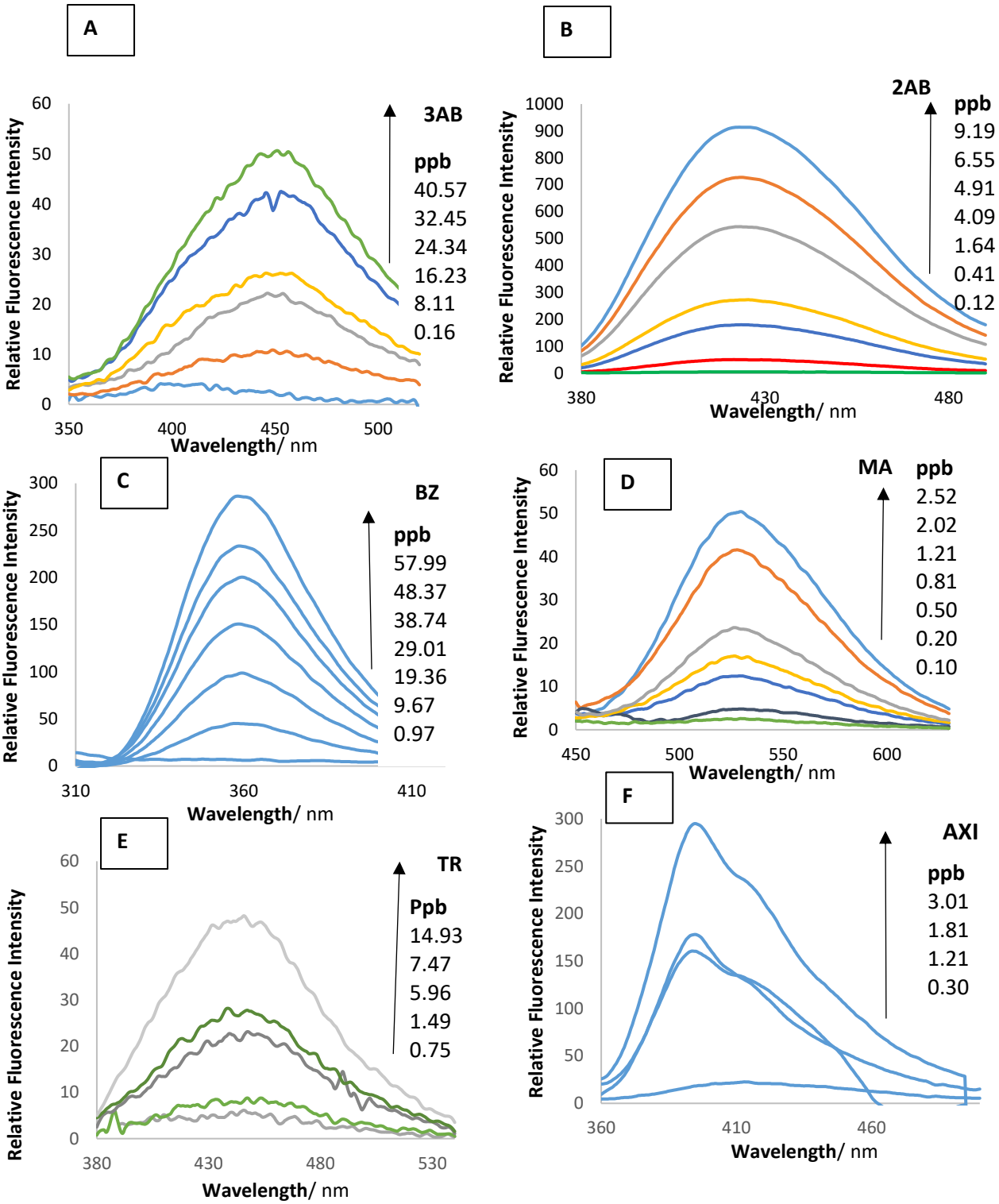

Figure 8: Evolution of calibration concentrations of (A) 3AB, (B) 2AB, (C) BZ and (D) MA in buffer pH=7, (E) TR in pH=4 and (F) AXI in water and ethanol (98/2), at room temperature

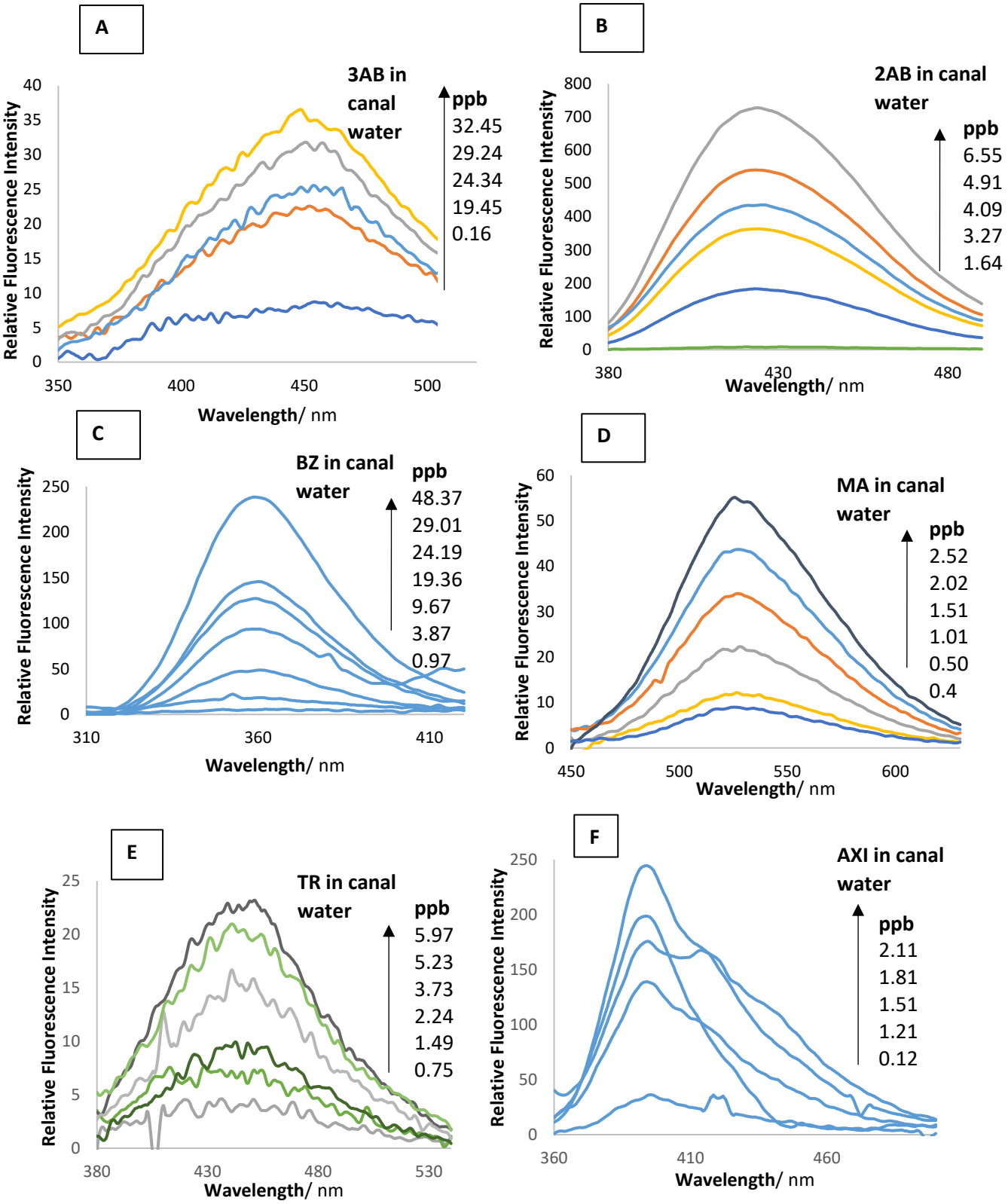

Figure 9: Evolution of calibration concentrations of (A) 3AB, (B) 2AB, (C) BZ, (D) MA, (E) TR and (F) AXI in canal water, at room temperature

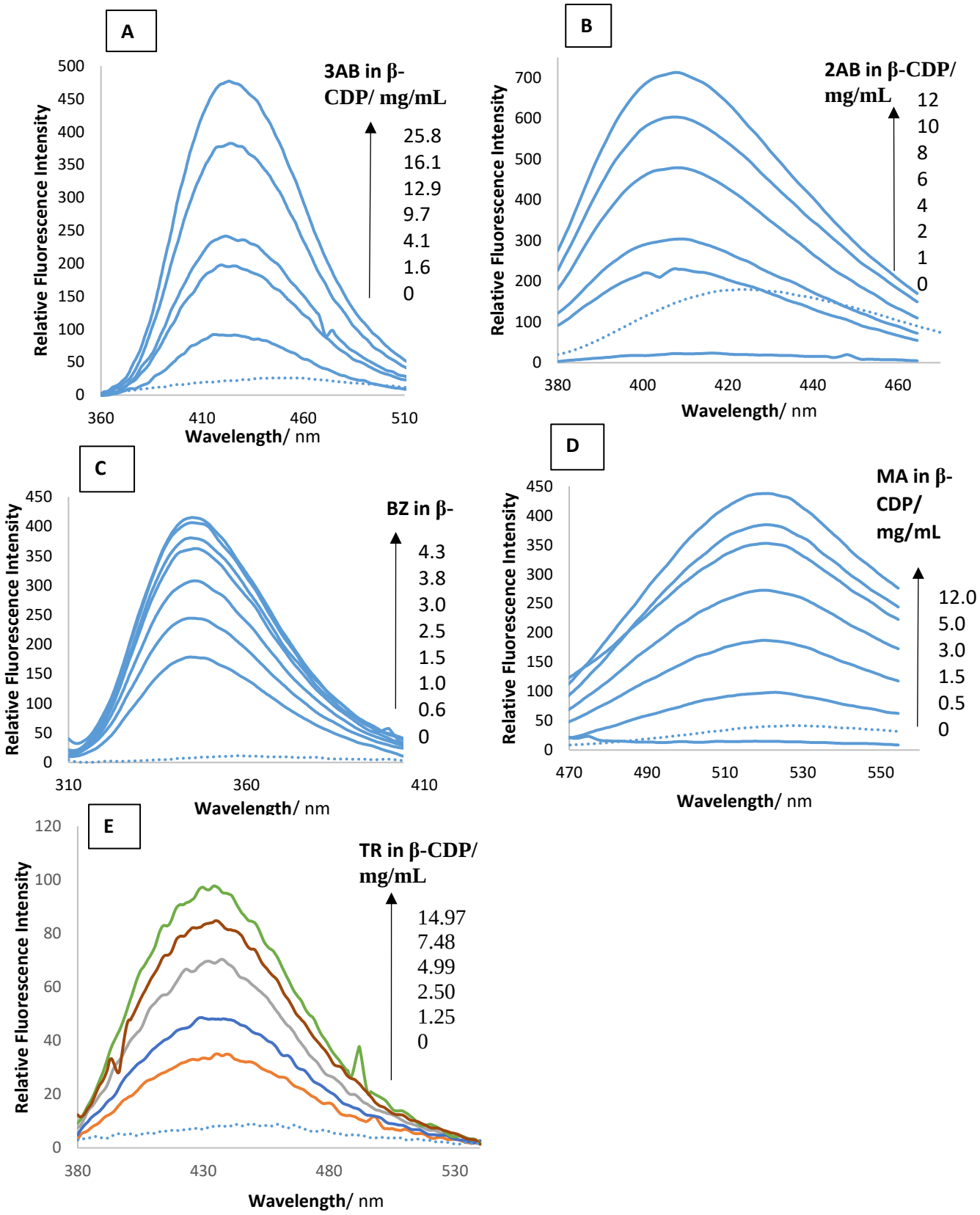

Figure 10: Evolution of the fluorescence emission spectra of (A) 2.60ppb 3AB, (B) 0.98ppb 2AB, (C) 2.90ppb BZ and (D) 4.19ppb MZ in water and (E) 1.49ppb TR in buffer pH=4, with increasing concentrations of β-CDP, at room temperature

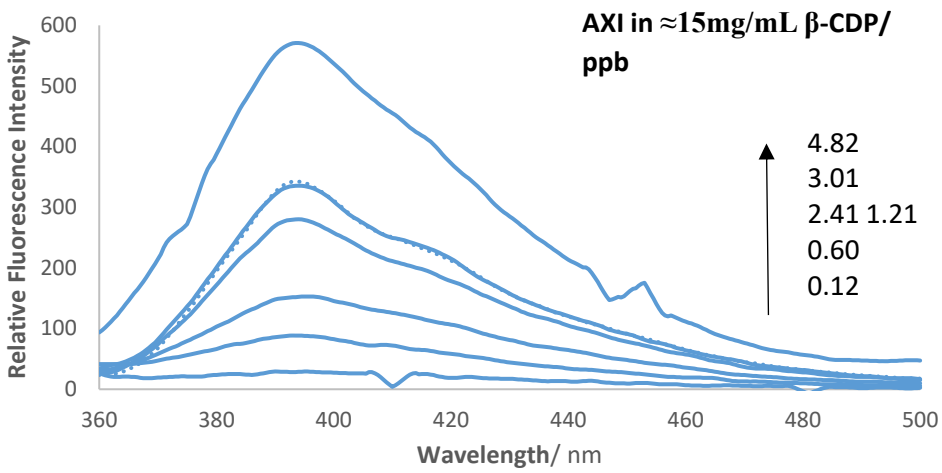

Figure 11: Effect on maximum intensity of various concentrations of AXI after 3 hours in water and ethanol (98/2)(dashed line) and ≈15mg/mL β-CDP, at room temperature (solid lines)

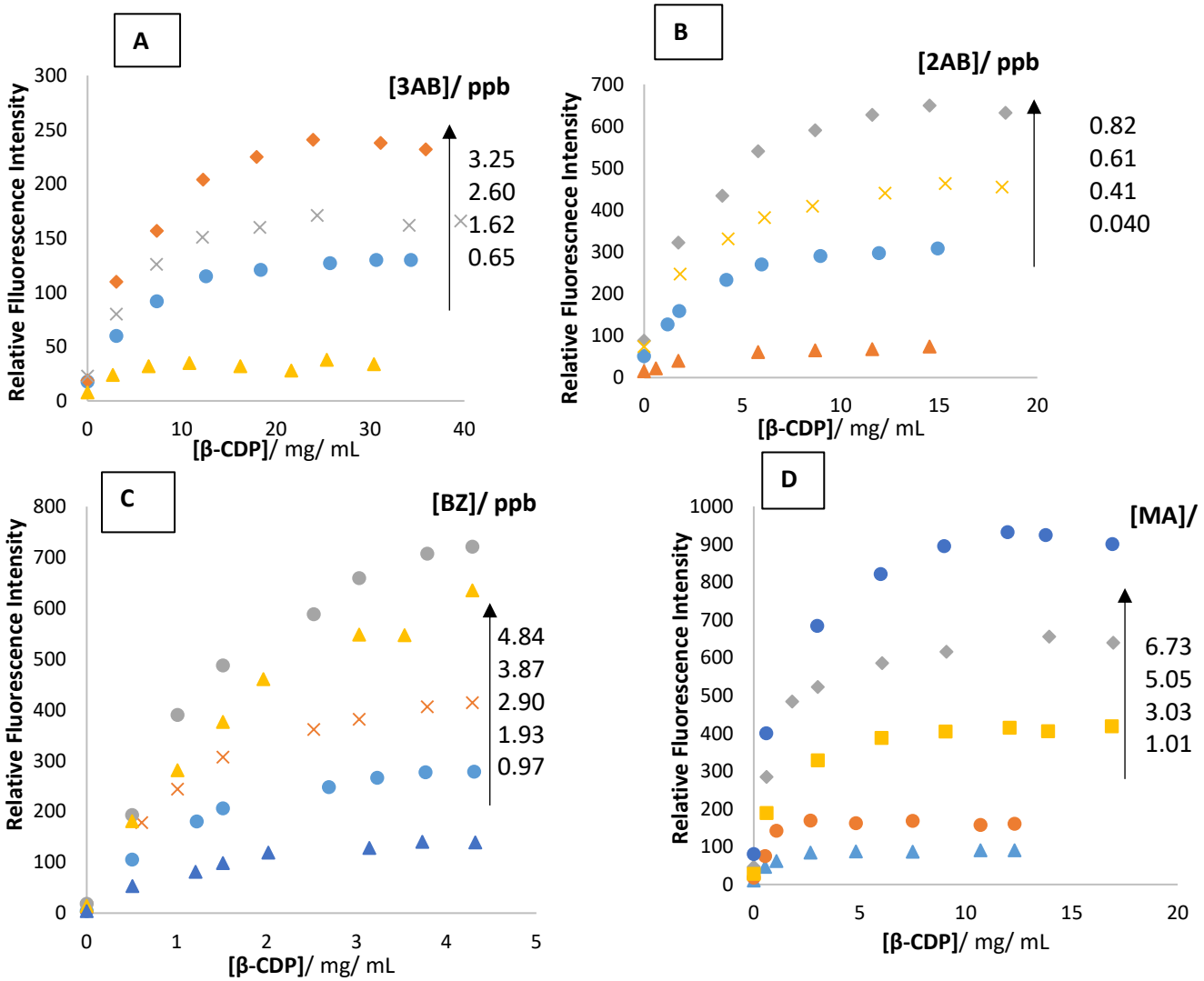

Figure 12: Isotherms of varying (A) 3AB, (B) 2AB, (C) BZ and (D) MA concentrations ((A) 0.65-3.25ppb, (B) 0.04-0.82ppb, (C) 0.97-4.84ppb and (D) 0.50ppb-2.49ppb, respectively), in water

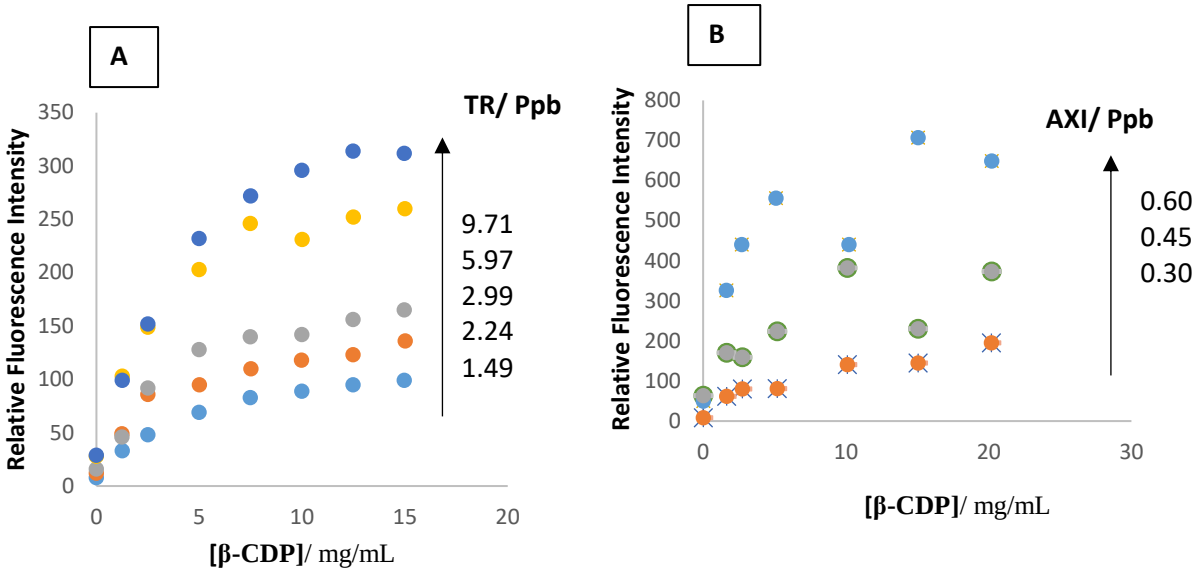

Figure 13: Isotherms of varying concentrations of (A) TR (1.49-9.71ppb) in buffer pH=4, and (B) AXI (0.3-0.6ppb) (after 3 hours) in water and ethanol (98/2), with increasing concentrations of β-CDP, at room temperature

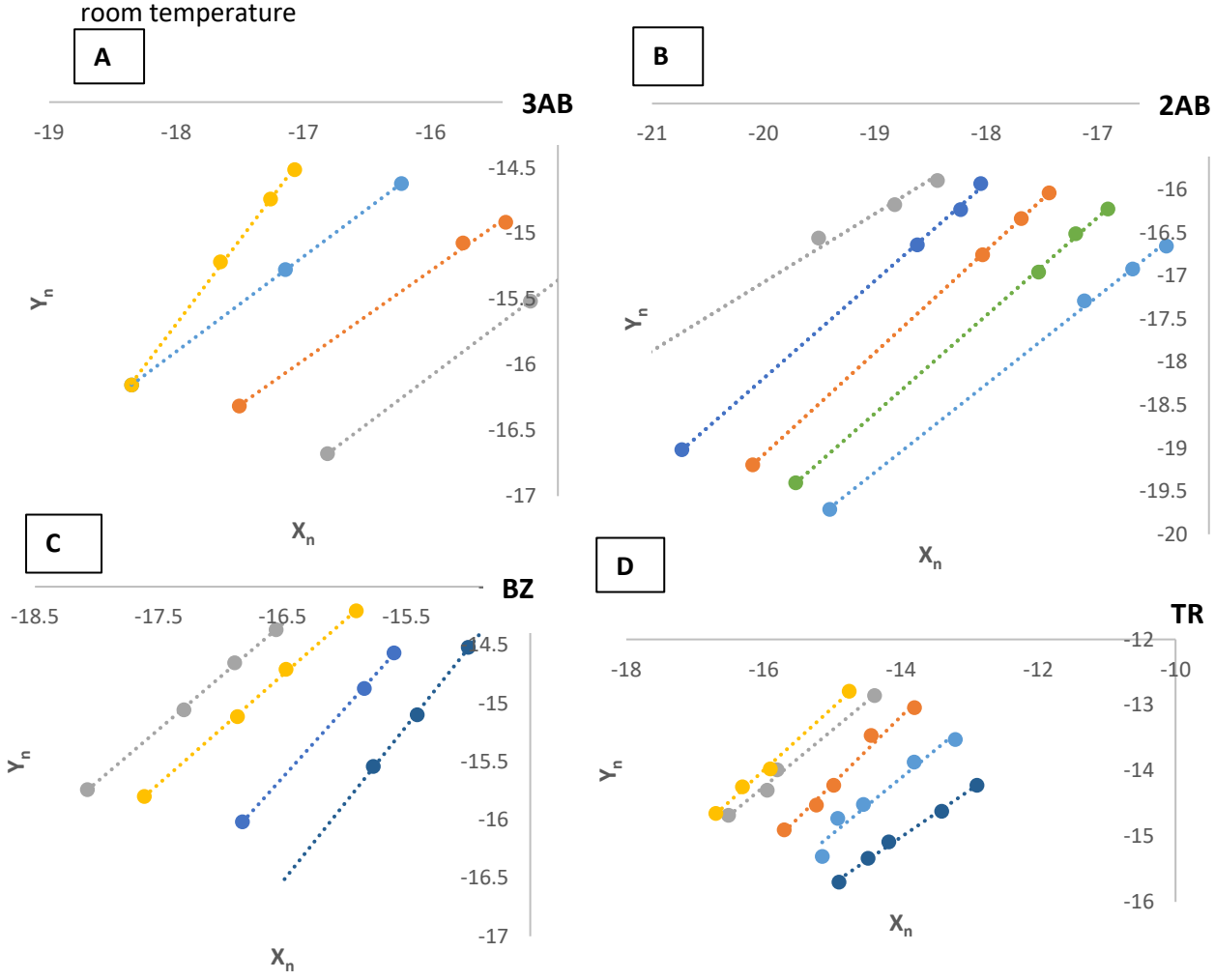

Figure 14: Determination of coefficient 'n' for (A) 3AB, (B) 2AB, (C) BZ and (D) TR complexes

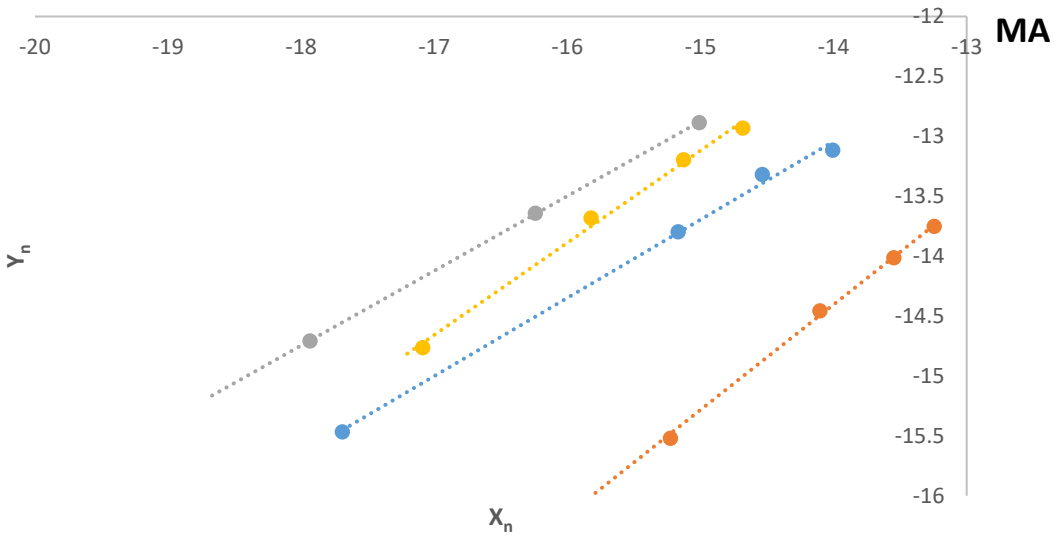

Figure 15: Determination of coefficient 'n' for MA complexes

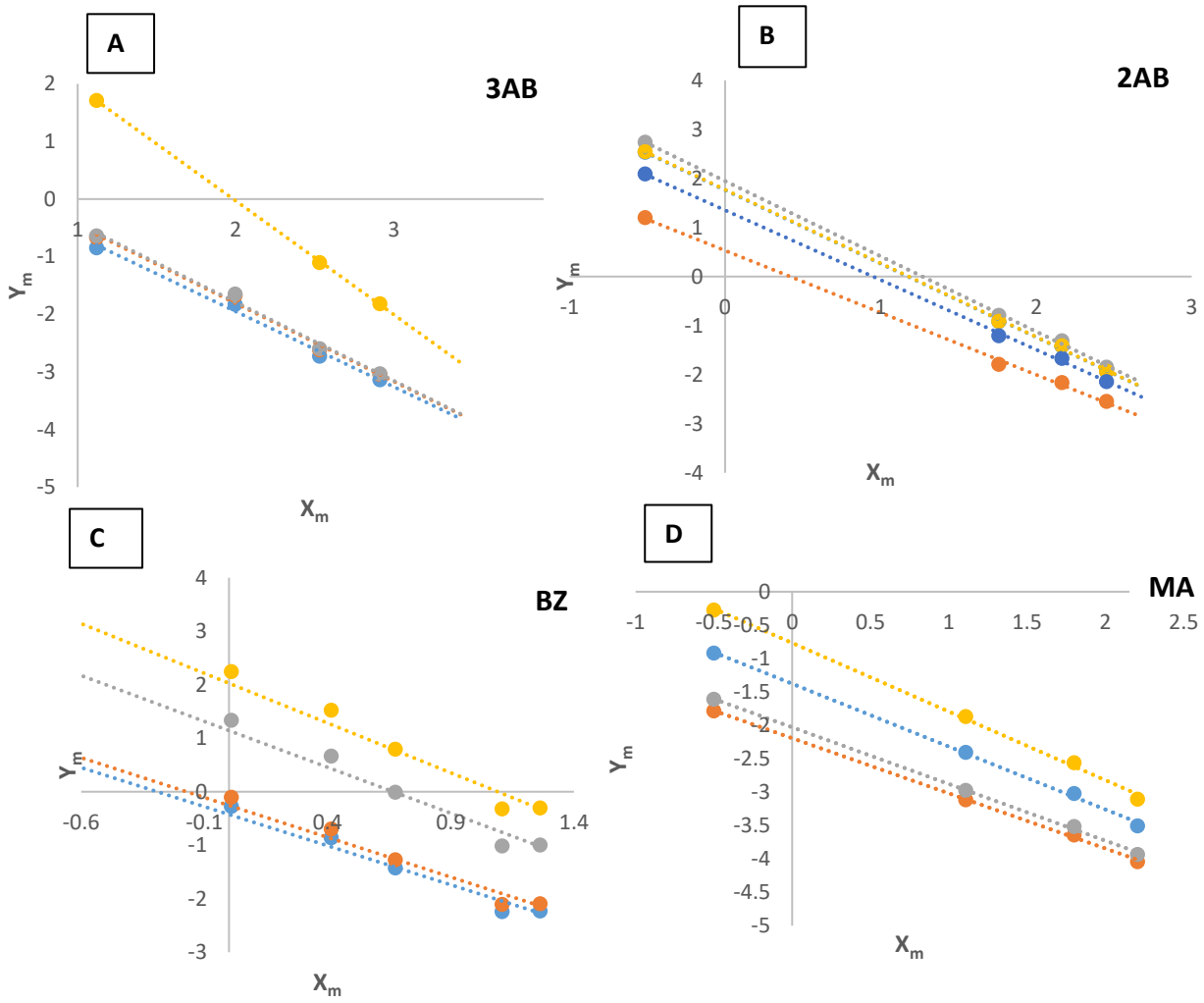

Figure 16: Determination of coefficient 'm' for (A) 3AB, (B) 2AB, (C) BZ and (D) MA complexes

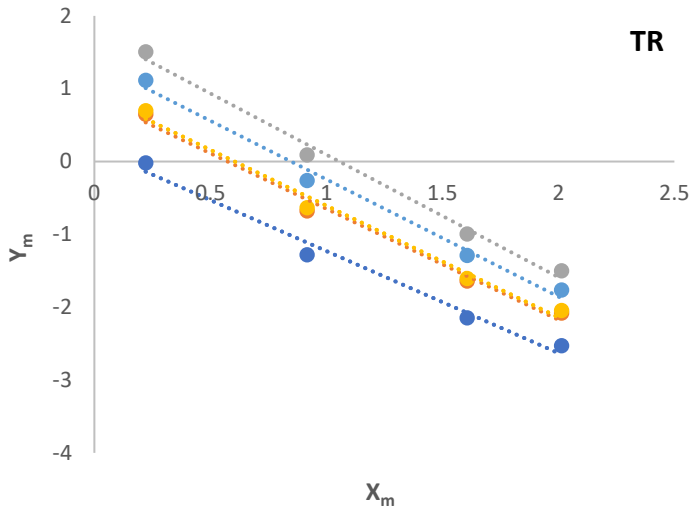

Figure 17: Determination of coefficient ‘m’ for TR complexes

Table 1: Statistical results of 3AB, 2AB, BZ, MA, TR and AXI in water (W) and canal water (C), and calibration of AXI in 0.0011ppb HSA, RFI= Relative Fluorescence Intensity, s.d.= Standard deviation

Compound		**3AB**		**2AB**		**BZ**		**MA**		**TR**		**AXI**		
	Medium	**W**	**C**	**W**	**C**	**W**	**C**	**W**	**C**	**W**	**C**	**W**	**C**	**HSA**
Gradient/ x $10^8 M^{-1}$	**Average**	0.083	0.047	6.69	6.68	0.29	0.30	0.48	0.51	0.093	0.10	2.47	0.92	0.031
	s.d.	0.00055	0.000033	0.030	0.12	0.0057	0.0037	0.013	0.013	0.0022	0.00057	0.017	0.0024	0.00084
	RSD/ %	1.44	0.069	0.53	1.77	1.95	1.25	0.82	2.63	2.37	0.56	0.69	2.61	2.67
Intercept/ RFI	**Average**	3.30	-0.0025	1.40	1.21	4.50	-1.05	1.02	0.51	2.38	2.25	-6.38	-1.62	103.79
	s.d.	0.83	0.86	0.85	0.51	1.75	0.58	0.37	0.23	0.42	0.090	1.80	2.56	2.90
	RSD/ %	-	-	-	-	-	-	-	-	-	-	-	-	-
Average regression correlation coefficient		0.997	0.995	0.999	0.999	0.998	0.997	0.998	0.998	0.994	0.990	0.996	0.981	0.918
Average linearity range/ ppb		0.16-48.68	5.46-34.09	0.013-8.19	0.013-8.19	0.998 0.97-57.99	1.61-48.37	0.10-2.52	0.10-2.52	0.75-14.93	0.75-6.47	0.30-3.01	2.14-57.16	10.72-27.69

Table 2: Analytical parameters of 3AB, 2AB, BZ, MA, TR and AXI, in water (W) and canal water (C),in approximately 25mg/mL, 12mg/mL, 12mg/mL, 4mg/mL, 12mg/mL and 15mg/mL β-CDP, respectively, RFI= Relative Fluorescence Intensity, s.d.= Standard deviation

Compound		**3AB**		**2AB**		**BZ**		**MA**		**TR**		**AXI**	
Medium		**W**	**C**	**W**	**C**	**W**	**C**	**W**	**C**	**W**	**C**	**W**	**C**
Gradient/ x $10^8 M^{-1}$	**Average**	0.79	8.17	44.40	43.33	9.33	8.32	4.13	3.77	1.27	1.72	2.57	0.42
	s.d.	0.14	0.23	0.57	1.30	0.084	0.25	0.12	0.12	0.0059	0.036	0.036	0.015
	RSD/ %	2.12	2.78	1.28	3.01	0.90	3.02	2.95	3.07	0.46	2.10	1.39	3.67
Intercept/ RFI	**Average**	2.59	7.15	3.67	10.71	0.81	2.32	5.80	4.81	8.90	26.79	50.62	83.35
	s.d.	2.65	2.44	3.48	4.41	2.56	4.84	2.45	4.10	5.40	0.052	5.16	4.40
	RSD/ %	-	-	-	-	-	-	-	-	-	-	-	-
Average regression correlation coefficient		0.996	0.997	0.997	0.998	0.999	0.999	0.998	0.997	0.998	0.993	0.997	0.992
Average linearity range/ ppb		0.65-3.03	0.65-3.25	0.013-0.98	0.013-0.98	0.13-4.84	0.19-1.42	0.10-2.52	0.20-2.07	0.20-3.98	0.17-2.86	0.15-1.21	1.34-8.93

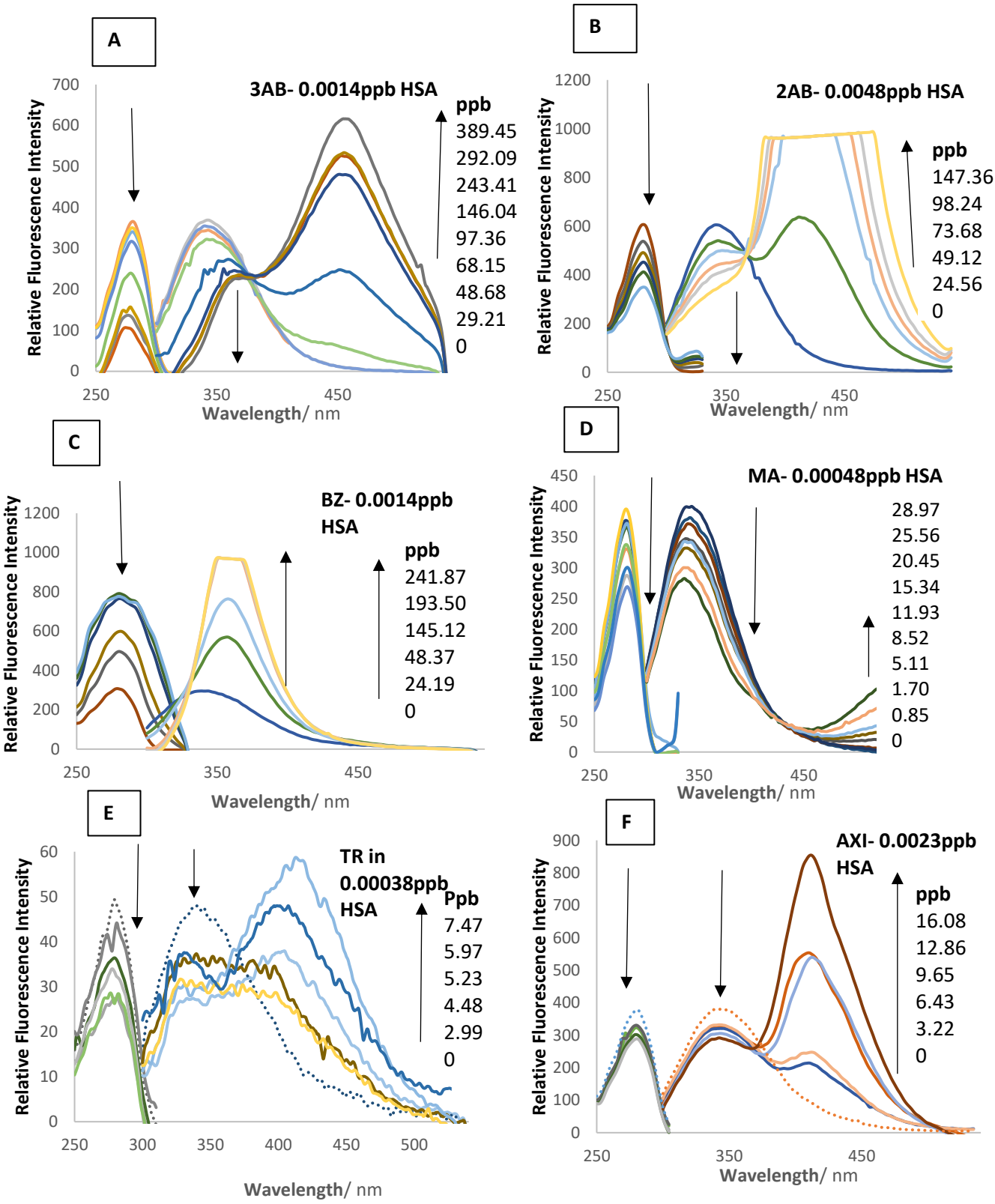

Figure 18: The effect of increasing concentrations of (A) 3AB, (B) 2AB, (C) BZ, (D) MA, (E) TR and (F) AXI on the fluorescence excitation and emission spectra of a specified concentration of human serum albumin

Table 3: Fluorescence features of HSA in the presence and absence of 3AB, 2AB, BZ, MA, TR and AXI

Compound	Medium	Fluorescence excitation (nm)[a]	Fluorescence emission (nm)	Stoke's shift (nm)[b]	$\frac{Fl^{obs}}{Fl^{obs}}_{c}$
HSA	Water	280	343	63	1
	3AB	274	359	85	0.57
	2AB	280	343	63	0.89
	BZ	280	-	-	-
	MA	280	343	63	0.68
	TR	280	343	63	0.63
	AXI	282	339	57	0.92

[a] The maximum excitation and emission spectra of the compounds, alone are underlined, whilst shoulders are displayed in brackets

[b] The Stoke's shift is calculated from the difference in the energy of the maximum emission spectra and the maximum excitation spectra of the compound

[c] The fluorescence intensity of the numerator corresponds to either the maximum fluorescence intensity of 0.0014ppb HSA in water, 0.0014ppb HSA in 38.95ppb 3AB, 0.0048ppb HSA in water, 0.0048ppb HSA in 24.56ppb 2AB, 0.0014ppb HSA in water, 0.0014ppb HSA in 24.19ppb BZ, 0.0014ppb HSA in water, 0.0014ppb HSA in 28.97ppb MA, 0.0038ppb HSA in water, 0.0038ppb HSA in 7.47ppb TR, 0.0017ppb HSA in water or 0.0017ppb HSA in 3.01ppb AXI, respectively ($Fl^{obs}$is equal to $Fl^{\lambda obs}_{0,G,i}$)

[d] The fluorescence intensity of the denominator corresponds to the fluorescence intensity of 0.0014ppb, 0.0048ppb, 0.0014ppb, 0.0014ppb, 0.0038ppb and 0.0017ppb HSA in water, respectively

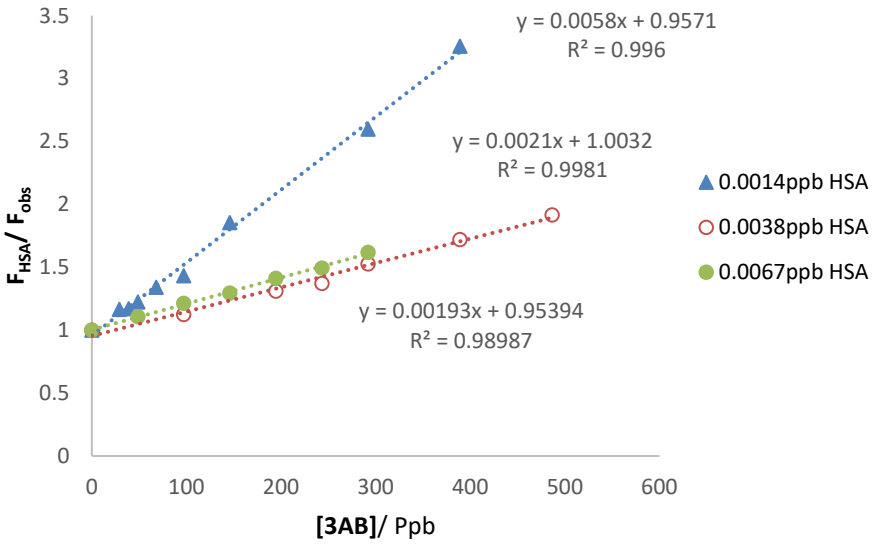

Figure 19: Average Stern-Volmer plot of 0.0014ppb, 0.0038ppb and 0.0067ppb HSA in increasing concentrations of 3AB

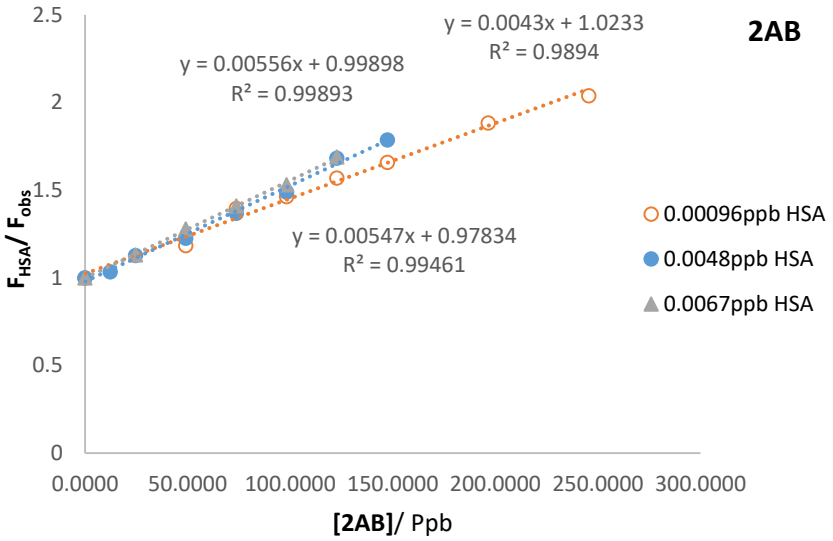

Figure 20: Average Stern-Volmer plot of 0.00096ppb, 0.0048ppb and 0.0067ppb HSA in increasing concentrations of 2AB

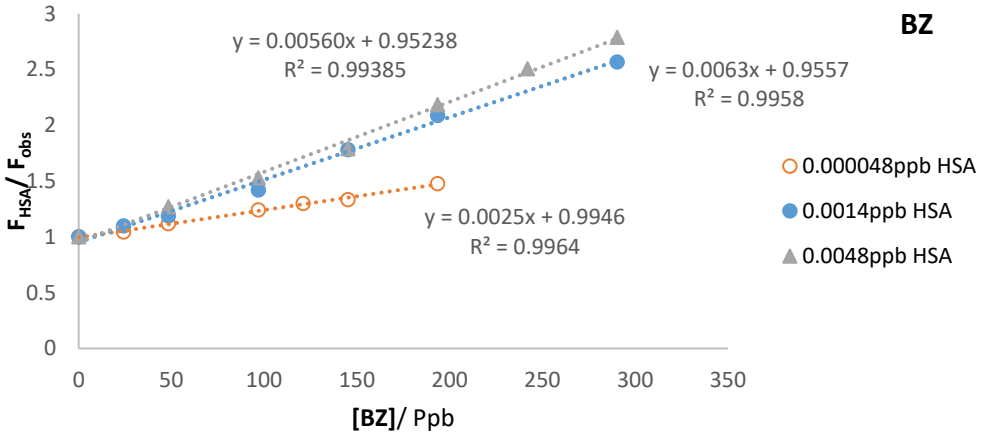

Figure 21: Average Stern-Volmer plot of 0.000048ppb, 0.0014ppb and 0.0048ppb BZ HSA in increasing concentrations of BZ

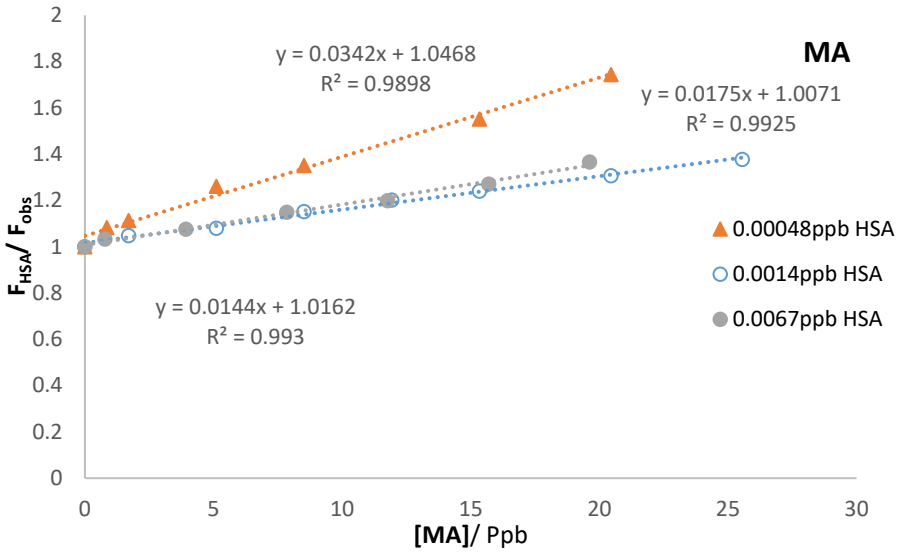

Figure 22: Average Stern-Volmer plot of 0.00048ppb, 0.0014ppb and 0.0067ppb HSA in increasing concentrations of MA

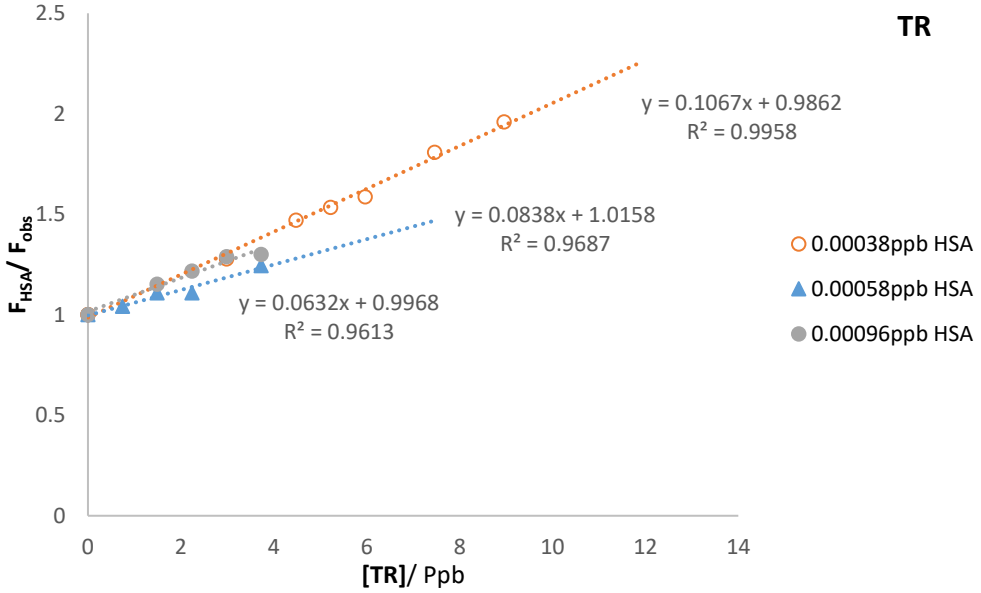

Figure 23: Average Stern-Volmer plot of 0.00038ppb, 0.00058ppb and 0.00096ppb HSA in increasing concentrations of TR

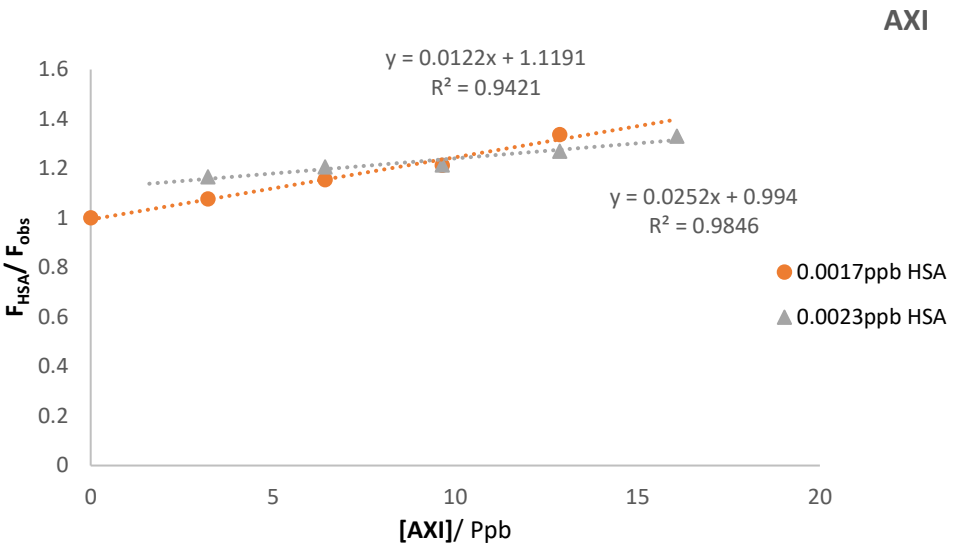

Figure 24: Average Stern-Volmer plot of 0.0017ppb and 0.0023ppb HSA in increasing concentrations of AXI

Table 4: Quenching calibration graphs of 3AB, 2AB, BZ, MA, TR and AXI in the presence of various concentrations of HSA, RFI= Relative Fluorescence Intensity, s.d.= Standard deviation

Compound		**3AB**			**2AB**			**BZ**			**MA**			**TR**			**AXI**	
Concentration of HSA/ Ppb		**0.0014**	**0.0038**	**0.0067**	**0.00096**	**0.0048**	**0.0067**	**0.000048**	**0.0048**	**0.0014**	**0.00048**	**0.0014**	**0.0067**	**0.00038**	**0.00058**	**0.00096**	**0.0017**	**0.0023**
Gradient/ x 10^6M^{-1}	**Average**	0.0056	0.0019	0.0021	0.0046	0.0053	0.0056	0.0025	0.0063	0.0057	0.035	0.015	0.018	0.32	0.015	0.26	0.062	0.031
	s.d.	0.00010	0.000064	0.000029	0.00034	0.00026	0.00023	0.00012	0.00036	0.000029	0.00039	0.00057	0.00072	0.0092	0.17	0.0086	0.0021	0.00067
	RSD/ %	1.70	3.30	1.42	7.29	4.96	4.20	4.74	2.17	0.50	1.01	3.91	3.95	2.86	8.39	3.28	3.43	2.18
Intercept/ RFI	**Average**	0.90	0.96	1.00	1.00	0.98	1.00	1.00	0.95	0.95	1.06	1.00	1.00	1.00	1.00	1.03	1.00	1.13
	s.d.	0.031	0.016	0.0042	0.019	0.0067	0.013	0.0078	0.017	0.017	0.014	0.0083	0.0067	0.014	0.0037	0.009	0.0074	0.0095
	RSD/ %	3.43	1.68	0.42	1.94	0.68	1.33	0.78	1.79	1.77	1.29	0.83	0.67	1.42	0.37	0.97	0.74	0.84
Average regression correlation coefficient		0.989	0.992	0.997	0.990	0.995	0.997	0.988	0.994	0.986	0.985	0.992	0.995	0.995	0.944	0.950	0.982	0.890
Average linearity range/ ppb		74.64-389.45	97.36-486.82	64.91-292.09	49.12-212.86	20.47-147.36	24.56-122.80	32.25-193.50	48.37-290.24	24.19-225.75	1.14-20.45	5.11-23.86	2.88-18.31	2.74-9.21	1.00-4.98	1.00-3.73	4.29-15.01	3.22-16.08

Table 5: Percentage recoveries of 3AB, 2AB, BZ, MA, TR and AXI obtained in the presence of the specified concentrations of human serum albumin (+C_{Add}/ ppb=Concentration added, ≠C_{Det}/ ppb=Average concentration detected,*%$_{REC}$= Average percentage recovery, [HSA]= Concentration of HSA

Compound	**[HSA]/ ppb**	**+C_{Add}/ ppb**	**≠C_{Det}/ ppb**	***%$_{REC}$**	**[HSA]/ ppb**	**+C_{Add}/ ppb**	**≠C_{Det}/ ppb**	***%$_{REC}$**	**[HSA]/ ppb**	**+C_{Add}/ ppb**	**≠C_{Det}/ ppb**	***%$_{REC}$**
3AB	0.0014	292.09	261.19	92.63	0.0038	389.45	368.90	91.80	0.0067	292.09	305.85	101.86
			285.95				357.43				303.02	
			264.56				346.27				283.74	
		97.36	92.65	98.01		194.73	191.29	94.93		197.67	194.73	91.67
			101.12				168.28				167.66	
			98.01				194.98				170.16	
		194.73	167.96	96.01		97.36	97.95	98.76		97.36	94.11	102.09
			214.43								98.60	
			178.47								105.47	
2AB	0.00095	49.12	55.17	100.88	0.0047	24.56	24.14	99.62	0.0067	122.80	114.92	96.81
			45.07				27.71				109.59	
			48.42				21.54				132.13	
		98.24	107.68	105.43		98.24	109.47	109.36		49.12	50.45	107.82
			93.80				103.37				56.88	
			109.26				109.47				51.56	
		196.49	211.57	104.99		147.36	125.89	97.98		7.37	6.70	91.98
			224.64				140.37				6.70	
			182.65				166.93				6.94	
BZ	0.00048	24.19	25.52	96.11	0.0014	15.48	13.41	87.16	0.0047	48.37	51.07	110.88
			22.25				13.71				54.24	
			21.97				13.35				55.60	
		145.12	126.77	97.00		24.19	22.23	99.86		145.12	138.86	94.17
			162.85				25.91				132.27	
			132.70				24.31				138.86	
		290.24	301.75	104.81		241.87	216.26	92.01		290.24	259.56	92.74

			300.05				219.19				259.19	
			310.80				232.22				288.36	
MA	0.00048	6.28	6.70	93.39	0.0014	3.92	3.80	107.51	0.069	3.92	4.43	101.55
			6.70				4.43				3.66	
			6.70				4.43				3.87	
		17.27	18.22	111.02		23.55	23.05	103.52		11.77	11.96	93.14
			19.64				23.05				10.47	
			19.64				27.02				10.47	
		1.57	1.69	107.35		51.02	46.96	94.83		17.27	19.63	98.89
			1.69				49.09				16.27	
			1.69				49.09				15.33	
TR	0.00038	1.49	1.44	93.93	0.00058	1.49	1.65	97.99	0.00096	0.45	0.51	106.65
			1.34				1.37				0.51	
			1.43				1.37				0.41	
		5.97	6.69	106.07		2.24	2.36	105.19		1.49	1.68	101.66
			6.84				2.36				1.45	
			5.47				2.36				1.42	
		8.96	7.89	95.39		5.97	5.82	92.16		2.99	2.54	91.10
			9.08				5.35				2.54	
			8.69				5.35				3.08	
AXI	0.0017	3.22	2.97	95.91	0.0023	3.22	3.66	106.15	0.0011	8.04	9.25	110.03
			3.51				2.98				8.64	
			2.78				3.61				8.64	
		9.65	8.38	105.54		9.65	8.72	100.57		16.08	15.93	90.73
			11.08				10.57				13.93	
			11.08				9.82				13.90	
		16.08	14.07	93.18		16.08	17.07	102.47		26.79	29.77	105.37
			14.07				17.86				27.13	
			16.81				14.49				27.80	

Table 6: Percentage recoveries obtained for 3AB, 2AB, BZ, MA, TR and AXI, after making small changes in the wavelengths used (±2-5nm)(+C_{Add}/ ppb=Concentration added, ≠C_{Det}/ ppb=Average concentration detected,*$\%_{REC}$= Average percentage recovery

Compound	Wavelengths used/ nm	+C_{Add}/ ppb	≠C_{Det}/ ppb	*$\%_{REC}$	Wavelenth used/ nm	≠C_{Det}/ ppb	*$\%_{REC}$
3AB	λexc 306 λemi 448	9.74	10.99	107.41	λexc 302 λemi 444	9.39	96.43
			10.99			9.39	
			9.39			9.39	
		29.21	30.23	107.15		31.83	99.84
			31.83			25.42	
			31.83			30.23	
		38.95	41.45	111.93		44.66	114.67
			44.66			44.66	
			44.66			44.66	
2AB	λexc 331 λemi 426	0.049	0.051	104.48	λexc 327 λemi 422	0.051	98.37
			0.051			0.051	
			0.051			0.042	
		0.49	0.50	106.94		0.47	94.12
			0.52			0.44	
			0.56			0.47	
		0.88	1.01	107.59		0.89	97.08
			0.91			0.87	
			0.94			0.82	
BZ	λexc 288 λemi 362	3.87	4.19	103.01	λexc 284 λemi 358	4.19	103.01
			4.19			3.99	
			3.58			3.78	
		11.61	12.34	102.76		12.95	106.27
			11.32			11.12	
			12.13			12.95	
		17.41	18.04	105.94		18.65	109.45
			18.25			18.86	
			19.06			19.67	
MA	λexc 376 λemi 519	0.11	0.12	110.03	λexc 372 λemi 515	0.12	110.03
			0.12			0.12	
			0.12			0.12	
		0.84	0.76	95.92		0.81	97.87
			0.81			0.90	
			0.86			0.76	
		1.96	1.94	100.39		1.94	92.88
			1.94			1.74	
			2.04			1.79	
TR	λexc 328 λemi 446	0.75	0.83	111.55	λexc 318 λemi 436	0.83	111.55
			0.83			0.83	
			0.83			0.83	
		7.47	7.49	101.79		7.49	98.95
			7.81			6.54	
			7.49			8.13	
		14.93	13.20	87.00		13.52	96.21
			12.89			14.47	

			12.89			15.11	
AXI	λexc 336 λemi 396	7.72	7.66	99.29	λexc 332 λemi 392	7.66	99.29
			7.66			7.66	
			7.66			7.66	
		8.04	7.66	106.05		8.96	100.68
			8.96			7.66	
			8.96			7.66	
		9.32	8.96	96.05		10.25	100.67
			10.25			8.96	
			7.66			8.96	

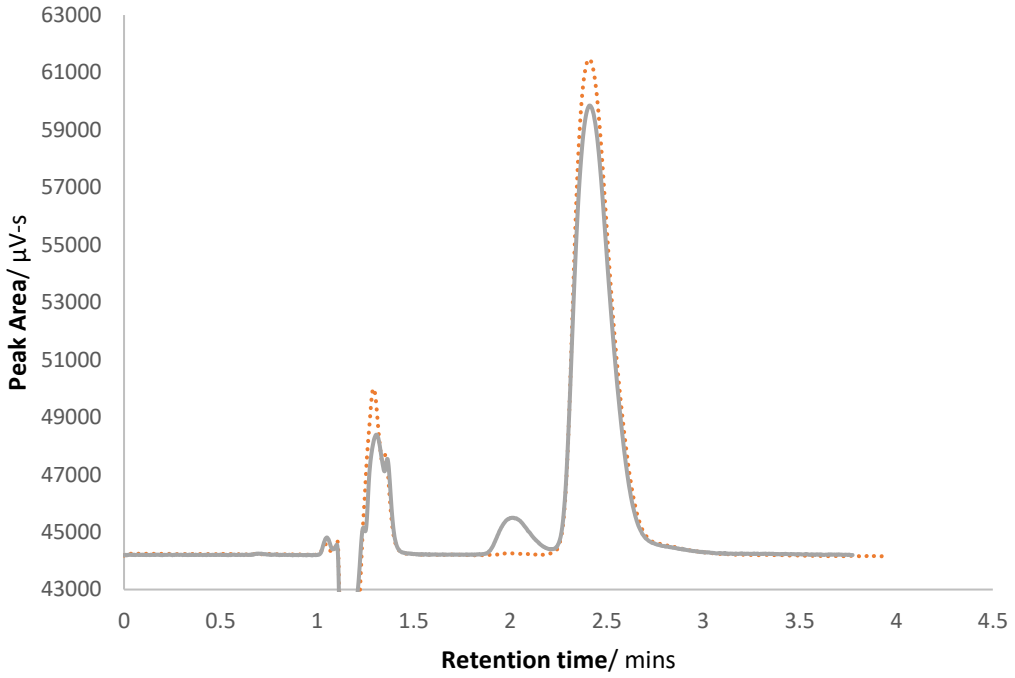

Figure 25: HPLC spectra of 1.53 x 10^{-5}M TR in ethanol solution, at room temperature, when irradiated for 0 mins (dashed line) and 30 minutes (sold line) in the presence of UV light